DYNAMIC REMEDIAL ACTION SCHEME USING ONLINE TRANSIENT STABILITY ANALYSIS

by

Arun Shrestha

A dissertation submitted to the faculty of
The University of North Carolina at Charlotte
in partial fulfillment of the requirements
for the degree of Doctor of Philosophy in
Electrical Engineering

Charlotte

2016

Approved by:

_____
Dr. Valentina Cecchi

_____
Dr. Robert W. Cox

_____
Dr. Sukumar Kamalasadan

_____
Dr. Badrul Chowdhury

_____
Dr. Harish Cherukuri

©2016
Arun Shrestha
ALL RIGHTS RESERVED

ABSTRACT

ARUN SHRESTHA. Dynamic remedial action scheme using online transient stability analysis. (Under the direction of DR. VALENTINA CECCHI)

Economic pressure and environmental factors have forced the modern power systems to operate closer to their stability limits. However, maintaining transient stability is a fundamental requirement for the operation of interconnected power systems. In North America, power systems are planned and operated to withstand the loss of any single or multiple elements without violating North American Electric Reliability Corporation (NERC) system performance criteria. For a contingency resulting in the loss of multiple elements (Category C), emergency transient stability controls may be necessary to stabilize the power system. Emergency control is designed to sense abnormal conditions and subsequently take pre-determined remedial actions to prevent instability. Commonly known as either Remedial Action Schemes (RAS) or as Special/System Protection Schemes (SPS), these emergency control approaches have been extensively adopted by utilities. RAS are designed to address specific problems, e.g. to increase power transfer, to provide reactive support, to address generator instability, to limit thermal overloads, etc. Possible remedial actions include generator tripping, load shedding, capacitor and reactor switching, static VAR control, etc. Among various RAS types, generation shedding is the most effective and widely used emergency control means for maintaining system stability.

In this dissertation, an optimal power flow (OPF)-based generation-shedding RAS is proposed. This scheme uses online transient stability calculation and generator cost function to determine appropriate remedial actions. For transient stability calculation, SIngle Machine Equivalent (SIME) technique is used, which reduces the multimachine power system model to a One-Machine Infinite Bus (OMIB) equivalent and identifies critical machines. Unlike conventional RAS, which are designed using

offline simulations, online stability calculations make the proposed RAS dynamic and adapting to any power system configuration and operating state. The generation-shedding cost is calculated using pre-RAS and post-RAS OPF costs. The criteria for selecting generators to trip is based on the minimum cost rather than minimum amount of generation to shed. For an unstable Category C contingency, the RAS control action that results in stable system with minimum generation shedding cost is selected among possible candidate solutions. The RAS control actions update whenever there is a change in operating condition, system configuration, or cost functions. The effectiveness of the proposed technique is demonstrated by simulations on the IEEE 9-bus system, the IEEE 39-bus system, and IEEE 145-bus system.

This dissertation also proposes an improved, yet relatively simple, technique for solving Transient Stability-Constrained Optimal Power Flow (TSC-OPF) problem. Using the SIME method, the sets of dynamic and transient stability constraints are reduced to a single stability constraint, decreasing the overall size of the optimization problem. The transient stability constraint is formulated using the critical machines' power at the initial time step, rather than using the machine rotor angles. This avoids the addition of machine steady state stator algebraic equations in the conventional OPF algorithm. A systematic approach to reach an optimal solution is developed by exploring the quasi-linear behavior of critical machine power and stability margin. The proposed method shifts critical machines active power based on generator costs using an OPF algorithm. Moreover, the transient stability limit is based on stability margin, and not on a heuristically set limit on OMIB rotor angle. As a result, the proposed TSC-OPF solution is more economical and transparent. The proposed technique enables the use of fast and robust commercial OPF tool and time-domain simulation software for solving large scale TSC-OPF problem, which makes the proposed method also suitable for real-time application.

ACKNOWLEDGEMENTS

Many people have contributed to the research work reported in this dissertation in various ways and their efforts are most sincerely appreciated.

First and foremost, I would like to express my sincere gratitude to my advisor, Dr. Valentina Cecchi, for all the help, guidance, and support she offered me throughout my doctoral research. Her incisive comments and ideas were instrumental in bringing out this work. Working with her has been a wonderful and learning experience.

Next, I wish to express my deep appreciation to my co-advisor, Dr. Robert W. Cox, not only for his guidance in the research, but also for his help and encouragement to face the challenges in my life. His profound knowledge has helped me a great deal.

I would like to thank the members of my committee, Dr. Sukumar Kamalasadan, Professor Badrul Chowdhury, and Dr. Harish Cherukuri for their guidance and valuable suggestions. I am grateful to Dr. Kamalasadan for his outstanding lectures on power system stability.

I am indebted to University of North Carolina at Charlotte (UNCC) for supporting my graduate studies by providing financial support in the form of Graduate Assistant Support Program (GASP). I also wish to gratefully acknowledge Schweitzer Engineering Laboratories Inc., Pullman, WA for donating protective relays and automation products used in my research work, and financial support for last few years of my doctoral studies.

Special thanks to my friends and family, who always supported me during both good and difficult times.

Finally, I would like to thank my wife for her love and support. Her unconditional love and support is the source of my inspiration and strength to accomplish this work. Without her support and encouragement, this dissertation would not have been possible.

DEDICATION

This dissertation is dedicated to my wife, Parmita Shrestha, for her unconditional love and support, and my parents, Tirtha Man Shrestha and Sanu Maiya Shrestha, for always encouraging me to follow my dreams.

TABLE OF CONTENTS

LIST OF TABLES xi

LIST OF FIGURES xiii

LIST OF ABBREVIATIONS xvii

LIST OF SYMBOLS xviii

CHAPTER 1: INTRODUCTION 1

1.1. Overview 1

1.2. Motivation 1

1.2.1. Preventive Transient Stability Control 3

1.2.2. Emergency Transient Stability Control 5

1.3. Problem Statement 8

1.4. Thesis Overview and Research Contributions 9

1.5. Thesis Organization 12

CHAPTER 2: TRANSIENT STABILITY, OPTIMAL POWER FLOW, AND REMEDIAL ACTION SCHEME 13

2.1. Overview 13

2.2. Transient Stability 14

2.2.1. Time-domain Method 17

2.2.2. Direct Method 17

2.2.3. Hybrid Method 19

2.3. Online Transient Stability Analysis 19

2.4. Optimal Power Flow 22

2.5. Transient Stability-Constrained Optimal Power Flow 24

2.6. Remedial Action Scheme 26

CHAPTER 3: PROPOSED TRANSIENT STABILITY-CONSTRAINED OPF 30

3.1. Overview 30

3.2. Proposed TSC-OPF 30

3.3. SIME for Online Transient Stability Analysis 31

3.3.1. SIME Mathematical Formulation 32

3.3.2. SIME Quasi-Linear Behavior 40

3.4. Formulation of TSC-OPF Problem 43

3.4.1. Conventional OPF 44

3.4.2. Transient Stability Constraints 47

3.4.3. Proposed TSC-OPF Algorithm 48

CHAPTER 4: PROPOSED DYNAMIC REMEDIAL ACTION SCHEME 51

4.1. Overview 51

4.2. Proposed Dynamic RAS 51

4.3. Formulation of Dynamic RAS Problem 53

4.3.1. OPF-Based Generation-Shedding Selection 54

4.3.2. OPF-Based Generation-Shedding Cost 56

CHAPTER 5: REAL-TIME TEST PLATFORM 60

5.1. Overview 60

5.2. Need for Real-Time Test Platform 60

5.3. Real-Time Test Platform 63

5.3.1. The Real Time Digital Simulator 65

5.3.2. The Phasor Measurement Units (PMUs) 66

5.3.3. The Protocol Gateway 67

5.3.4. The MATLAB Based TSA and RAS Determination Tool 67

5.3.5. RAS Logic Controller 68

5.4. Capabilities of the Real-Time Test Platform 68

CHAPTER 6: TEST CASES AND RESULTS 70

6.1. Overview 70

6.2. Test Cases For TSC-OPF 70

6.2.1. IEEE 9-Bus, 3-Machine System 71

6.2.2. IEEE 39-Bus, 10-Machine System 76

6.2.3. IEEE 145-Bus, 50-Machine System 80

6.2.4. Summary Of Results And Observations 84

6.3. Test Cases For Generation Shedding Dynamic RAS 85

6.3.1. IEEE 9-Bus, 8-Machine System 85

6.3.2. IEEE 39-Bus, 16-Machine System 90

6.3.3. IEEE 145-Bus, 50-Machine System 97

6.3.4. Summary Of Results And Observations 101

CHAPTER 7: CONCLUSIONS 103

7.1. Concluding Remarks 103

7.2. Summary of Research Contributions 105

7.3. Future Work 106

REFERENCES 108

APPENDIX A: IEEE TEST POWER SYSTEMS 115

A.1. IEEE 9-Bus, 3-Machine System 116

A.2. IEEE 9-Bus, 8-Machine System 119

A.3. IEEE 39-Bus, 10-Machine System 120

A.4. IEEE 39-Bus, 16-Machine System 124

A.5. IEEE 145-Bus, 50-Machine System 127

LIST OF TABLES

TABLE 2.1: Overview of RAS by NERC region 28

TABLE 2.2: SIPS purpose classification 28

TABLE 6.1: Cost function and optimal loading for IEEE 9-bus system 71

TABLE 6.2: TSC-OPF calculations for IEEE 9-bus system - Case A 72

TABLE 6.3: TSC-OPF costs comparison for IEEE 9-bus system 75

TABLE 6.4: Optimal solutions for IEEE 9-bus system 75

TABLE 6.5: Cost function and optimal loading for IEEE 39-bus system 76

TABLE 6.6: TSC-OPF calculations for IEEE 39-bus system - Case B 78

TABLE 6.7: Comparison of total costs for IEEE 39-bus system 80

TABLE 6.8: Optimal solutions for IEEE 39-bus system 80

TABLE 6.9: TSC-OPF calculations for IEEE 145-bus system - Case A 81

TABLE 6.10: TSC-OPF calculations for IEEE 145-bus Case B 84

TABLE 6.11: Plant cost function I and optimal loading for IEEE 39-bus system - Case A 92

TABLE 6.12: Generation-shedding cost For IEEE 39-bus system - Case A ($/h) 94

TABLE 6.13: Plant cost function II and optimal loading for IEEE 39-bus system - Case B 95

TABLE 6.14: Generation-shedding cost For IEEE 39-bus System - Case B ($/h) 96

TABLE 6.15: Generation shedding cost For IEEE 145-bus system ($/h) 100

TABLE A.1: OPF result for IEEE 9-bus system base case 116

TABLE A.2: Branch data for IEEE 9-bus system in 100 MVA base 117

TABLE A.3: Generator data for IEEE 9-bus system 117

TABLE A.4: Exciter data for IEEE 9-bus system 118

TABLE A.5: Turbine-governor data for IEEE 9-bus, 8-machine system 119

TABLE A.6: OPF result for IEEE 39-bus system base case 121

TABLE A.7: Branch data for IEEE 39-bus system in 100 MVA base 122

TABLE A.8: Generator data for IEEE 39-bus system 123

TABLE A.9: Exciter data for IEEE 39-bus system 124

TABLE A.10: Exciter data for IEEE 39-bus, 16-machine system 125

TABLE A.11: Turbine-governor data for IEEE 39-bus, 16-machine system 125

TABLE A.12: PSS data for IEEE 39-bus, 16-machine system 126

TABLE A.13: Loadflow result for IEEE 145-bus system 128

TABLE A.14: Branch data for IEEE 145-bus system in 100 MVA base 132

TABLE A.15: Generator data for IEEE 145-bus system 143

TABLE A.16: Exciter data for IEEE 145-bus system 144

LIST OF FIGURES

FIGURE 2.1: Classification of power system stability. 15

FIGURE 3.1: Machine rotor angles for: (top) an unstable and (bottom) a stable system. 35

FIGURE 3.2: Rotor angles and OMIB P–δ plot for a stable contingency. 38

FIGURE 3.3: Rotor angles and OMIB P–δ plot for an unstable contingency. 38

FIGURE 3.4: OMIB P–δ plot for a stable contingency. 39

FIGURE 3.5: (a) OMIB P–δ, (b) δ, and (c) ω plots for an unstable contingency. 40

FIGURE 3.6: Quasi-linear relationship exhibited by a contingency in the IEEE 9-bus system. (a) Stability margin (η) vs electrical power (P_e), (b) Stability margin (η) vs critical machines electrical power (P_{eC}), (c) Stability margin (η) vs rotor angle (δ). 42

FIGURE 3.7: Quasi-linear relationship exhibited by a contingency in the IEEE 39-bus system. (a) Stability margin (η) vs electrical power (P_e), (b) Stability margin (η) vs critical machines electrical power (P_{eC}), (c) Stability margin (η) vs rotor angle (δ). 42

FIGURE 3.8: Stability margin (η) calculated using SIME method and estimated using linear-extrapolation. (a) For IEEE 9-bus system, (b) For IEEE 39-bus system. 43

FIGURE 3.9: Steady state representation of the stator algebraic equations. 48

FIGURE 3.10: Flowchart for the proposed TSC-OPF technique. 50

FIGURE 4.1: Schematic overview of the Dynamic RAS. 53

FIGURE 4.2: Flowchart for the OPF-based generation-shedding selection. 55

FIGURE 5.1: Real-time test platform in the Duke Energy Smart Grid Lab at UNC Charlotte. 64

FIGURE 5.2: Hardware used for testing the proposed Dynamic RAS. 64

FIGURE 5.3: Real-time platform for testing the Dynamic RAS. 65

FIGURE 6.1: IEEE 9-bus system - Case A. Generator rotor angles and OMIB $P-\delta$ curves for the base case. 72

FIGURE 6.2: IEEE 9-bus system - Case A. Stable rotor angles and OMIB P-δ curves for the third iteration. 73

FIGURE 6.3: IEEE 9-bus system - Case B. Generator rotor angles and OMIB $P-\delta$ curves for the base case. 74

FIGURE 6.4: IEEE 9-bus system - Case B. Stable rotor angles and OMIB $P-\delta$ curves obtained for the sixth iteration. 75

FIGURE 6.5: IEEE 39-bus system - Case A. Generator rotor angles and OMIB $P-\delta$ curves for the base case. 77

FIGURE 6.6: IEEE 39-bus system - Case A. Stable rotor angles and OMIB P-δ curves obtained for the fourth iteration. 78

FIGURE 6.7: IEEE 39-bus system - Case B. Generator rotor angles and OMIB P-δ curves for the base case. 79

FIGURE 6.8: IEEE 39-bus system - Case B. Stable rotor angles and OMIB $P-\delta$ curves obtained for the fourth iteration. 79

FIGURE 6.9: IEEE 145-bus system - Case A. Generator rotor angles and OMIB $P-\delta$ curves for the base case. 82

FIGURE 6.10: IEEE 145-bus system - Case A. Stable rotor angles and OMIB $P-\delta$ curves obtained for the third iteration. 82

FIGURE 6.11: IEEE 145-bus system - Case B. Generator rotor angles and OMIB $P-\delta$ curves for the base case. 83

FIGURE 6.12: IEEE 145-bus system - Case B. Stable rotor angles and OMIB P-δ curves obtained for the third iteration. 84

FIGURE 6.13: OMIB $P-\delta$ curve and generator speed curves for Test Case A without remedial action. The contingency drives the system to instability. 87

FIGURE 6.14: OMIB $P-\delta$ curve and generator speed curves for Test Case A with Gen21 trip remedial action. The remedial action stabilizes the system. 88

FIGURE 6.15: OMIB $P-\delta$ curve and generator speed curves for Test Case B (5% increase in Gen21-Gen24 P) with Gen21 trip remedial action. 88

FIGURE 6.16: OMIB $P-\delta$ curve and generator speed curves for Test Case B (5% increase in Gen21-Gen24 P) with Gen21-Gen22 trip remedial action. Additional generator trip is needed to stabilize the system. 89

FIGURE 6.17: OMIB $P-\delta$ curve and generator speed curves for Case C (5% decrease in Gen21-Gen24 P). The system is stable and no remedial action is needed. 89

FIGURE 6.18: OMIB $P-\delta$ curve and generator speed curves for Case D (5% decrease in Gen1 $|V|$). The system is stable and no remedial action is needed. 90

FIGURE 6.19: OMIB $P-\delta$ curve and generator speed curves for Case E (3% decrease in Gen21-Gen24 $|V|$). The system is unstable even with Gen21 tripping. 91

FIGURE 6.20: (a) Generator rotor angles for 3-phase fault on a single line between Bus 16-17. (b) Generator rotor angles for 3-phase fault on both lines. The system is stable for the first case and is unstable for the second case. 93

FIGURE 6.21: OMIB $P-\delta$ curve and generator rotor angles for G51 RAS choice. Shedding generator G51 stabilizes the system. 94

FIGURE 6.22: OMIB $P-\delta$ curve and generator rotor angles for G41 RAS choice. Shedding generator G41 does not stabilize the system. 95

FIGURE 6.23: OMIB $P-\delta$ curves for 3-phase fault on a single and double lines between Bus 16-17. The system is stable for the first case and is unstable for the second case. 96

FIGURE 6.24: OMIB P-δ curve and generator rotor angles for G71 RAS choice. Shedding generators G71 stabilizes the system. 97

FIGURE 6.25: OMIB P-δ curve and generator rotor angles for G51 RAS choice. Shedding generators G51 stabilizes the system. 97

FIGURE 6.26: (a) Generator rotor angles for 3-phase fault on a single line between Bus 25-12. (b) Generator rotor angles for 3-phase fault on both lines. The system is stable for the first case and is unstable for the second case 99

FIGURE 6.27: OMIB P-δ curve and generator rotor angles for G15 RAS choice. Shedding generator G15 does not stabilize the system. 100

FIGURE 6.28: OMIB P-δ curve and generator rotor angles for G34 RAS choice. Shedding generator G34 stabilizes the system. 101

FIGURE 6.29: OMIB P-δ curve and generator rotor angles for G9 RAS choice. Shedding generator G9 stabilizes the system. 101

FIGURE A.1: IEEE 9-bus, 3-machine test power system. 116

FIGURE A.2: IEEE 9-bus, 8-machine test power system. 119

FIGURE A.3: IEEE 39-bus test power system. 120

FIGURE A.4: IEEE 39-bus 16-machine test power system. 124

FIGURE A.5: IEEE 145-bus, 50-machine test power system. 127

LIST OF ABBREVIATIONS

ATC	Available Transfer Capacity
AVR	Automatic Voltage Regulator
CM	Critical Machines
DSA	Dynamic Security Assessment
EAC	Equal-Area Criterion
FACTS	Flexible Alternating Current Transmission System
IEEE	Institute of Electrical and Electronics Engineers
ISO	Independent System Operator
NERC	North American Electric Reliability Corporation
NM	Non-Critical Machines
OMIB	One-Machine Infinite Bus
OPF	Optimal Power Flow
PMU	Phasor Measurement Unit
PSS	Power System Stabilizer
RAS	Remedial Action Scheme
RTDS	Real-Time Digital Simulator
SIME	SIngle Machine Equivalent
SPS	Special Protection Scheme
SVC	Static Var Compensator
TSA	Transient Stability Assessment
TSC-OPF	Transient Stability-Constrained Optimal Power Flow
WACS	Wide-Area Control System
WAMS	Wide-Area Monitoring System

LIST OF SYMBOLS

P_{Gi}	real power output of machine i
Q_{Gi}	reactive power output of machine i
P_{Di}	real power demand of load i
Q_{Di}	reactive power demand of load i
V_i	voltage magnitude of bus i
S_i	complex power flow in line i
θ_n	voltage angle at bus n
δ_i	rotor angle of machine i
δ	rotor angle of the OMIB equivalent
δ_C	rotor angle of the equivalent critical machine
δ_N	rotor angle of the equivalent non-critical machine
δ_r	return angle of the OMIB equivalent
δ_u	unstable angle of the OMIB equivalent
ω_i	rotor speed of machine i
ω	rotor speed of the OMIB equivalent
ω_C	rotor speed of the equivalent critical machine
ω_N	rotor speed of the equivalent non-critical machine
P_m	mechanical power of the OMIB equivalent
P_{mC}	mechanical power of the equivalent critical machine
P_{mN}	mechanical power of the equivalent noncritical machine
P_e	electrical active power of the OMIB equivalent
P_{eC}	electrical active power of the equivalent critical machine
P_{eN}	electrical active power of the equivalent non-critical machine
η	stability margin
E'_{qi}	q-axis transient voltage of machine i
E'_{di}	d-axis transient voltage of machine i

E_{qi}	q-axis steady state voltage of machine i
E_{di}	d-axis steady state voltage of machine i
X'_{di}	d-axis transient reactance of machine i
X'_{qi}	q-axis transient reactance of machine i
X_{di}	d-axis synchronous reactance of machine i
X_{qi}	q-axis synchronous reactance of machine i
R_{si}	stator resistance of machine i
I_{di}	d-axis current of machine i
I_{qi}	d-axis current of machine i
E_{fdi}	field voltage of machine i
τ'_{d0i}	d-axis transient open circuit time constant of machine i
τ'_{q0i}	q-axis transient open circuit time constant of machine i
M_i	moment of inertia of machine i
H_i	inertia constant of machine i
D_i	damping constant of machine i
Y_{ik}	admittance between bus i and bus k

CHAPTER 1: INTRODUCTION

1.1 Overview

This thesis is focused on the development of solution techniques for improving transient stability during grid disturbances. Two solution techniques are proposed in this thesis. The first is the development of the proposed transient stability constrained-optimal power flow solution technique and the second is the proposed dynamic remedial action scheme using online transient stability analysis. The proposed techniques can function as valuable tools for system operators and assist in real-time operation of power systems.

This chapter is organized as follows. Section 1.2 provides a background and motivation for this work. The thesis' problem statement is presented in Section 1.3. In Section 1.4, a summary of research contributions is given. Finally, an overview of the thesis organization is presented in Section 1.5.

1.2 Motivation

The electric power system is perhaps the largest, most complicated man-made machine ever created. Its operation should be reliable, secure, and economical. The supply of reliable and economical electrical power has a major impact on the economy of a nation. In recent years, economic pressure and environmental factors have forced modern power systems to operate within tighter margins and with less redundancy. Transmission networks, for instance, have experienced increased stress since regulatory processes, high capital costs, and right-of-way restrictions limit new construction. Further complications have resulted from the introduction of intermittent resources, market competition, heavy inter-area exchanges, and the use of Flexible Alternating

Current Transmission Systems (FACTS). The combined effect of these trends has greater concern over transient stability margins. As a result, many large-scale blackouts have occurred worldwide during major grid disturbances [1]. Such disturbances affect millions of people and billions of dollars in financial loss. A summary of the major blackouts that occurred in the last two decades is discussed below.

- Blackout of July 31, 2012 in northern, eastern, and north-eastern India [2]

  On July 31, 2012 a major grid disturbance occurred at 13:00 hours in the northern, eastern and north-eastern electricity grids. Approximately 48 GW of load across 21 States and 1 Union Territory were affected. Over 600 million people (nearly half of India's population), were left without power.

- Blackout of July 30, 2012 in northern India [2]

  The grid disturbance of July 30, 2012 in northern India affected more than 300 million people (about 25% of India's population). Around 32 GW of load was interrupted in 8 northern states.

- Blackout of August 14, 2003 in North America [1]

  The U.S.-Canadian blackout of August 14, 2003 affected approximately 50 million people in eight U.S. states and two Canadian provinces. Roughly 63 GW of load was interrupted, which equates to approximately 11% of the total load served in the Eastern Interconnection of the North American system. Financial loss of $6 billion was estimated. During this event, over 400 transmission lines and 531 generating units at 261 power plants tripped.

- Blackout of August 10, 1996 in western North America [3]

  On August 10, 1996, a major failure occurred in the Western Systems Coordinating Council (WSCC) system resulting in break-up into four islands. This power outage affected customers in seven western U.S. states, two Canadian

provinces, and Baja California, Mexico. Around 30.39 GW of load was lost, affecting 7.5 million customers, and costing an estimated of $2 billion in financial loss.

To avoid major grid disturbances, the power systems shall be designed and operated with sufficient redundancy. In North America, the power systems are planned and operated to withstand the loss of any single or multiple elements without violating North American Electric Reliability Corporation (NERC) system performance criteria [4,5]. For a contingency resulting in the loss of a single element (Category B), the power system must remain stable with all equipment loaded to within its normal operating limits. To withstand Category B contingency, preventive type transient stability control is implemented [6]. Preventive control enables the system to withstand contingencies by rescheduling generation. It is usually achieved by adding transient stability constraints in the optimal power flow (OPF) algorithm [7]. For a contingency resulting in the loss of multiple elements (Category C), emergency transient stability controls like load shedding, generation shedding, or curtailment of contracted power may be necessary to stabilize the power system [5]. Application of preventive control for Category C contingency can impact the economic operation of the power systems. Emergency control is designed to sense abnormal conditions and subsequently take pre-determined remedial actions to prevent instability.

1.2.1 Preventive Transient Stability Control

For a given unstable contingency, preventive transient stability control moves the system state to a secure operating region in order to withstand the contingency. The preventive control actions include redispatching of generating units, adjustments of the voltage set point, adjustments of transformers taps, and adjustments of load demands. However, the movement of the system state to a secure operating region impacts the economic operation of the power system. To reconcile between economics and security, the preventive control is normally achieved by adding transient stability

constraints within the OPF problem formulation; this is referred to as Transient Stability-Constrained OPF (TSC-OPF). The detailed literature review on transient stability analysis, optimal power flow, and TSC-OPF is presented in Chapter 2.

TSC-OPF is a nonlinear optimization problem that extends the OPF to include transient stability constraints. The solution techniques for the TSC-OPF can be broadly classified into three different classes: dynamic optimization, extended equal area criterion, and computational intelligence. These methods exhibit two distinct characteristics in regards to: (i) inclusion of the stability constraints in the OPF algorithm, and (ii) the method used to compute stability margins.

In dynamic optimization-based approach, the power system transient stability model is converted into an algebraic set of equations for each time step of time-domain simulation, and are then included as equality constraints in the OPF problem [7–9]. This approach increases the TSC-OPF problem dimension by several orders of magnitude with respect to conventional OPF. Thus, its solution generally requires large memory and computational capabilities. In extended equal area approach, the transient stability constraints are directly converted into conventional constraints of a standard OPF program. Transient Stability Assessment (TSA) is carried out outside the OPF algorithm, resulting in a reduced number of stability constraints to be incorporated in the OPF formulation [6, 10, 11]. This technique significantly reduces OPF problem complexity and dimension. Moreover, this type of approach is compatible with any power system dynamic model and stability scenarios. The TSC-OPF problem has also been solved using computational intelligence solution techniques such as differential evolution and evolutionary algorithms [12, 13].

Recently, preventive control problem has also been solved using SIngle Machine Equivalent (SIME) method [14, 15]. Using time-domain simulation, SIME transforms the dynamics of the multi-machine power system into a suitable One Machine Infinite Bus (OMIB) system, and the stability margin is calculated using the equal-area

criterion [16]. Since the OMIB represents the dynamics of the multi-machine power system, the sets of dynamic and transient stability constraints can be reduced to a single, time independent stability constraints, decreasing the overall size of the OPF problem. In [14], a single transient stability constraint based on the OMIB rotor angle at initial time step is proposed. Although very powerful, the method proposed in [14] requires addition of generator stator algebraic equations and higher generator reactive power limits ($Q_{Gi\ max}$ and $Q_{Gi\ min}$), to incorporate for reactive power absorb by generator synchronous reactance, in the OPF formulation. Since generator stator algebraic equations are not included in the conventional OPF formulation, the proposed method requires modification of the conventional OPF problem [17]. This can be a challenging task for large-scale power systems.

The TSC-OPF solution technique for preventive control can be improved by:

- exploring quasi-linear behavior of the OMIB stability margin and machine active power and developing a systematic approach for reaching an optimal solution.
- developing a single, time-independent, stability constraint based on the machines' active power, as opposed to the OMIB rotor angle. This avoids the addition of generator stator algebraic equations in the OPF formulation and enables the use of conventional OPF. It also allows the implementation of actual generator reactive power limits ($Q_{Gi\ max}$ and $Q_{Gi\ min}$) in the OPF algorithm.
- setting the stability limit based on stability margin, rather than heuristically set limit on the OMIB rotor angle. It allows the solution technique to become transparent and more economical solutions can be obtained.

1.2.2 Emergency Transient Stability Control

Emergency transient stability controls are designed to sense abnormal power system conditions and subsequently take pre-determined remedial actions to prevent the contingencies from escalating into major system disturbances. Commonly known as

either Remedial Action Schemes (RAS) or Special Protection Schemes (SPS), these emergency control approaches have been extensively adopted by utilities [18]. These schemes are designed to address specific problems, e.g. increase power transfer, provide reactive support, mitigate overfrequency or underfrequency issues, address generator instability, limit line and other equipment thermal overloads, etc. Possible remedial actions include generator tripping, turbine fast valving, braking resistor insertion, load shedding, capacitor and reactor switching, static VAR control, system separation, etc. These schemes have become more common because they are less costly and quicker to permit, design, and build than other alternatives such as the construction of new transmission lines and power plants [19, 20]. The detailed literature review on RAS is presented in Chapter 2.

The current practice in RAS design is to use extensive offline simulations [21–23]. These simulations consider system behavior following large disturbances occurring during stressed conditions. The remedial actions are designed using repeated offline transient simulations that consider numerous combinations of contingencies, power-system configurations, and load-flow scenarios. For example, if X contingencies require remedial actions, and there are Y possible power-system configurations and Z load-flow scenarios, the design process requires $X * Y * Z$ simulation runs [22]. Trying to predict all possible power system operating states in offline studies leads to a large number of test cases to simulate. This leads to long design, validation and commissioning periods. Also, the current RAS design method cannot easily account for any future addition of transmission lines or power plants.

RAS logic is triggered into action whenever a Wide-Area Monitoring System (WAMS) detects a particular contingency. Although tremendously useful, the logic is static and thus it can be somewhat draconian in its approach. For instance, system loading conditions and parameters may be quite different from those assumed during the design stage, thus resulting in excessive load or generation shedding. Also some of the con-

tingencies considered non-severe during design can become severe due to changes in system loading.

In recent years, deployment of phasor measurement units (PMU) has revolutionized the way power systems are monitored and controlled. Instead of estimating power system states, PMUs measure system states in real-time. Similarly, advancement in communication and computing technology has made online transient stability analysis (TSA) possible. As a result, a growing number of system operators have implemented online TSA in the energy management systems [24]. Online TSA evaluates stability limits based on real-time system conditions and topology. It greatly enhances the operational decision making capability of an operator and significantly reduces the risk of cascading blackouts. The current RAS design can clearly be improved through the application of online TSA.

Moreover, traditionally the design of RAS considers only technical aspects of the power system. The effect of a RAS control action on the economic operation of the power system is generally not considered. These schemes might therefore be acceptable in a regulated energy market, but they are not an attractive option in a competitive energy market. In today's deregulated power industry, economic operation of the power system depends on various factors such as load demand, cost of generation, time-varying bid price of generator power, power purchase agreement, etc. Hence, a RAS scheme designed using both operation costs and technical constraints can result in optimal economic operation while maintaining security limits.

The shortcomings of current RAS design can be addressed by:

- incorporating online transient stability analysis to determine appropriate remedial actions based on current system states, i.e. making RAS more dynamic and adaptable. It also reduces the number of contingencies to be analyzed for remedial action determination.

- implementing SIME method to separate the generators into two categories,

namely Critical Machines (CMs) and Non-critical Machines (NMs). Identification of critical machines greatly reduces the number of machines to be considered for determining remedial actions.

- incorporating an appropriate cost function to assist in selecting an optimal remedial action. A cost-based RAS scheme can guarantee the most economic power system operation in the post remedial action phase.

1.3 Problem Statement

The main objective of this thesis is to develop control techniques for both preventive and emergency transient stability controls to assist system operators. For preventive control, the objective is to develop a solution technique for solving TSC-OPF problem. Similarly, for emergency control, the goal of this thesis is to develop dynamic generation shedding RAS using online transient stability analysis. Specific objectives and assumptions for each control technique are stated below:

1. TSC-OPF solution technique

   - Objectives

     - To develop a global, time-independent, transient stability constraint based on quasi-linear behavior of the OMIB stability margin and critical machines' active power.
     - To establish an objective criterion to determine the transient stability limit.
     - To design a security constrained OPF tool by combining a global transient stability constraint and a conventional OPF formulation.

   - Assumptions

     - It is assumed that a list of credible contingency is provided to the TSC-OPF algorithm. Only single contingency is be considered in this

work.

  - Multi-swing instability is not considered.

2. Dynamic generation shedding RAS

   - Objectives

     - To develop a dynamic generation shedding RAS by incorporating on-line transient stability analysis and SIME method.
     - To formulate an OPF problem that calculates generation shedding cost for each remedial action and for a given unstable contingency.
     - To identify generation shedding RAS choice which results in minimum generation-shedding cost and stable system following the RAS action.
     - To develop a real-time hardware-in-the-loop test platform for testing dynamic RAS.

   - Assumptions

     - It is assumed that real-time power system states information is made available by State Estimator. Similarly, a list of credible contingency is provided to the dynamic RAS algorithm.
     - Power system model used to determine remedial actions closely matches the actual power system.
     - The remedial action does not change the mode of disturbance [25].

1.4 Thesis Overview and Research Contributions

In this thesis, two control techniques for improving transient stability are developed: (i) TSC-OPF solution technique and (ii) dynamic generation shedding RAS.

An improved, yet relatively simple, method for solving TSC-OPF problem is developed in this thesis. Using SIME technique, the multi-machine power system model

is reduced to a OMIB equivalent to compute stability margins. The quasi-linear behavior of the OMIB stability margin and critical machine(s) active power is explored to formulate a single, time-independent transient stability constraint. This avoids the addition of the generator stator algebraic equations in the OPF formulation and enabling the use of conventional OPF. The proposed method shifts critical machines active power based on generator costs using an OPF algorithm. Effectiveness of the proposed TSC-OPF solution technique is demonstrated by simulations on the IEEE 9-bus, 3-machine system, IEEE 39-bus, 10-machine system, and IEEE 145-bus, 50-machine system.

A dynamic generation shedding RAS which combines online stability calculations and generator cost function is proposed in this thesis. The SIME method is used for identification of critical machines and fast calculation of stability margins. An optimization problem is formulated using generator cost function to determine minimum cost generation shedding remedial action. Robustness of the proposed method is evaluated for change in operating condition, system configuration, and cost function.

A real-time hardware-in-the-loop test platform is developed for testing the proposed dynamic generation shedding RAS. Effectiveness of the proposed dynamic RAS is demonstrated by real-time simulations on the IEEE 9-bus, 8-machine system and IEEE 39-bus, 16-machine system using the real-time test platform. The proposed dynamic RAS is also tested using offline simulation on the IEEE 145-bus, 50-machine system.

The thesis' contributions are summarized below:

1. Formulation of a TSC-OPF optimization problem for security dispatch [26].
    - Given: an unstable contingency and generator fuel cost function,
    - Determine: transient security dispatch at minimum operation cost.
2. Formulation of a TSC-OPF optimization problem for security redispatch [26].

- Given: an unstable contingency and market-clearing or spot price,
- Determine: transient security redispatch at minimum cost increase.

The proposed TSC-OPF solution technique is an improved, yet relatively simple method. It uses a single, time-independent stability constraint and a conventional OPF to calculate an optimal solution.

3. Formulation of a dynamic generation shedding RAS optimization problem for traditional electricity markets [27, 28].

   - Given: a list of credible contingencies and generator fuel cost function,
   - Determine: generation-shedding RAS choice with minimum generation-shedding cost.

4. Formulation of a dynamic generation shedding RAS optimization problem for deregulated energy markets [29].

   - Given: a list of credible contingencies and market-clearing or spot price,
   - Determine: generation-shedding RAS choice with minimum generation-shedding cost.

   It is noted that the concept of dynamic RAS is novel. It uses available real-time power system data and cost function to determine most appropriate remedial actions with minimum cost.

5. Development of the real-time hardware-in-the-loop test platform specifically for validation and testing of the proposed dynamic RAS [30].

6. Development of a fast solution for converting synchrophasor data (IEEE C37.118 format) into analog values that are readable by any controller [31].

   It is noted that the real-time test platform is suitable for the design, testing, and validation of both continuous and discontinuous wide-area controllers. This

makes the test platform a powerful tool for any state-of-the-art 'Smart Grid' laboratory.

1.5 Thesis Organization

The remaining chapters of this dissertation are organized as follows. In Chapter 2, detailed literature review of transient stability, optimal power flow, and remedial action schemes are presented. The proposed transient stability constrained-optimal power flow solution technique is discussed in Chapter 3. In Chapter 4, formulation of the OPF-based dynamic generation shedding RAS is presented. Chapter 5 describes the real-time hardware-in-the-loop test platform designed and developed specifically for validation and testing of the proposed dynamic RAS. Chapter 6 then presents the test cases and results for the proposed TSC-OPF solution technique and the proposed OPF-based dynamic generation shedding RAS. Finally, in Chapter 7, the research contributions of this thesis are summarized, and directions for future research work are suggested.

CHAPTER 2: TRANSIENT STABILITY, OPTIMAL POWER FLOW, AND REMEDIAL ACTION SCHEME

2.1 Overview

The economic and secure operation of power systems is of paramount importance to the utilities and regulatory authorities around the world. Environmental and economic issues have forced modern power systems to operate within tighter margins and with less redundancy. These factors have resulted in stability-limited power networks and made transient stability a primary concern to the system operators. However, maintaining transient stability is a fundamental requirement for the operation of interconnected power systems. In order to enhance transient stability, two distinct varieties of transient stability control are available to system operators, namely preventive control and emergency control [6,32]. Transient stability constrained-optimal power flow (TSC-OPF) is one type of preventive control and remedial action scheme falls under emergency control.

This chapter is organized as follows. Section 2.2 provides an overview of transient stability and reviews three available techniques for conducting transient stability analysis. The advantages and challenges of moving transient stability analysis from the offline mode to the online mode is discussed in Section 2.3. Section 2.4 provides a brief description of an optimal power flow. Various techniques found in the literature for solving TSC-OPF problem are presented in Section 2.5. Similarly, various types of remedial action schemes implemented in the industry are discussed in Section 2.6.

2.2 Transient Stability

Modern power systems are large and complex systems whose operation should be reliable, secure, and economical. The supply of reliable and economic electric energy has a major impact on economic security of a nation and the standard of living of its citizens. Indeed, recent major blackouts in North America and in Europe have vividly demonstrated that power interruptions, grid congestions, or blackouts significantly impact the economy and society. Hence, the economic and secure operation of electrical power systems is of paramount importance to the utilities and regulatory authorities around the world.

Economic and environmental issues have forced modern power systems to operate within tighter margins and with less redundancy. Transmission networks, for instance, experience increased stress since regulatory processes, high capital costs, and right-of-way restrictions limit new construction. Further complications result from the introduction of intermittent resources, market competition, heavy inter-area exchanges, and the use of Flexible Alternating Current Transmission Systems (FACTS). These factors have resulted in stability-limited power networks and made transient stability a primary concern to the system operators.

Power system stability is defined as the property of a power system that enables it to remain in a state of operating equilibrium under normal operating conditions and to regain an acceptable state of equilibrium after being subjected to a disturbance [33]. The classification of power system stability, according to IEEE/CIGRE Joint Task Force on Stability Terms and Definitions [34], is shown in Fig. 2.1.

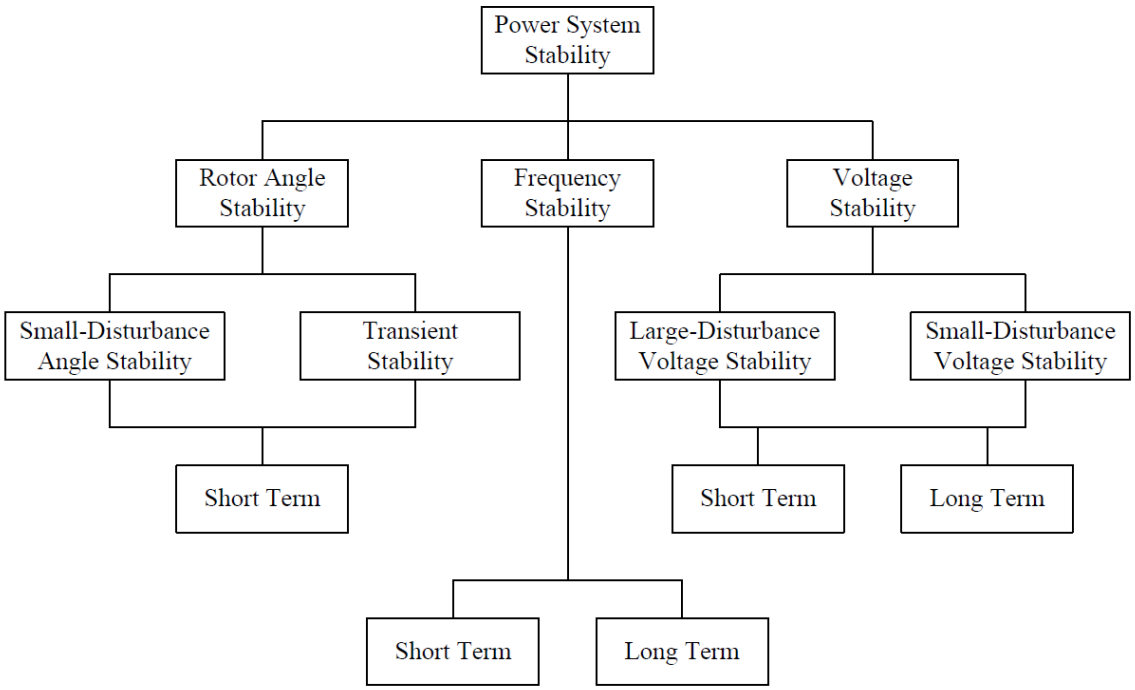

Figure 2.1: Classification of power system stability.

Power systems continually experience two types of disturbances: load variations and event disturbances. Small disturbances in the form of load variations occur continually and the system must be able to adjust to the changing conditions and operate satisfactorily. The system must also be able to survive numerous event disturbances, such as a short circuit on a transmission line or loss of a large generator. A large event disturbance may lead to new system configuration due to the isolation of the faulted elements.

Transient stability refers to the behavior of interconnected synchronous machines when subjected to a large disturbance. Such situations cause large excursions between rotor angles, and synchronism may be lost. The ability to maintain synchronism depends upon the equilibrium between electromagnetic torque and mechanical torque of each synchronous machine in the system. The time frame for preventing this scenario might only be a few seconds. Transient instability is usually identified by increasing angular swings of some generators leading to their loss of synchronism

with other generators. Because of the severity and short recovery window, transient stability is a key concern in most power systems. The stresses created by the changing landscape in the power industry only exacerbate concerns over stable operation during large disturbances.

Transient Stability Assessment (TSA) is the study of power system's response to a set of credible large disturbances. The assessment involves selecting a set of credible contingencies and evaluating system's response to those contingencies. The time frame of interest in transient stability studies is usually three to five seconds following the disturbance. It may extend to 10 - 20 seconds for very large systems with dominant inter-area swing. The dynamics of the excitation system, automatic voltage regulators, SVCs, underfrequency load shedding, and undervoltage load shedding are all active in this time frame.

In North America, the power systems are planned and operated to withstand the loss of any single or multiple elements without violating North American Electric Reliability Corporation (NERC) system performance criteria [4,5]. For a contingency resulting in the loss of a single element (Category B), the power system must remain stable with all equipment loaded to within its normal operating limits. In order to meet NERC system performance criteria, system operators periodically perform transient stability assessment to ensure that the power system can withstand a set of credible contingencies. Most modern energy management systems (EMS) house some sort of software package to carry out transient stability assessment task.

Three commonly used techniques to carry out transient stability assessment are as follows:

- Time-domain method
- Direct method
- Hybrid method

2.2.1 Time-domain Method

In the time-domain method, transient stability assessment is carried out using step-by-step numerical integrations of differential-algebraic equations representing the power system stability models [35]. Power system stability is assessed by monitoring the evolution of machine rotor angles and other system variables with respect to time in the post-fault period. For a stable system, machine rotor angles stabilize to a new equilibrium state. However, for an unstable condition, the machine rotor angles diverge. A simulation time period of three seconds is deemed appropriate for simplified modeling, and 15 seconds for full detailed modeling of the system and if multiswing instability is of concern [16].

The biggest advantage of this method is that it can incorporate any power system modeling and stability scenario. Complex power system models like HVDC, SVC, WACS, and FACTS devices can be easily modeled and simulated using time-domain method. In the past, this method was considered time-consuming and computationally expensive. With the rapid development of fast and cheap microprocessors, this limitation no longer holds true. Today power system software package using time-domain method finds its extensive application in modern energy management systems.

Although very powerful, this method does not provide information regarding the degree of stability (for stable system) and the degree of instability (for unstable system) of a power system. The stability margin is very useful for computing sensitivity analysis, which in turn can be used in preventive control. This information is valuable for both power system planning and operations.

2.2.2 Direct Method

The deficiencies of the time-domain method led to the development of an alternate approach to transient stability analysis known as direct method. Direct methods use

some form of energy function and assess transient stability by applying Lyapunov second criteria [36, 37]. There are three basic direct methods, with a number of variations on each method: (i) Lowest energy unstable equilibrium point (u.e.p.) method [38], (ii) Potential Energy Boundary Surface (PEBS) method [39], and (iii) Controlling u.e.p. method [40]. Direct methods can determine transient stability without the time-consuming numerical integration of a postfault power system. This method restricts the time-domain simulations solely to the fault period, avoiding all repetitive runs. This reduces simulation to a very small percentage of the overall computing effort of time-domain method. In addition to its computational speed, direct methods also provide sound stability margins, which in turn can provide useful information regarding preventive control and enhancement control actions for power system stability.

Despite the promising technique for computing stability margin, direct methods suffer from two main limitations [16]: (i) difficulty of constructing a suitable Lyapunov functions for a detailed multimachine power system, and (ii) difficulty of defining practical stability domain, that is suitable in terms of both computational efficiency and accuracy. Due to these limitations, direct methods have been considered impractical by many researchers.

Recent developments of the family of boundary of stability region controlling unstable equilibrium point (BCU) method have revived the controlling u.e.p. method [41, 42]. The BCU method can efficiently compute the controlling u.e.p. and now emerges as a practical tool for solving large-scale transient stability assessment problems. Extensive evaluations of the BCU-based controlling u.e.p. method on large-scale power systems such as a 12,000-bus power system have reported promising results [42]. The BCU method based transient stability assessment tool has been installed in several modern energy management systems in large utilities.

2.2.3 Hybrid Method

The hybrid method combines the strength of both the time-domain method and the direct method for evaluating transient stability. The use of time-domain simulations allows the hybrid method to consider any power-system modeling and stability scenario while providing essential information on system dynamics with respect to time. In this method, the actual system trajectory is first computed using time-domain simulation, then a transient energy margin is estimated and used as a stability index.

Two distinct types of hybrid method exist. The first type considers a Lyapunov function constructed for the multimachine power system and computed along the multimachine trajectory using step-by-step time-domain simulation results [43]. For this method, it is difficult to establish an appropriate stability limit. In the second type, one-machine equivalent is constructed from the multimachine system, and the stability margin is calculated using the equal-area criterion (EAC) [16]. The SIME method (for SIngle Machine Equivalent) belongs to this latter family. The use of EAC greatly simplifies the task of determining stability limit for the one-machine equivalent method.

The SIME method is used for transient stability analysis and computing stability margin in this dissertation.

2.3 Online Transient Stability Analysis

An important activity in power system planning and operation is the study of the impact a set of credible disturbances has on transient stability. Traditionally, transient stability analysis has been performed using offline calculations. In this process, detailed stability analysis is conducted for each credible contingency under a variety of operating conditions. The computations needed to assess the security are technically rigorous and require considerable effort. As a result, transient stability analysis has been historically conducted in an offline operation-planning environment

in which the stability of the near-term forecasted system conditions are exhaustively determined. The results of the offline studies are loaded into look-up tables and are accessed online by the operator.

In the new competitive environment, power systems can no longer be operated in a structured and conservative manner. The system loading conditions and parameters assumed at the planning stage may be quite different than in actual operation. In many power systems, it has become impossible to operate systems with an acceptable degree of security based on offline calculation of stability limits. This has been illustrated by the major system disturbances that have recently occurred in different systems around the world, highlighting the importance of being able to monitor and ensure system stability online.

Online power system stability analysis takes measurements of the actual system condition and performs security analysis in near real time, thereby reducing the uncertainty that exists in offline analysis using forecasted conditions. Transient stability analysis conducted in a near real time greatly enhances the operational decision making capability of an operator and significantly reduces the risk of cascading blackouts by evaluating limits based on real-time system conditions and topology.

There are several significant benefits and potential applications from the movement of transient stability analysis from the offline mode to the online operating environment. The first benefit is that a power system can be operated with lower operating margins if the transient stability analysis is based on the actual system configuration and actual operating conditions instead of assumed worst-case conditions, as is done in offline studies. This ability is especially significant since current environments have pushed power systems to operate with low reserve margins closer to their stability limits [42]. A second benefit is that the online analysis can be reduced to those contingencies relevant to the actual operating conditions; more accurate operating margins can be then determined and higher power transfer among different areas, or different

zones of power networks, can be realized [44].

A growing number of system operators is implementing online TSA in the energy management systems [24]. When a cycle of an online TSA is initiated, a list of credible contingencies, along with information from the state estimator and topological analysis, is applied to the online TSA program whose basic function is to identify unstable contingencies from the contingency list. Online TSA provides system operators with critical system stability information including (i) TSA of the current operating condition subject to a list of contingencies, and (ii) available transfer limits at key interfaces subject to transient stability constraints. A brief description of the online TSA tools implemented in large control centers and their capabilities are described below:

- The transient stability control (TCS) system is the world's first real-time stability control system developed for application to the trunk power system of Chubu Electric Power Co. (CEPCO) [45, 46]. Installed in 1995, the TSC system performed detailed stability calculations based on on-line information telemetered from the actual network, and it periodically evaluated the stability of the power system against contingencies with a high degree of accuracy. The TSC system evaluates stability for about 100 contingencies within 5 minutes.

- The Guangxi Electric Power Company (GXEP) online system, installed in 2003, consists of two main functions: transient security assessment using the TSAT program (jointly developed by Powertech Labs and NARI) and voltage security assessment using the VSAT program (developed by Powertech Labs) [47]. The online GXEP system model contains 1876 buses and 248 generators (including some external equivalents). At the normal condition, 4 Dell 2650 servers are designated for DSA computations (3 for transient stability and 1 for voltage stability). The DSA system is able to complete the entire assessment cycle for 80-90 contingencies within 5 minutes.

- An on-line Transient Stability Analysis & Control (TSA&C) system, designed by Powertech Labs, was implemented at PJM system control center in 2006 [48]. The PJM EMS model consists of 13,500 buses and 2,500 generators. With the planned model expansion, the system size can grow to 25,000 buses and 3,000 generators in the near future. The TSA&C system can process 3,000 contingencies and calculate 16 interface stability limits within 15 minutes assessment cycle.

- TEPCO-BCU was selected as a fast real-time transient stability screening tool for PJM's TSA system in 2010 [44]. The TEPCO-BCU tool was implemented on the system size of 14,000 buses, a total number of 5,293,691 contingencies, and the assessment cycle of 15 minutes. The assessment results from TEPCO-BCU software include the ranking of each contingency in terms of energy margins or estimated CCTs for each contingency, the stability status, the computation time consumed, the estimated CCT, and the energy margin.

2.4 Optimal Power Flow

An optimal power flow (OPF) is a steady-state optimization tool for power system operators, both in planning and operation stages. It is extensively used in power system planning and operation for security, reliability, and economic efficiency. The goal of an OPF algorithm is to find the operating point that optimizes the system objective functions such as total generation cost, network loss, reactive power reserve, etc. while satisfying different constraints such as power balance, line flows, voltage limits, and capacity limits [49]. In contrast to the load flow problem, where active power generations are specified, in an OPF, the optimal generations are sought to minimize the operating cost of the system. However, such a solution is valid only for steady-state operation. An optimal power flow being a steady-state operational tool is incapable of incorporating dynamic security constraints and may result in unstable

dynamics.

Commonly used objective functions in OPF problems include minimum generation cost, minimum active power losses, minimum deviation from a specific operation condition, minimum control shift to alleviate violations, and minimum emissions. An optimal solution of the objective function is determined by adjusting the control variables. A partial list of such variables would include: generator real and reactive power, bus voltage, transformer tap position, switched capacitor settings, reactive injection for a static VAR compensator, and stability margin [17].

Amongst a number of different operational objectives that an OPF problem may be formulated, a widely considered objective is to minimize the fuel cost subject to network and generator operation constraints. Many mathematical programming techniques such as Newton method, gradient method, nonlinear programming (NLP), quadratic programming (QP), linear programming (LP), and modified interior point methods (MIP) have been applied to solve the OPF problem successfully [50]. However, these classical optimization methods are limited in handling algebraic functions and unable to consider the dynamic characteristic such as the transient stability performance in the optimization.

Conventionally, only static physical and operating limits are considered in the OPF constraint set [17]. In recent years, to protect the system against large severe disturbances, there has been increasing interest and need to take into account the dynamic security constraints in the OPF computations. Correspondingly, there are small-signal stability- [51], voltage stability- [52], and transient stability- [7, 8] constrained OPF models proposed to fulfill the dynamic security requirements in optimizing a power system operating state. The extension to the procedure to add dynamic security constraints allows the OPF to meet pre-contingency limits as well as post-contingency limits.

2.5 Transient Stability-Constrained Optimal Power Flow

Deregulation of the power industry has forced the modern power systems to operate within tighter margins and with less redundancy. As fewer new transmission lines are being built because of high capital costs, new regulatory requirements for transmission open access, and environmental concern, the existing transmission networks are heavily loaded. These factors have resulted in stability-limited power networks making transient stability a primary concern to system operators [1]. Hence, system operators are faced with the challenge of operating the power system in both an economical and secure manner against credible contingencies.

Traditionally, an OPF is used to determine the most economic operating condition of the power system. To reconcile between economics and security, transient stability constraints are added to the OPF problem; this is referred to as Transient Stability-Constrained OPF (TSC-OPF). TSC-OPF is a nonlinear optimization problem that extends the OPF to include transient stability constraints. The solution methods for the TSC-OPF can be broadly classified into three different classes: dynamic optimization [7], SIME method [6], and computational intelligence [12]. These solution methods exhibit two distinct characteristics. The first in terms of how they include stability constraints in the OPF algorithm, and the second in terms of the method they use for computing the stability margin.

In [7–9], the generator differential equations are converted to nonlinear algebraic equations for all time steps, and are then included as equality constraints in the OPF problem. This approach increases the TSC-OPF problem dimension by several orders of magnitude with respect to conventional OPF. Thus, its solution generally requires large memory and computational capabilities. In [6,10,11,14,15,53], Transient Stability Assessment (TSA) is carried out outside the OPF algorithm, resulting in a reduced number of stability constraints to be incorporated in the OPF formulation. Hence, OPF problem complexity and dimension are significantly lessened. Moreover, this

type of approach is compatible with any power system dynamic model. In regards to the method used for stability margin determination, various TSA techniques have been proposed in the literature. The most common method is to run time-domain simulation and access transient stability in terms of machine rotor angles' deviation from a set limit [7, 53]. Due to the robustness in convergence, low computational time, and capability to treat inequality constraints, direct methods, e.g. Potential Energy Boundary Surface (PEBS) [8, 54, 55], and Boundary Controlling Unstable Equilibrium Point (BCU) [56], have also been used. The main limitation of direct methods is that their success depends upon the availability of a suitable Lyapunov function. A hybrid TSA method, which combines time-domain simulation and direct methods, is implemented in [6, 9, 14, 15]. In hybrid TSA method, one-machine equivalent is constructed from the multimachine system, and the stability margin is calculated using the equal-area criterion (EAC). This method seems to be quite computationally efficient and promising for online use. However, one-machine equivalent is only an approximation of the multi-machine system dynamics. Recent work has shown non-monotonic variation of stability margin with respect to critical parameters and other complicated phenomenon like isolated stability domain (ISD) under multi-swing unstable conditions [57]. This thesis uses the hybrid method proposed in [16]. The TSC-OPF problem has also been solved using computational intelligence solution techniques (e.g. differential evolution and evolutionary algorithms [12, 13]).

In this dissertation, an improved, yet relatively simple, method for solving TSC-OPF problem is proposed. Using SIngle Machine Equivalent (SIME) method, multi-machine power system model is reduced to one-machine infinite bus (OMIB) equivalent to compute stability margin. The quasi-linear behavior of OMIB stability margin and critical machine(s) active power is explored to formulate transient stability constraint. Since the stability constraint is based on the OMIB equivalent, the dynamic and stability constraints of multi-machine system is reduced to a single, time inde-

pendent constraint. A single stability constraint is formulated as a limit on the sum of critical machines active power, and not on the OMIB rotor angle. This avoids the addition of generator stator algebraic equations in the the OPF problem and enables to use conventional OPF formulation. In [10, 11] SIME based compensation schemes have been proposed to enhance transient stability by shifting active power from critical machines to noncritical machines. Unlike compensation schemes, the proposed method shifts the active power from the critical machines based on generator costs using an OPF algorithm. Also, the transient stability limit is based on stability margin, and not on heuristically set limit on OMIB rotor angle. As a result, the proposed TSC-OPF solution is more economical and transparent. The proposed technique enables the use of fast and robust commercial OPF tool and time-domain simulation software for solving large scale TSC-OPF problem. This makes the proposed method suitable for real-time application.

2.6 Remedial Action Scheme

Remedial Action Schemes (RAS) are emergency transient stability controls designed to sense abnormal conditions and subsequently take pre-determined corrective actions to prevent instability. RAS supplement ordinary protection and control devices (fault protection, reclosing, AVR, PSS, governors, AGC, etc) to prevent violations of the NERC Reliability Criteria for Category B and more severe events. RAS are designed to address specific problems, e.g. to increase power transfer, to provide reactive support, to mitigate overfrequency or underfrequency issues, to address generator instability, to limit line and other equipment thermal overloads, etc. Possible remedial actions include generator tripping, turbine fast valving, braking resistor insertion, load shedding, capacitor and reactor switching, static VAR control, system separation, etc [19]. A RAS solution will typically be considered when other operating and construction options are substantially more expensive or cannot be implemented in time to avoid problems identified by the initial studies. These schemes

have become more common because they are less costly and quicker to permit, design, and build than other alternatives such as the construction of new transmission lines and power plants. Commonly known as either RAS or as Special/System Protection Schemes (SPS), these emergency control approaches have been extensively adopted by utilities [18, 58].

NERC defines RAS as, *"An automatic protection system designed to detect abnormal or predetermined system conditions, and take corrective actions other than and/or in addition to the isolation of faulted components to maintain system reliability. Such action may include changes in demand, generation (MW and Mvar), or system configuration to maintain system stability, acceptable voltage, or power flows."* [59]. The number of RAS implemented in NERC regions is listed in Table 2.1 As of 2011, a total of 462 RAS have been implemented in NERC regions [59].

System integrity protection schemes (SIPS) encompasses special protection system (SPS), remedial action schemes (RAS), as well as other system integrity schemes, such as underfrequency (UF), undervoltage (UV), out-of-step (OOS), etc [18]. The SIPS are installed to protect the integrity of the power system or strategic portions thereof, as opposed to conventional protection systems that are dedicated to a specific power system element. These schemes provide reasonable countermeasures to slow and/or stop cascading outages caused by extreme contingencies.

Table 2.1: Overview of RAS by NERC region

Region	**Total Number**
FRCC	20
MRO	36
NPCC	117
RFC	47
SERC	20
SPP	6
TRE	24
WECC	192

Table 2.2 shows a summary of overall SIPS purpose classification into five major categories as described in the survey [18]. Out of 958 total entries, 22% of the entries are applications to address "normal" system conditions. This fact demonstrates that SIPS are no longer applied solely for system security purposes.

Table 2.2: SIPS purpose classification

SIPS Purpose	**Distribution**
Essential	22%
Increased security	36%
Increased power flow capability	19%
Normal	22%
Important	8%

Depending upon the input variables, RAS are classified into one of four types: event-based, parameter-based, response-based, or a combination [20]. One growing trend is to combine event-based schemes to detect contingencies with parameter-based schemes to determine power flows [21–23]. No matter the approach, RAS

requires a fast telecommunications system and WAMS to monitor system parameters (i.e. line flows, node voltages, system configuration, contingencies, etc.). Most of the RAS control actions are designed using extensive offline transient simulations by considering numerous combinations of contingencies, power-system configurations, and load-flow scenarios.

Among various RAS types, generation shedding is the most effective and widely used emergency control means for maintaining system stability [18]. The existing generation-shedding schemes are focused towards determining the minimum amount of generation to shed [25, 60] to stabilize the system. The world's first real-time transient stability control (TSC) system applied on a large power system is described in [45, 46]. The TSC system selects the optimum generator to shed based on online stability calculation. The complexity and challenges associated with implementing generation shedding RAS in real world power systems are described in [21–23]. Various hybrid methods for generation tripping are discussed in [61, 62]. Although very effective, these schemes do not consider the generation-shedding cost when selecting remedial action. In today's deregulated power industry, generation-shedding scheme using both operation costs and technical constraints can be an attractive alternative.

CHAPTER 3: PROPOSED TRANSIENT STABILITY-CONSTRAINED OPF

3.1 Overview

This chapter describes the proposed Transient Stability-Constrained Optimal Power Flow (TSC-OPF) solution technique for preventive control. An improved, yet relatively simple, technique for solving TSC-OPF problem is proposed. Using the SIngle Machine Equivalent (SIME) method, a single, time-independent transient stability constraint is formulated using the critical machines' power at the initial time step. The TSC-OPF problem is then solved by adding the stability constraint to a conventional OPF formulation.

This chapter is organized as follows. Section 3.2 presents the brief overview of the proposed TSC-OPF technique. Section 3.3 reviews the SIME method and explores the quasi-linear behavior of the OMIB stability margin and critical machines power. The mathematical formulation of the proposed TSC-OPF solution technique is described in Section 3.4.

3.2 Proposed TSC-OPF

In this thesis, an improved, yet relatively simple, method for solving TSC-OPF problem is proposed. Using SIngle Machine Equivalent (SIME) technique, the multi-machine power system model is reduced to a One-Machine Infinite Bus (OMIB) equivalent to compute stability margins. The quasi-linear behavior of the OMIB stability margin and critical machine(s) active power is explored to formulate the transient stability constraint. Since the stability constraint is based on the OMIB equivalent, the multi-machine system's dynamic and stability constraints are reduced to a single, time independent constraint. In [15], a single transient stability constraint is pro-

posed based on the OMIB rotor angle. Although very powerful, the proposed method requires addition of generator stator algebraic equations and higher generator reactive power limits ($Q_{Gi\ max}$ and $Q_{Gi\ min}$), to incorporate for reactive power absorb by generator synchronous reactance, in the OPF formulation. In the proposed method, a single stability constraint is formulated as a limit on the sum of critical machines' active power, as opposed to on the OMIB rotor angle, avoiding the addition of the generator stator algebraic equations in the OPF formulation and enabling the use of conventional OPF. This allow to implement actual generator reactive power limits in the OPF algorithm. The proposed method shifts critical machines active power based on generator costs using an OPF algorithm. Moreover, the transient stability limit is based on stability margin, and not on a heuristically set limit on OMIB rotor angle. As a result, the proposed TSC-OPF solution is more economical and transparent. The proposed technique enables the use of fast and robust commercial OPF tool and time-domain simulation software for solving large scale TSC-OPF problem, which makes the proposed method also suitable for real-time application.

3.3 SIME for Online Transient Stability Analysis

SIME is a hybrid transient stability analysis method that uses the generalized One-Machine Infinite Bus (OMIB) system [16]. It combines the strength of both time-domain and direct transient stability methods. The use of time-domain simulations allows SIME to consider any power-system modeling and stability scenario while providing essential information on system dynamics with respect to time. Detailed generator, exciter, and PSS model, FACTS devices, balanced and unbalanced faults, and various switching actions can be considered for stability analysis using SIME. Using a time-domain simulation, SIME transforms the dynamics of the multi-machine power system into a suitable OMIB system. Due to its robustness, SIME method is implemented in DSATools Software by Powertech Labs Inc., a leading commercial software for online dynamic security analysis, for fast and accurate calculation of

transient stability index [63].

For an unstable system, SIME separates the generators into two categories, namely Critical Machines (CMs) and Noncritical Machines (NMs). To identify critical machines, SIME observes the post-fault swing curves of the system machines. At each time step, SIME sorts the machines according to their rotor angles, identifies the very first larger rotor angular deviations between adjacent machines, and considers as candidate CMs those which are above each one of these larger distances [16]. In this context, machines deemed critical are those that can become out-of-step during a severe disturbance.

Once machines are grouped into critical and non-critical machines, SIME transforms two groups of machines into a suitable OMIB equivalent, defined by its angle, speed, mechanical power, electrical power, and inertia coefficient. Using equal-area criteria (EAC) on the OMIB system, SIME provides accurate and fast transient stability analysis of the multimachine power system. Besides stability margin, SIME also provides crucial information like identification of critical machines, time to instability, and time to first-swing stability. This information enables SIME to carryout both preventive and emergency types of control. These salient features make SIME a suitable tool for online transient stability analysis. The SIME method has also been implemented in DSATools Software by Powertech Labs Inc., a leading commercial software for online dynamic security analysis, for fast and accurate calculation of transient stability index [63].

3.3.1 SIME Mathematical Formulation

A multimachine power system can be represented by a set of differential-algebraic equations in time-domain method. For transient stability studies, machines are modeled using a two-axis machine model with no saturation and both the stator and the network transients are neglected [35]. Also linear damping is assumed and the subtransient reactances and saturation for machines are neglected. Differential-algebraic

model for a multimachine power system with n machines and m bus system takes the following form.

A. Differential Equations

$$\tau'_{d0i}\frac{dE'_{qi}}{dt} = -E'_{qi} - (X_{di} - X'_{di})I_{di} + E_{fdi} \quad i = 1, 2, ..., n \tag{3.1}$$

$$\tau'_{q0i}\frac{dE'_{di}}{dt} = -E'_{di} + (X_{qi} - X'_{qi})I_{qi} \quad i = 1, 2, ..., n \tag{3.2}$$

$$\frac{d\delta_i}{dt} = \omega_i - \omega_s \quad i = 1, 2, ..., n \tag{3.3}$$

$$\begin{gathered}\frac{2H_i}{\omega_s}\frac{d\omega_i}{dt} + D_i(\omega_i - \omega_s) = \tau_{Mi} - E'_{di}I_{di} \\ -E'_{qi}I_{qi} - (X'_{qi} - X'_{di})I_{di}I_{qi} \quad i = 1, 2, ..., n\end{gathered} \tag{3.4}$$

B. Algebraic Equations

The algebraic equations consist of the stator and network algebraic equations.

B.1 Stator Algebraic Equations

$$\begin{gathered}V_i e^{j\theta_i} + (R_{si} + jX'_{di})(I_{di} + jI_{qi})e^{j(\delta_i - \frac{\pi}{2})} \\ -[E'_{di} + (X'_{qi} - X'_{di})I_{qi} + jE'_{qi}]e^{j(\delta_i - \frac{\pi}{2})} = 0 \quad i = 1, 2, ..., n\end{gathered} \tag{3.5}$$

B.2 Network Algebraic Equations

B.2.1 Generator Buses

$$\begin{gathered}V_i e^{j\theta_i}(I_{di} - jI_{qi})e^{-j(\delta_i - \frac{\pi}{2})} + P_{Li}(V_i) + jQ_{Li}(V_i) = \\ \sum_{k=1}^{n} V_i V_k Y_{ik} e^{j(\theta_i - \theta_k - \alpha_{ik})} \quad i = 1, 2, ..., n\end{gathered} \tag{3.6}$$

B.2.2 Load Buses

$$P_{Li}(V_i) + jQ_{Li}(V_i) = \sum_{k=1}^{n} V_i V_k Y_{ik} e^{j(\theta_i - \theta_k - \alpha_{ik})} \quad i = n+1, ..., m \tag{3.7}$$

The complex electrical power injected by machine i is given by,

$$P_{ei} + jQ_{ei} = V_i e^{j\theta_i}(I_{di} - jI_{qi})e^{-j(\delta_i - \frac{\pi}{2})} \tag{3.8}$$

Equation (3.4) can be rearranged to develop swing equations for the i-th generator in an n machine power system, which is

$$M_i \frac{d^2\delta_i}{dt^2} + D_i \frac{d\delta_i}{dt} = P_{mi} - P_{ei} \quad i = 1, 2, ..., n \tag{3.9}$$

The dynamics of the multimachine power system with n machines can be studied by solving (3.1)-(3.9). Next, the rotor angles are transformed into the Center of Inertia (COI) reference by subtracting angle of center of inertia. In COI reference frame, we use the terms angle of center of inertia (δ_0), center of speed (ω_0), and total moment of inertia (M_T). These quantities are defined as

$$\delta_0 = \frac{1}{M_T} \sum_{i=1}^{n} M_i \delta_i \tag{3.10}$$

$$\omega_0 = \frac{1}{M_T} \sum_{i=1}^{n} M_i \omega_i \tag{3.11}$$

$$M_T = \sum_{i=1}^{n} M_i \tag{3.12}$$

Machine rotor angles for an unstable and a stable system in COI reference frame are shown in Fig. 3.1. The rotor angles diverge for an unstable system whereas they converge for a stable system.

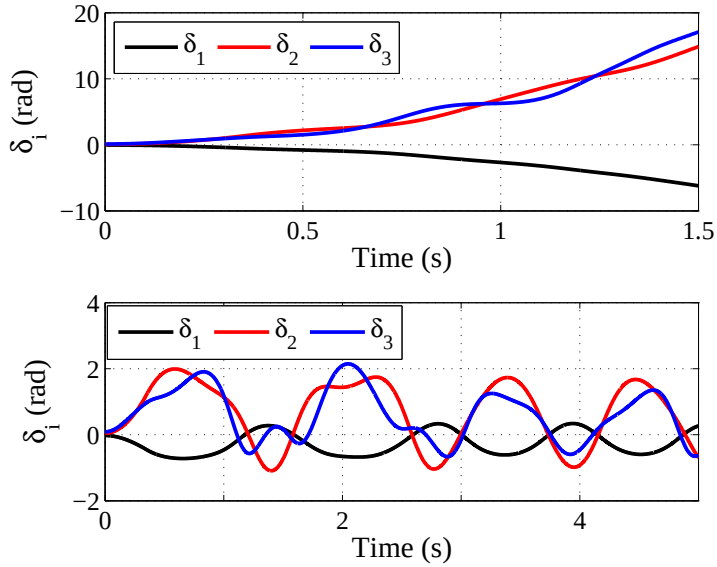

Figure 3.1: Machine rotor angles for: (top) an unstable and (bottom) a stable system.

3.3.1.1 Identification of Critical Machines

In order to identify critical machine(s) for a given contingency, SIME runs the time-domain simulation program for the fault-on and the post-fault configuration. As soon as the system enters the post-fault configuration, SIME starts constructing candidate OMIB equivalents at each time step. At each time step of the post-fault simulation, SIME sorts the machines according to their rotor angles, and calculates the maximum difference (distance) between two adjacent rotor angles, say δ_i - δ_j. The machines representing these two rotor angles represent the critical and non-critical machine respectively. The machines whose rotor angles are closer to δ_i are considered as critical machines and the machines whose rotor angles are closer to δ_j are considered as non-critical machines. Next, candidate OMIB equivalents are constructed using the critical and non-critical machine group. The first OMIB equivalent that reaches instability condition defined by EAC is selected as the critical OMIB equivalent.

3.3.1.2 OMIB Time-Varying Parameters

The transformation of total machines into two groups of critical and non-critical machines allows SIME to compute time-varying OMIB parameters like δ, ω, M, P_m, and P_e. These parameters are updated at every time step of the time-domain program and represent the overall dynamics of the multimachine power system. The machines are separated into critical and non-critical machines and aggregated by determining the Center of Angle (COA) for each group. For a system with C critical machines and N non-critical machines, these aggregate angles are given by:

$$\delta_C(t) = \frac{1}{M_C} \sum_{k \in C} M_k \delta_k(t) \tag{3.13}$$

$$\delta_N(t) = \frac{1}{M_N} \sum_{j \in N} M_j \delta_j(t) \tag{3.14}$$

where,

$$M_C = \sum_{k \in C} M_k \qquad M_N = \sum_{j \in N} M_j$$

Similarly, the center of speed for each group is given by:

$$\omega_C(t) = \frac{1}{M_C} \sum_{k \in C} M_k \omega_k(t) \tag{3.15}$$

$$\omega_N(t) = \frac{1}{M_N} \sum_{j \in N} M_j \omega_j(t) \tag{3.16}$$

The corresponding OMIB rotor angle and rotor speed are computed as follows:

$$\delta(t) = \delta_C(t) - \delta_N(t) \tag{3.17}$$

$$\omega(t) = \omega_C(t) - \omega_N(t) \tag{3.18}$$

The equivalent OMIB mechanical and electrical power are expressed as follows:

$$P_m(t) = M\left(\frac{1}{M_C}\sum_{k\in C} P_{mk}(t) - \frac{1}{M_N}\sum_{j\in N} P_{mj}(t)\right) \tag{3.19}$$

$$P_e(t) = M\left(\frac{1}{M_C}\sum_{k\in C} P_{ek}(t) - \frac{1}{M_N}\sum_{j\in N} P_{ej}(t)\right) \tag{3.20}$$

The critical and non-critical machine electrical powers are defined as follows:

$$P_{eC}(t) = \frac{M}{M_C}\sum_{k\in C} P_{ek}(t) \tag{3.21}$$

$$P_{eN}(t) = \frac{M}{M_N}\sum_{j\in N} P_{ej}(t) \tag{3.22}$$

and the equivalent OMIB inertia coefficient M is calculated as follows:

$$M = \frac{M_C M_N}{M_C + M_N}$$

Finally, the OMIB accelerating power is expressed as follows:

$$P_a(t) = P_m(t) - P_e(t) \tag{3.23}$$

3.3.1.3 Stability Margin

The stability margin provides a measure of degree of criticality (or instability) of the multimachine power system against contingencies. First, SIME plots the OMIB P–δ curves using the OMIB parameters computed in (3.13)-(3.23). Using the equal-area criterion, the stability margin η is computed as follows:

$$\eta = A_{dec} - A_{acc} \tag{3.24}$$

where A_{acc} is the accelerating area and A_{dec} is the decelerating area in the P–δ plane. The accelerating area represents the kinetic energy stored during the fault-on period, while the decelerating area represents the maximum potential energy that the power system can dissipate in the post fault configuration.

Fig. 3.2 and Fig. 3.3 show the transformation of machine rotor angles to OMIB parameters for a stable and an unstable contingency, respectively. Notice the aggregation of machines as critical and non-critical during both the stable and the unstable condition. For a stable contingency, the machine rotor angles are within bounds and $A_{dec} > A_{acc}$. On the other hand, the machine rotor angles diverge and $A_{dec} < A_{acc}$ for an unstable contingency.

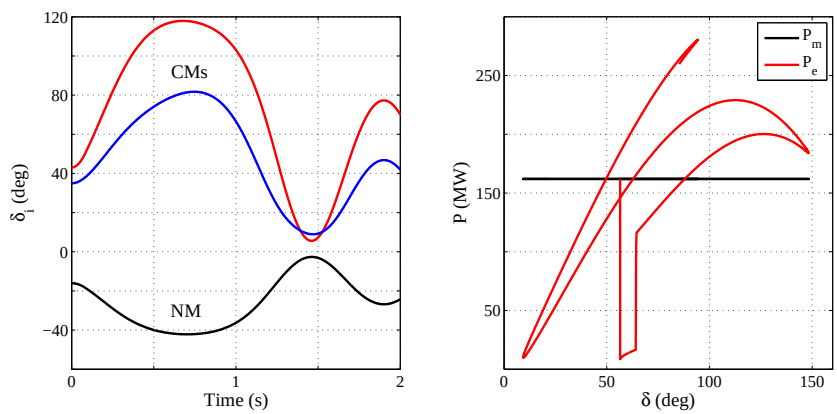

Figure 3.2: Rotor angles and OMIB P–δ plot for a stable contingency.

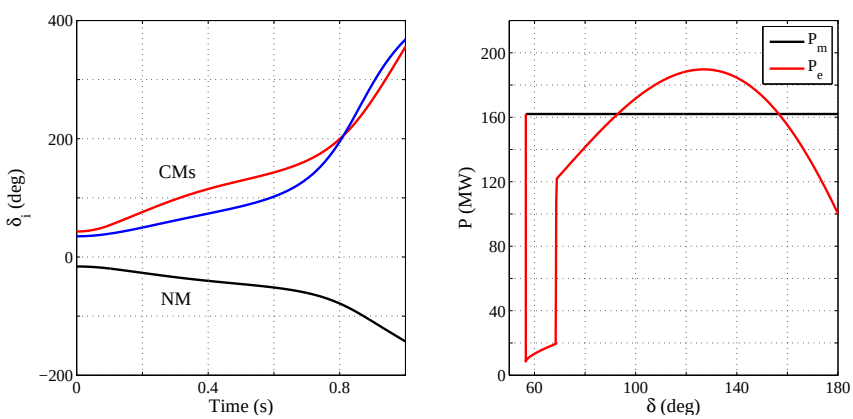

Figure 3.3: Rotor angles and OMIB P–δ plot for an unstable contingency.

A. Stability margin - stable contingency

The OMIB P - δ plot with A_{acc} and A_{dec} area is shown in Fig. 3.4. For the stable system, P_e returns back at the return angle of δ_r without crossing P_m. The OMIB P_e and P_e curves are extrapolated from the return angle (δ_r) until they intersect at the unstable angle (δ_u). The stable stability margin (η_{st}) is calculated by integrating the area between (δ_r) and (δ_u).

$$\eta_{st} = -\int_{\delta_r}^{\delta_u} P_a d\delta \tag{3.25}$$

$$\eta_{st} = \int_{\delta_r}^{\delta_u} \mid P_m - P_e \mid d\delta \tag{3.26}$$

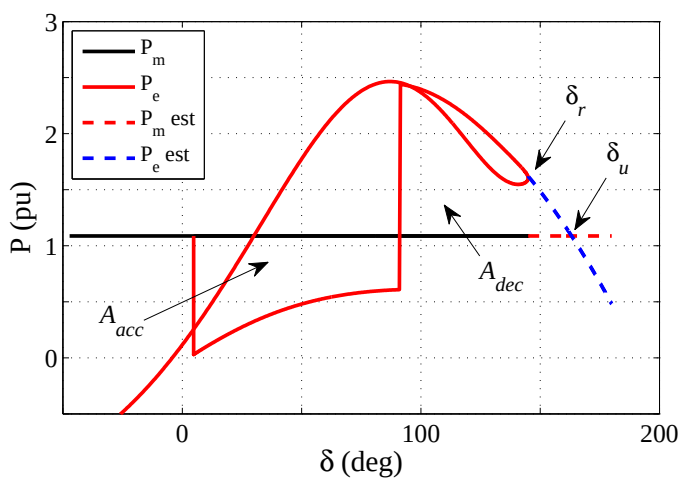

Figure 3.4: OMIB P–δ plot for a stable contingency.

B. Stability margin - unstable contingency

For an unstable system, the unstable stability margin (η_u) is computed using M and the OMIB rotor speed (ω) at time to instability (t_u).

$$\eta_u = -\frac{1}{2}M(\omega(t_u)^2) \tag{3.27}$$

Fig. 3.5 shows OMIB P–δ, δ, and ω plots for an unstable contingency. At first,

using OMIB P–δ plot, the unstable angle δ_u (intersection between P_e and P_m) is determined. Next, the time to instability (t_u) is calculated at δ_u using OMIB δ plot. Once t_u is known, the value of OMIB rotor speed (ω) is extracted from the OMIB ω plot. Finally, using (3.27), the unstable stability margin is calculated.

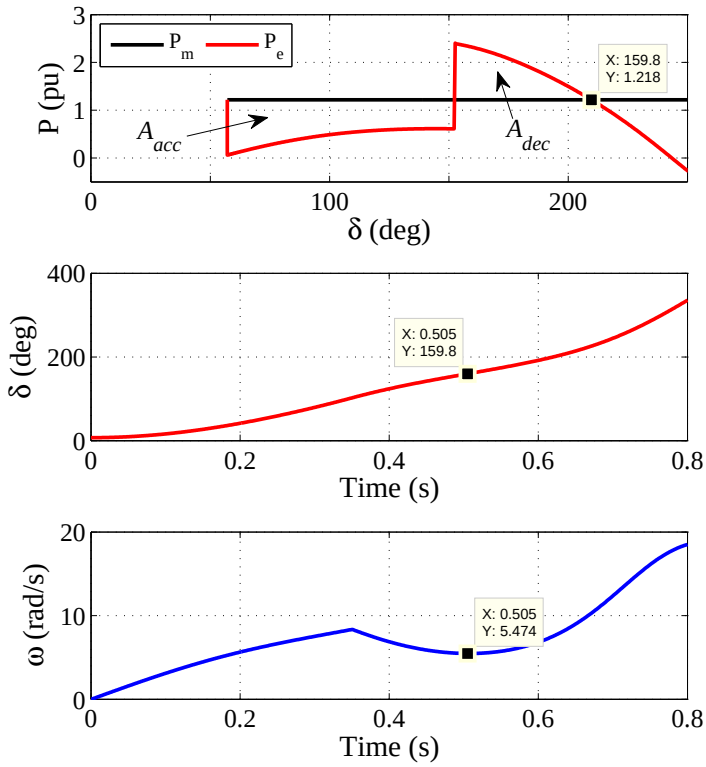

Figure 3.5: (a) OMIB P–δ, (b) δ, and (c) ω plots for an unstable contingency.

3.3.2 SIME Quasi-Linear Behavior

Among various salient features provided by the SIME method, the quasi-linear relationship between OMIB stability margin (η) and parameters like fault clearing time (t_e), active power (P_m and P_e), and OMIB rotor angle (δ), make SIME suitable for sensitivity analysis. Simulations carried out on a large variety of power systems, with number of machines varying between 3 and over 600, have corroborated these quasi-linear relationships [16]. The quasi-linear behavior is true for negative and

small positive stability margins. The advantage of this property is that the stability margin can be estimated within the quasi-linear region by using linear extrapolation (or interpolation) methods. The linear extrapolation of the OMIB stability margin is valid as long as successive simulations are not too far away from each other, and the set of critical machines does not change.

Fig. 3.6 shows the quasi-linear relationship between OMIB stability margin and OMIB parameters for a contingency in the IEEE 9-bus system. Similarly, Fig. 3.7 shows the quasi-linear relationship for the IEEE 39-bus system. OMIB parameters (P_e, P_{eC}, and δ) are computed at the initial simulation time, i.e. t=0s, and the stability margin is computed using the SIME method. The successive data points are calculated by decreasing the critical machines active power by 1.5% from the previous value. The distribution of active power among both critical and noncritical machines is carried out using the proposed TSC-OPF technique described in Section 3.4. The quasi-linear relationships exhibited by the OMIB electrical power (P_e), critical machines electrical power (P_{eC}), and rotor angle (δ) with respect to the stability margin (η) have similar slope. The linear extrapolation of any quasi-linear characteristics can be used to stabilize an unstable system. In [14], the quasi-linear relationship between the OMIB stability margin and rotor angle at the initial time-step is used to solve TSC-OPF problem. This thesis uses the quasi-linear relationship between OMIB stability margin and critical machines active power at the initial timestep.

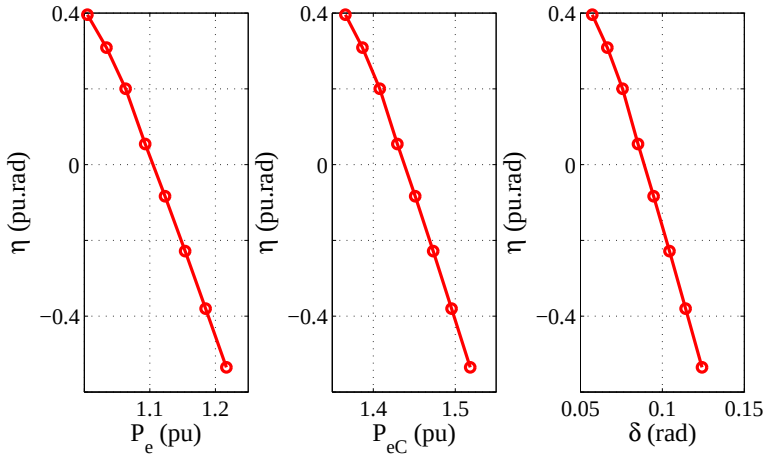

Figure 3.6: Quasi-linear relationship exhibited by a contingency in the IEEE 9-bus system. (a) Stability margin (η) vs electrical power (P_e), (b) Stability margin (η) vs critical machines electrical power (P_{eC}), (c) Stability margin (η) vs rotor angle (δ).

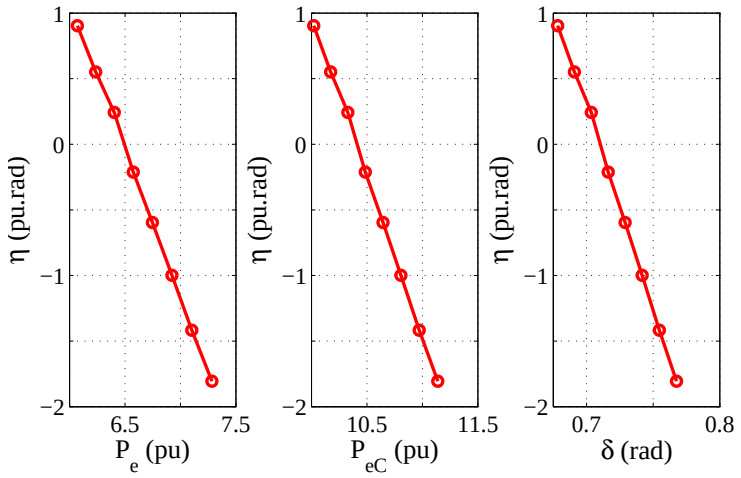

Figure 3.7: Quasi-linear relationship exhibited by a contingency in the IEEE 39-bus system. (a) Stability margin (η) vs electrical power (P_e), (b) Stability margin (η) vs critical machines electrical power (P_{eC}), (c) Stability margin (η) vs rotor angle (δ).

Fig. 3.8 shows the stability margin calculated using the SIME method and estimated using linear-extrapolation for the system described in Fig. 3.6 and Fig. 3.7 respectively. The two most unstable data points (two large negative stability margins) are used to estimate the stability margins for the remaining critical machines active power (P_{eC}) values. The estimated value of stability margin (η^k) for k^{th} data

point is calculated using (3.28).

$$\eta^k = \left(\frac{\eta^{k-1} - \eta^{k-2}}{P_{eC}^{k-1} - P_{eC}^{k-2}} \right) (P_{eC}^k - P_{eC}^{k-1}) + \eta^{k-1} \tag{3.28}$$

Note, the estimated stability margins are very close to the values calculated using the SIME method in the unstable region. As the system transitions from the unstable to the stable region, the difference between the two slowly increases. The quasi-linear relationship of stability margin and critical machines power provides a systematic approach to solve the TSC-OPF problem.

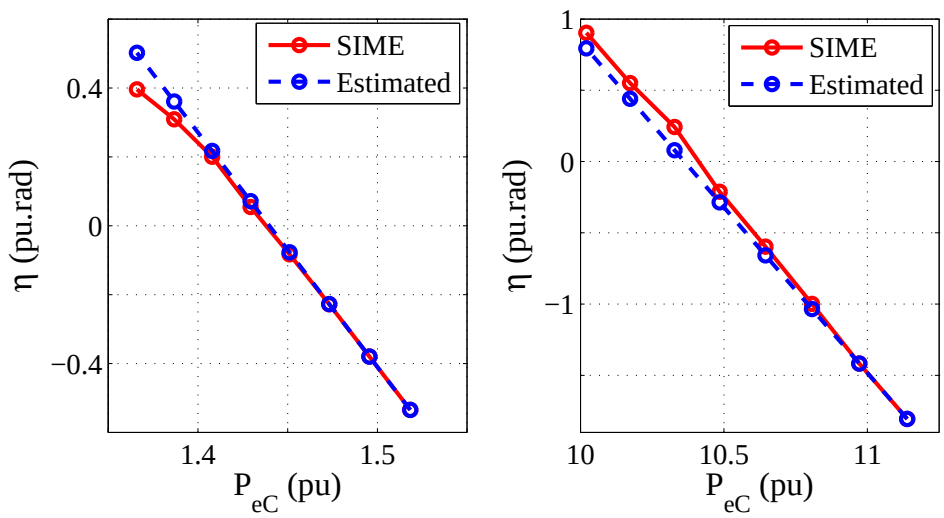

Figure 3.8: Stability margin (η) calculated using SIME method and estimated using linear-extrapolation. (a) For IEEE 9-bus system, (b) For IEEE 39-bus system.

3.4 Formulation of TSC-OPF Problem

A TSC-OPF problem is formulated by combining transient stability constraints in a conventional OPF problem. In the proposed TSC-OPF method, the transient stability constraint is expressed in terms of limit on the sum of critical machines' active power. Using the quasi-linear relationship between η and P_{eC}, the value of sum of critical machines' active power is updated at each OPF iteration, until a stable and economical condition is reached.

The formulation of the TSC-OPF problem using a conventional OPF and objective functions are described below.

3.4.1 Conventional OPF

An OPF is a steady-state optimization tool for power system operators, both in planning and operation stages. The goal of an OPF algorithm is to find the optimal operation point that optimizes the system objective functions such as total generation cost, network loss, reactive power reserve, etc while satisfying different constraints such as power balance, line flows, voltage limits, and capacity limits [49].

For a power system with n buses, a conventional OPF problem for minimizing an objective function can be formulated as follows:

$$\text{Min} \quad f(\cdot) \tag{3.29}$$

subject to power flow equality constraints,

$$P_{Gi} - P_{Di} - V_i \sum_{j=1}^{N} V_j (G_{ij} cos\theta_{ij} + B_{ij} sin\theta_{ij}) = 0 \tag{3.30}$$

$$Q_{Gi} - Q_{Di} - V_i \sum_{j=1}^{N} V_j (G_{ij} sin\theta_{ij} - B_{ij} cos\theta_{ij}) = 0 \tag{3.31}$$

and inequality constraints in the form of technical limits,

$$P_{Gi\,min} \leq P_{Gi} \leq P_{Gi\,max} \tag{3.32}$$

$$Q_{Gi\,min} \leq Q_{Gi} \leq Q_{Gi\,max} \tag{3.33}$$

$$V_{i\,min} \leq V_i \leq V_{i\,max} \tag{3.34}$$

$$S_i \leq S_{i\,max} \tag{3.35}$$

where,

P_{Gi}/Q_{Gi} :	real/reactive power output of generator i
P_{Di}/Q_{Di} :	real/reactive power demand of load i
V_i :	voltage magnitude at bus i
S_i :	apparent power flow in line i
$P_{Gi\,max}/P_{Gi\,min}$:	upper/lower active power limit of generator i
$Q_{Gi\,max}/Q_{Gi\,min}$:	upper/lower reactive power limit of generator i
$V_{i\,max}/V_{i\,min}$:	upper/lower voltage limit at bus i
$S_{i\,max}$:	upper apparent power flow limit in line i

3.4.1.1 Objective Functions

The OPF problem is formulated as a minimization or maximization of a certain objective function subjected to a variety of equality and inequality constraints. These objective functions vary from generator fuel cost, active and/or reactive power transmission loss, reactive power reserve margin, security margin index, and emission, environmental, index. Two types of objective functions are considered in this thesis for the TSC-OPF problem.

When TSC-OPF is used as a dispatching tool, total generator fuel cost is selected as an objective function.

$$f(P_{Gi}) = \sum_{i=1}^{NG}(a_i P_{Gi}^2 + b_i P_{Gi} + c_i) \tag{3.36}$$

where P_{Gi} is the active power output of generator i and a_i, b_i, and c_i represents its fuel cost coefficients.

When TSC-OPF is used as a redispatching tool, the objective function represents the total cost associated with generator power adjustments [64].

$$f(\Delta P_{Gi}^{\text{up}}, \Delta P_{Gi}^{\text{down}}) = \sum_{i=1}^{NG}(r_{Gi}^{\text{up}} \Delta P_{Gi}^{\text{up}} + r_{Gi}^{\text{down}} \Delta P_{Gi}^{\text{down}}) \tag{3.37}$$

where $\Delta P_{Gi}^{\text{up}}$ and $\Delta P_{Gi}^{\text{down}}$ are the power adjustments of generator i and r_{Gi}^{up} and r_{Gi}^{down} are the prices offered by the generator to increase or decrease its power dispatch for transient stability requirement, respectively. The active power generation P_{Gi} for this TSC-OPF case is defined as follows:

$$P_{Gi} = P_{Gi}^{0} + \Delta P_{Gi}^{\text{up}} - \Delta P_{Gi}^{\text{down}} \tag{3.38}$$

where P_{Gi}^{0} represents the base case active power generation of generator i. P_{Gi}^{0} is obtained from market-clearing mechanics and represents constant power in (3.38). The power adjustments need the following additional constraints:

$$\Delta P_{Gi}^{\text{up}} \geq 0, \quad \Delta P_{Gi}^{\text{down}} \geq 0 \tag{3.39}$$

This objective function is suitable for a day-ahead electric energy market based on a pool. Within this pool, producers and retailers/consumers submit production and consumption bids to the market operator, which, in turn, clears the market using an appropriate market-clearing procedure. This procedure results in 24 hourly energy prices to be paid by consumers and to be charged by producers [65]. Equation (3.37) represents the total cost associated with up/down power adjustments by the ISO to ensure a secure operation. In this thesis, any change from the market-clearing conditions implies a payment to the agent involved. It should be noted that while the time framework for the day-ahead electric energy market is 24 hours, the time framework for TSC-OPF is one hour, as preventive controls based on TSC-OPF are considered hour by hour. It is noted that the objective function is also suitable for the real-time market. For the real-time market, r_{Gi}^{up} and r_{Gi}^{down} represent the Locational Marginal Prices (LMP) at each generator node, calculated at five-minute intervals based on actual grid operating conditions.

3.4.2 Transient Stability Constraints

The stability constraints to be included in the conventional OPF problem depend on factors such as whether the machine dynamic equations are solved inside or outside the OPF, and the transient stability index used for stability assessment. If the power system differential equations are solved within the OPF, these equations are discretized and added as difference algebraic equations. The discretization of the dynamic equation leads to a large number of equality constraints to be incorporated. The technique to discretize dynamic equations is described in [7, 9]. The number of dynamic and transient stability constraints included in the OPF problem for different TSC-OPF methods proposed in the literature are tabulated in [14].

Even when the power system dynamic equations are solved outside the OPF and the transient stability constraints are formulated using machines rotor angles [14, 53], the algebraic constraints associated with generator stator equations shall be added in the conventional OPF formulation. The steady state generator internal voltage and rotor angle are computed in the OPF algorithm by adding the algebraic equations shown graphically in Fig. 3.9. The transient stability constraint is typically included in the form of limits on individual generator rotor angles [7, 53], or a limit on the OMIB rotor angle [9, 14], or transient energy function (which uses generator rotor angles to determine the stability margin) [8, 54].

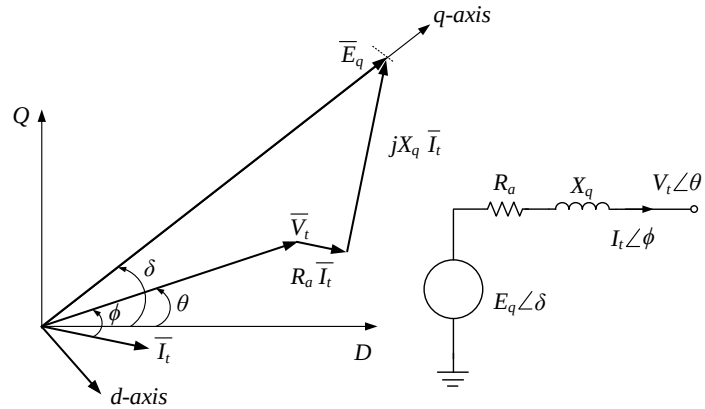

Figure 3.9: Steady state representation of the stator algebraic equations.

In this thesis, the transient stability constraint is expressed in terms of limit on the sum of critical machines active power, as shown in (3.40). Since the SIME method is used, only one constraint is sufficient to include dynamic and stability limits of the multi-machine power system. The value of P_{eC*} is estimated using (3.28), i.e. linear extrapolation technique on the quasi-linear relationship between critical machines active power and stability margin, as described in Section 3.3.2. If the difference between the calculated (SIME) and estimated stability margin is outside the tolerance value, the P_{eC*} is re-estimated. The process is continued until the calculated stability margin is within acceptable range.

$$\sum_{k \in C} P_{ek} \leq \frac{M_C}{M} P_{eC*} \tag{3.40}$$

3.4.3 Proposed TSC-OPF Algorithm

The flowchart for the proposed TSC-OPF technique is illustrated in Fig. 3.10. The main steps for ensuring transient stability using the proposed method are listed below.

Step (1) Set $i = 1$. Run a conventional OPF to obtain the base case solution for the given system.

Step (2) Using the base case solution, run transient stability assessment with the SIME method for a given contingency x. Compute the OMIB equivalent parameters (C, N, M, M_C, M_N, P_{eC}, δ, δ_u, ω_u, δ_r) and the stability margin (η).

Step (3) If the OMIB system is stable, go to Step (8).

If the system is unstable and $P_e(t) < P_m(t)$ in the post-fault period, go to Step (4). This situation happens during highly stringent stability condition, when there is no intersection of P_m and P_e curves [16].

Else set $i = i + 1$.

If $i < 2$ go to Step (4), else proceed to Step (5).

Step (4) Decrease the value of P_{eC} by λ (say 1.5%). Using (3.40), add a transient stability constraint and run the OPF. Run TSA with the SIME method and compute the OMIB equivalent parameters and the stability margin. Go to Step (3).

Step (5) Using the last two values of η and P_{eC}, estimate the value of P_{eC*} for a known positive stability margin η_{ST}. The value of η_{ST} is set to $0.05 * A_{acc}$ pu.rad (where A_{acc} is the accelerating area in the OMIB $P - \delta$ plot from previous iteration).

Step (6) Update the transient stability constraint (3.40) and run the OPF. Run TSA and compute the OMIB equivalent parameters and the stability margin.

Step (7) If the stability margin (η) is outside the acceptable range ($\eta_{max} > \eta > \eta_{min}$), then go to Step (5).

Else proceed to Step (8).

For each iteration, η_{max} is set to $0.2 * A_{acc}$ pu.rad and η_{min} is set to 0 pu.rad (where A_{acc} is the accelerating area of the current OMIB $P - \delta$ plot).

Step (8) Display TSC-OPF result.

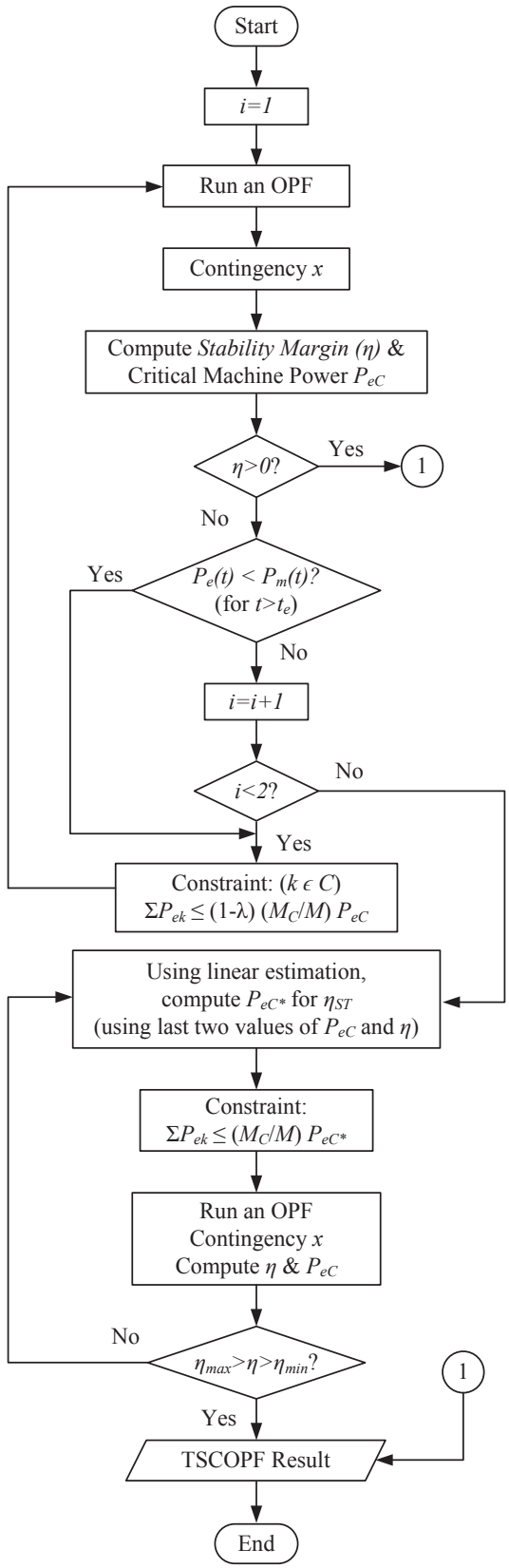

Figure 3.10: Flowchart for the proposed TSC-OPF technique.

CHAPTER 4: PROPOSED DYNAMIC REMEDIAL ACTION SCHEME

4.1 Overview

This chapter describes the proposed dynamic remedial action scheme in details. The proposed dynamic RAS technique is used to develop a generation shedding RAS. This scheme uses online stability calculations and generator cost functions to determine appropriate remedial actions. Unlike conventional RAS, which are designed using offline simulations, online stability calculations make the proposed technique dynamic and adapting to any power system configuration and operating state. The generation-shedding cost is calculated using pre-RAS and post-RAS OPF costs. The criteria for selecting generators to trip is based on the minimum cost rather than minimum amount of generation to shed. For an unstable Category C contingency, the RAS control action that results in stable system with minimum generation shedding cost is selected among possible candidate solutions. The RAS control actions update whenever there is a change in operating condition, system configuration, or cost functions.

This chapter is organized as follows. Section 4.2 presents the overview of the proposed dynamic RAS technique. The formulation of dynamic generation-shedding RAS problem is described in Section 4.3. The technique to select the appropriate generation-shedding RAS choice is described in Section 4.3.1. Finally, the calculation of OPF-based generation-shedding cost is presented in Section 4.3.2.

4.2 Proposed Dynamic RAS

Remedial action schemes supplement primary protection devices to prevent violations of the NERC reliability criteria for Category C and more severe events. RAS

are designed to address specific problems, e.g. to address generator instability, to increase power transfer, to mitigate overfrequency or underfrequency issues, etc. Possible remedial actions include generation shedding, load shedding, capacitor and reactor switching, etc. At present, most of the RAS control actions are designed using extensive offline simulations [18, 21, 22]. Numerous combinations of credible contingencies, power-system configurations, and load-flow scenarios are considered during the design phase. Trying to predict all possible power system operating states in offline studies leads to a large number of test cases to simulate [22]. This leads to long design, validation and commissioning periods.

The proposed dynamic RAS addresses the shortcomings of current RAS design by incorporating online transient stability analysis (TSA) and generation cost functions [27, 28]. The schematic overview of the proposed dynamic RAS is shown in Fig. 4.1. The 'Power System State' block estimates power system states using Phasor Measurement Units (PMU), SCADA, and a topology processor data. The 'Online TSA' block uses the real-time state data and model data of the power system to compute the stability margin for a list of credible contingencies. The Single Machine Equivalent (SIME) method is used for computing stability margin. The SIME method is a hybrid transient stability analysis tool that uses the generalized One-Machine Infinite Bus (OMIB) system [16]. For unstable contingencies, this block separates the generators into critical and non-critical machines. For each unstable case, the 'Online OPF-based RAS Action Determination' block computes the generation-shedding cost for all practical combinations of critical generators. Next the 'Online TSA' block computes the stability margin for the same unstable contingency followed by the least costly generation-shedding RAS action. If the stability margin is positive, then the selected RAS action is uploaded to the 'RAS Logic Controller'. If the stability margin is negative, then the next RAS choice is selected and the process is repeated. The 'RAS Logic Controller' monitors the power system using wide-area monitoring system

(WAMS). If the occurrence of critical contingency is identified, then it executes the pre-assigned remedial control action to stabilize the system. The proposed dynamic RAS is designed and tested in the real-time test platform described in Chapter 5.

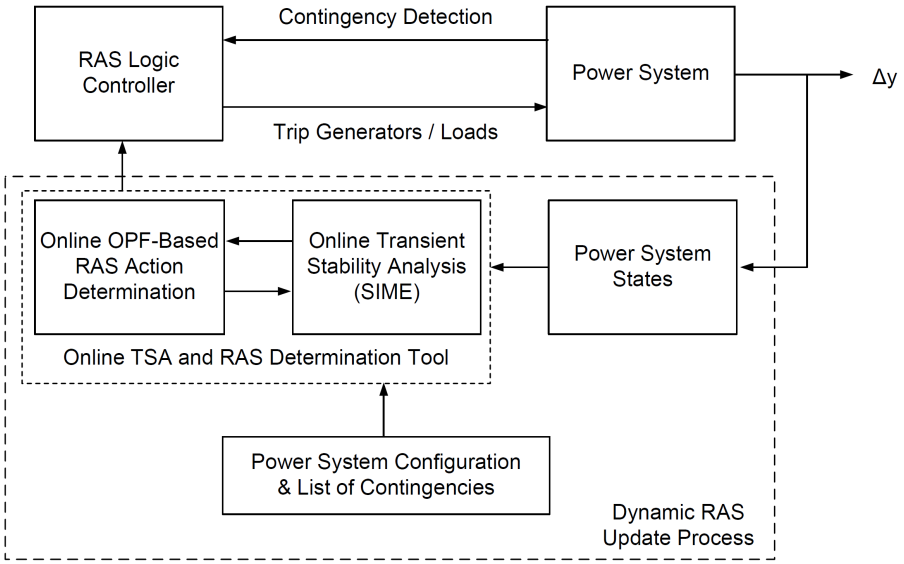

Figure 4.1: Schematic overview of the Dynamic RAS.

Among various RAS types, generation shedding is the most effective and widely used emergency control means for maintaining system stability [18]. Previous research on generation-shedding schemes are focused towards determining the minimum amount of generation to shed [25, 60]. The world's first real-time transient stability control (TSC) system applied on a large power system is described in [45, 46]. The TSC system selects the optimum generator to shed based on online stability calculation. Although very effective, these schemes do not consider the generation shedding cost when selecting remedial action. In today's deregulated power industry, generation shedding scheme using both operation costs and technical constraints can be an attractive alternative. In this thesis, dynamic generation shedding RAS is developed.

4.3 Formulation of Dynamic RAS Problem

A dynamic generation shedding RAS problem is formulated by combining online transient stability analysis with generation cost functions. For an unstable con-

tingency, the critical generators are identified using the SIME-based tool. Next, generation-shedding cost is calculated for each critical generator(s) using an optimal power flow tool. The critical generator(s), which can stabilize the system following generation shedding at minimum generation-shedding cost, is selected as the preferred RAS choice. The RAS choice is then stored in the RAS Logic Controller. The RAS choice is updated whenever there is a change in operating condition, system configuration, or cost functions.

4.3.1 OPF-Based Generation-Shedding Selection

The generation-shedding schemes discussed earlier are developed to shed the minimum amount of generation. The effect of generation shedding on the economic operation of the power system is generally not considered. These schemes might be applicable in regulated energy market, but they are not an attractive option in a competitive market. In today's deregulated power industry, economic operation of the power system depends on various factors like load demand, generating cost curves, time-varying bid price of generator power, power purchase agreement etc. Hence, a generation-shedding scheme designed using both operation costs and technical constraints can result in optimal economic operation of the system while operating within security limits.

The flowchart for selecting critical generator(s) for the generation-shedding scheme is shown in Fig. 4.2. The proposed scheme determines generation-shedding RAS control actions for all unstable multiple element contingencies. For an unstable contingency, the critical generators are separated from the non-critical generators using the SIME-based tool. This reduces the combination of generators to be considered for generation shedding from total online generators to total number of critical generators. This combination can be further reduced by identifying the critical generators with and without generation shedding capabilities and wide-area communication networks.

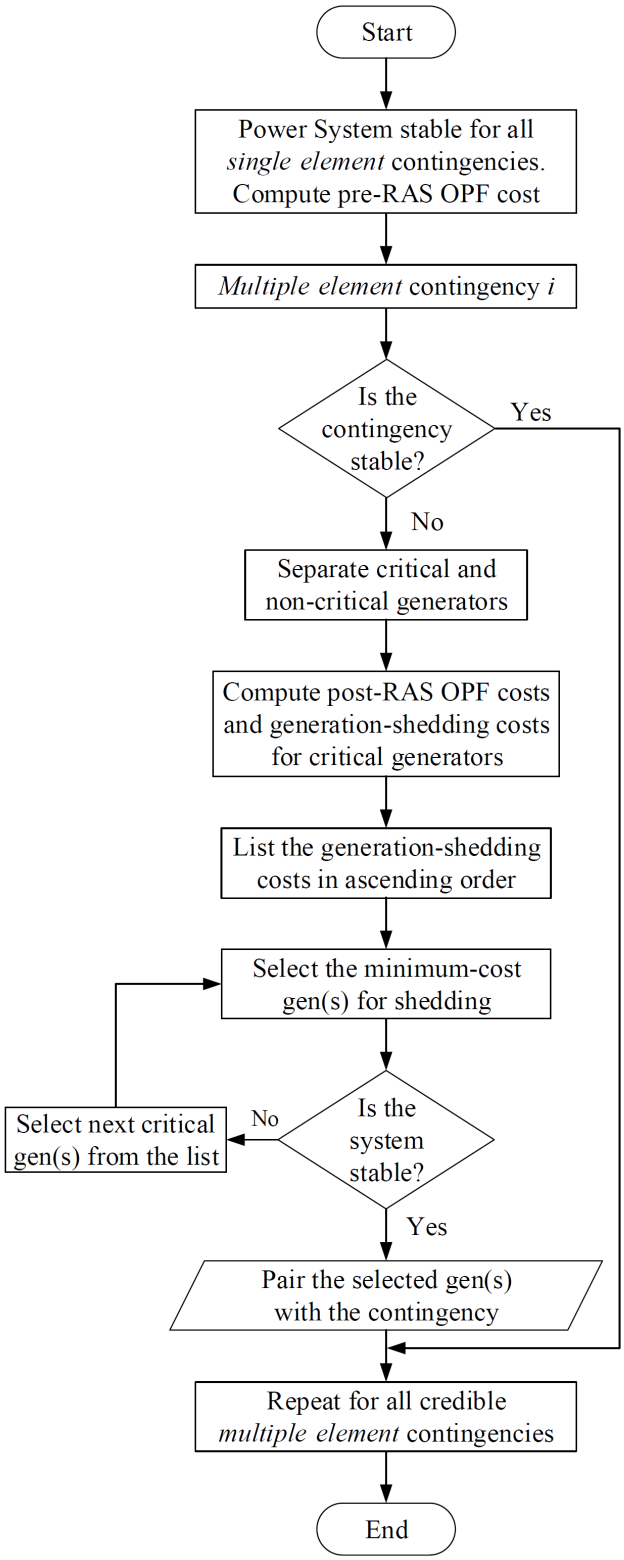

Figure 4.2: Flowchart for the OPF-based generation-shedding selection.

The generation-shedding cost is computed as a difference between optimal power system operating cost in post-RAS and pre-RAS periods. For an unstable contingency, the critical generator(s) that can stabilize the system at the minimum generation-shedding cost is selected as the RAS choice. Since the transient stability calculation and generation-shedding costs are calculated online, the control action can adapt to any change in power system operation and cost variations. This process is repeated for all credible contingencies.

4.3.2 OPF-Based Generation-Shedding Cost

The generation-shedding cost is calculated by minimizing the change in total generation operation cost when the system moves from pre-RAS phase to the post-RAS phase. The formulation of the OPF-based generation-shedding cost is shown below.

For a power system with n buses, an OPF problem for minimizing an objective function can be formulated as follows:

$$\text{Min} \quad f(\cdot) \tag{4.1}$$

subject to power flow equality constraints,

$$P_{Gi} - P_{Di} - V_i \sum_{j=1}^{N} V_j (G_{ij} cos\theta_{ij} + B_{ij} sin\theta_{ij}) = 0 \tag{4.2}$$

$$Q_{Gi} - Q_{Di} - V_i \sum_{j=1}^{N} V_j (G_{ij} sin\theta_{ij} - B_{ij} cos\theta_{ij}) = 0 \tag{4.3}$$

and inequality constraints in the form of technical limits,

$$P_{Gi\,min} \leq P_{Gi} \leq P_{Gi\,max} \tag{4.4}$$

$$Q_{Gi\,min} \leq Q_{Gi} \leq Q_{Gi\,max} \tag{4.5}$$

$$V_{i\,min} \leq V_i \leq V_{i\,max} \tag{4.6}$$

$$S_i \leq S_{i\,max} \tag{4.7}$$

where,

P_{Gi}/Q_{Gi} :	real/reactive power output of generator i
P_{Di}/Q_{Di} :	real/reactive power demand of load i
V_i :	voltage magnitude at bus i
S_i :	apparent power flow in line i
$P_{Gi\,max}/P_{Gi\,min}$:	upper/lower active power limit of generator i
$Q_{Gi\,max}/Q_{Gi\,min}$:	upper/lower reactive power limit of generator i
$V_{i\,max}/V_{i\,min}$:	upper/lower voltage limit at bus i
$S_{i\,max}$:	upper apparent power flow limit in line i

During pre-RAS period, all NG generators are online. The operating point of the generators is determined by OPF, which results in the minimum operating cost. The optimal operating cost of the power system during the pre-RAS period is given by:

$$f(pre - RAS) = \quad \text{Min} \quad \sum_{i=1}^{NG} f(\cdot) \tag{4.8}$$

For an unstable multiple element contingency, the total generators in the system are separated into C critical generators and N non-critical generators using the SIME method. Out of C critical generators, let CS represents a subset of critical generator(s) selected for generation shedding. The optimal operating cost of the power system in post-RAS period, i.e. following the contingency and generation-shedding RAS action, is given by:

$$f(post - RAS) = \quad \text{Min} \quad \sum_{i=1,\ i \neq CS}^{NG} f(\cdot) \tag{4.9}$$

The generation-shedding cost is defined as:

$$F_{GSi} = f(post - RAS) - f(pre - RAS) \tag{4.10}$$

Hence, the critical generators to shed (CS) are selected such that the generation-shedding cost is minimized, the system remains stable following the contingency, and the operating constraints (4.2) - (4.7) are not violated in the post-RAS period.

$$\text{Min} \quad F_{GSi}(i \in C) \tag{4.11}$$

4.3.2.1 Objective Functions

Two types of objective functions are considered for calculating generation-shedding cost. The first objective function is the total generator fuel cost. This type of objective function is applicable for traditional vertically structured electric utilities where energy prices are not determined by market-clearing procedure.

$$f(P_{Gi}) = \sum_{i=1}^{NG}(a_i P_{Gi}^2 + b_i P_{Gi} + c_i) \tag{4.12}$$

where P_{Gi} is the active power output of generator i and a_i, b_i, and c_i represents its fuel cost coefficients.

The second type of objective function represents the total cost associated with generator power adjustments [64]. This objective function is suitable for both a day-ahead electric energy market and a real-time market based on a pool. Within this pool, producers and retailers/consumers submit production and consumption bids to the market operator, which, in turn, clears the market using an appropriate market-clearing procedure.

$$f(\Delta P_{Gi}^{\text{up}}, \Delta P_{Gi}^{\text{down}}) = \sum_{i=1}^{NG}(r_{Gi}^{\text{up}} \Delta P_{Gi}^{\text{up}} + r_{Gi}^{\text{down}} \Delta P_{Gi}^{\text{down}}) \tag{4.13}$$

where $\Delta P_{Gi}^{\text{up}}$ and $\Delta P_{Gi}^{\text{down}}$ are the power adjustments of generator i and r_{Gi}^{up} and

r_{Gi}^{down} are the prices offered by the generator to increase or decrease its power dispatch, respectively. The active power generation P_{Gi} is defined as follows:

$$P_{Gi} = P_{Gi}^{0} + \Delta P_{Gi}^{\text{up}} - \Delta P_{Gi}^{\text{down}} \tag{4.14}$$

where P_{Gi}^{0} represents the base case active power generation of generator i. P_{Gi}^{0} is obtained from market-clearing mechanics and represents constant power in (4.14). The power adjustments need the following additional constraints:

$$\Delta P_{Gi}^{\text{up}} \geq 0, \quad \Delta P_{Gi}^{\text{down}} \geq 0 \tag{4.15}$$

Since, P_{Gi}^{0} represents pre-RAS active power generation of generator i, $\Delta P_{Gi}^{\text{up}}$ and $\Delta P_{Gi}^{\text{down}}$ are zero for pre-RAS period. This results in zero pre-RAS cost ($f(pre - RAS)$), and the generation-shedding cost for this objective function is given by post-RAS cost ($f(post - RAS)$).

CHAPTER 5: REAL-TIME TEST PLATFORM

5.1 Overview

This chapter describes the real-time hardware-in-the-loop test platform designed and developed specifically for validation and testing of the proposed dynamic RAS. This setup allows one to include all of the necessary hardware for control, measurement, communications, and protection. The test platform consists of multiple Real Time Digital Simulators (RTDS), multiple PMUs, a protocol gateway, and a MATLAB-based controller. The real-time platform is suitable for the design, testing, and validation of both continuous and discontinuous wide-area controllers. The solutions discussed in this chapter are expected to be helpful in any state-of-the-art 'Smart Grid' laboratory.

This chapter is organized as follows. The need for real-time test platform is discussed in details in Section 5.2. Section 5.3 provides an overview of the test platform developed for testing the proposed dynamic RAS. Each hardware used in the test platform is described in details. Finally, Section 5.4 presents the key capabilities of the test setup.

5.2 Need for Real-Time Test Platform

Modern power systems are large and complex systems. The constraints placed by economic and environmental factors has pushed power system operation to its stability limits. As a result, many large scale blackouts have occurred worldwide during major system-wide disturbances [1]. Due to the lack of global observability and coordination, local controllers like power system stabilizers (PSSs) and flexible alternating current transmission systems (FACTS) can provide only limited stabilizing control,

and cannot always prevent system instability. Research in wide-area control system (WACS) has proved that it is a robust tool for improving power system stability and reliability [66–68]. Wide-area controllers coordinate the activities of multiple distributed controllers using information from time-synchronized phasor measurement units (PMUs) and supervisory control and data-acquisition (SCADA).

Depending upon the output signal, WACS can be classified as continuous or discontinuous [66]. An example of continuous WACS is BPA's Pacific HVDC intertie project [69]. In 1976, BPA implemented modulation of the Pacific HVDC intertie using active power and later current magnitude signals from a remote substation on the parallel Pacific ac intertie. The continuous control damped electromechanical oscillations between groups of PNW generators and groups of Pacific Southwest generators. Other examples of continuous WACS are described in [70,71]. Discontinuous WACS supplement the basic continuous controls by relieving stress for very large disturbances, and a secure post disturbance operating point. Compared to continuous control, discontinuous control tends to be safer-action is only taken when necessary. RAS falls under discontinuous WACS. Modern RAS monitor the power system using PMU and SCADA data, and take discontinuous actions like generator tripping, load shedding, capacitor/reactor bank switching etc., upon detection of a predefined event. Examples of discontinuous WACS implemented by utilities are discussed in [21–23,66].

Advancement in wide-area measurement technology have led to wide-area applications progressing from being simply visualization, data archiving, and postmortem analysis tools to real-time control systems. Because of increased control leverage and continuous exposure to adverse interactions, design of wide-area control should be approached with caution compared to local control. The consequence of failure of a wide-area controller can result in large-scale blackouts. Testing, validation, commissioning, and training of new real-time wide-area controllers can become very challenging. Communications latency and its effect on the controller is another concern.

A real-time hardware-in-the-loop test platform comprising of real-time simulators, hardware controller, measurement and protection devices, and communication equipment can aid in the design and testing of new WACS. The need for real-time test platform is described below is details.

- Due to the complexity and critical nature of the power system, it is very difficult to test new control methods and algorithms on the real world power system. The real-time test platform can perform electromagnetic transient simulations of a power system and provide real-time signal to PMUs and controllers. It is a great R&D tool for designing and testing new control techniques. New wide-area controls implemented by the utilities all use real-time test platform during design and testing phase [66, 72].

- Remedial schemes using wide-area measurements have been extensively implemented by utilities [18]. These schemes are designed following industry guidelines like WECC and NERC [20,59]. A misoperation of a RAS control action can lead to a major outage. RAS should be thoroughly tested and validated before commissioning to avoid such situation. A real-time test platform is the preferred industry choice for the design, testing, and validation of RAS [21, 22, 73].

- WACS use PMUs and communication equipment to monitor the states of remote buses and generators. Communication latency can have significant negative impact on the controllers. The real-time test platform allows one to include all of the necessary hardware for control, measurement, and communications. This enables researchers to measure and estimate actual communication latency and include necessary remedy in the controllers. In [72], high-frequency constant amplitude oscillation caused by communication time delay was identified during real-time testing. Similar oscillation in wide-area PSS output is discussed in [31].

- Many wide-area protection and control applications have been proposed and

implemented using synchrophasor (PMU) data and protective relays [67, 68, 74]. Inter-area oscillation and mitigation, detection of out-of-step condition, distributed generation control, synchrophasor-based backup protection are few applications of wide-area control using protective relays. The real-time test platform is an ideal tool for the design, development and testing of power system protection and control designs.

- Dispatcher training simulator (DTS)-based blackout restoration drills have been mandated by the NERC due to reoccurring large-scale blackouts that affect tens of millions of customers and their economic activities [75]. The real-time test platform can operate as a powerful simulator for operators and dispatchers to train for emergency situations [76].

5.3 Real-Time Test Platform

A real-time test platform which addresses the needs described above is developed in the Duke Energy Smart Grid Laboratory within the Energy Production and Infrastructure Center (EPIC) at UNC Charlotte. The real-time platform is suitable for the design, testing, and validation of both continuous and discontinuous wide-area controllers [30, 31]. IEEE Standard C37.118 Synchrophasor and IEC 61850 Generic Object Oriented Substation Event (GOOSE) protocols are implemented for high speed wide-area communications. Fig. 5.1 shows the test platform which consists of multiple Real Time Digital Simulators (RTDS), multiple PMUs, a protocol gateway, and a MATLAB based controller. Since the platform allows one to use actual hardware for measurement, communications, protection, and control, it allows for the connection of all necessary external hardware. The solutions discussed here are expected to be helpful in any state-of-the-art 'Smart Grid' laboratory.

Figure 5.1: Real-time test platform in the Duke Energy Smart Grid Lab at UNC Charlotte.

The dynamic RAS proposed in Chapter 4 is tested on the real-time test platform. Fig. 5.2 shows the schematic overview of the proposed dynamic RAS and the hardware used for implementation. The power system is simulated in real-time in RTDS. The power system states are measured directly using physical PMUs (SEL-421 relays) and RTDS GTNET card. The 'Online TSA and RAS Determination Tool' is implemented using a series of MATLAB based tools. The output of this block is updated in the 'RAS Logic Controller', which is implemented in a SEL-421 relay.

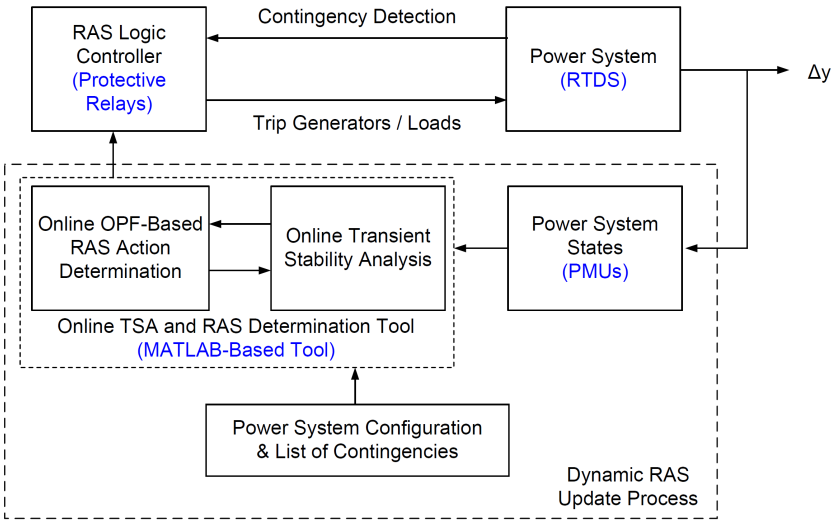

Figure 5.2: Hardware used for testing the proposed Dynamic RAS.

Fig. 5.3 illustrates the system architecture of the real-time test platform. Each element is discussed in details in the following subsections.

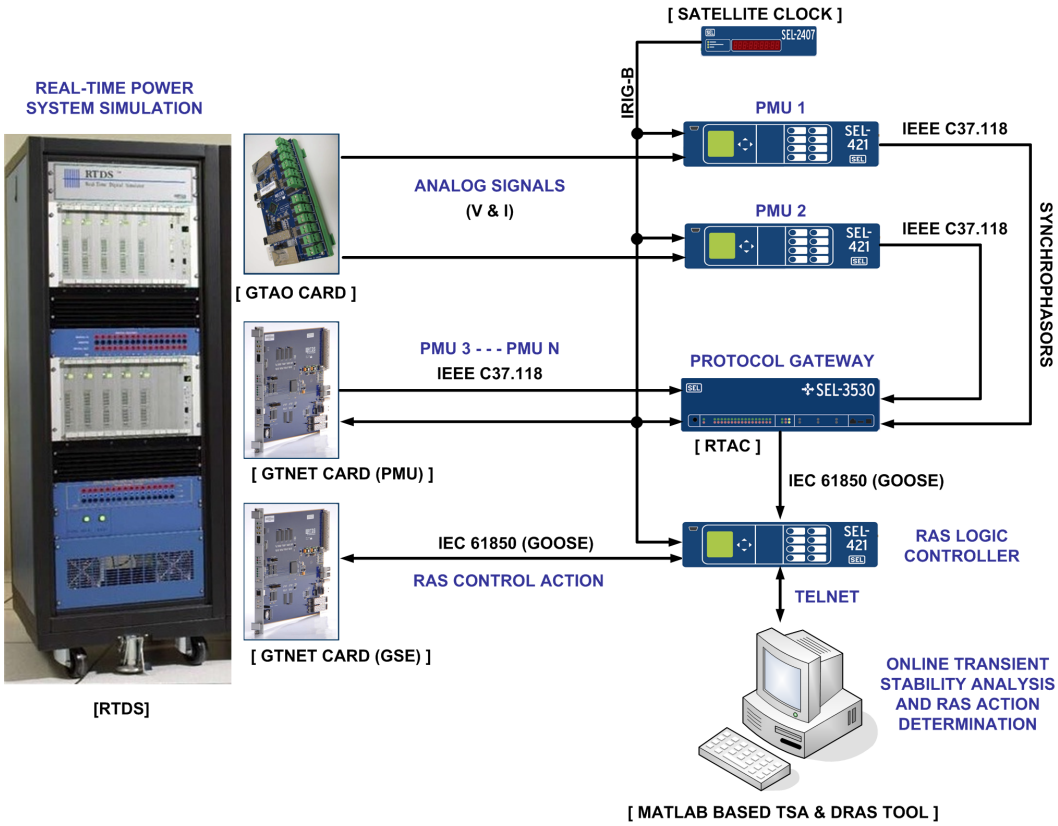

Figure 5.3: Real-time platform for testing the Dynamic RAS.

5.3.1 The Real Time Digital Simulator

The RTDS is a real-time digital simulator that can be used for detailed power-system studies, including hardware-in-the-loop (HIL) testing of protective relays and controllers as well as power hardware components. It performs electromagnetic transient simulations within a typical time step of 50 μs [77]. As such, the RTDS is a powerful research and development tool commonly used in both industrial and academic laboratories. It is widely viewed as an essential component for testing the impact of wide-area controllers and grid-connected power electronics.

The RTDS uses RSCAD as a graphical user interface to develop and simulate power systems. It supports a variety of input/output (I/O) cards, including those for

digital I/O, analog I/O, and various communications protocols. The two essential to the real-time test platform are the following:

- The Gigabit-Transceiver Analog Output (GTAO) Card is a rail mount component that provides 12 analog outputs in the range of ±10V peak, and whose output channels are optically isolated from the simulator. This card is used to provide voltage and current signals from the real-time simulation to SEL-421 relays to generate Synchrophasor data.

- The Gigabit Transceiver Network Interface System (GTNET) Card is a communication card which allows exchange of information between the RTDS and external intelligent electronic devices (IEDs) using communication protocols. This card supports a number of standard communications protocols, including IEC 61850 GSSE, GOOSE, PMU, SV, DNP, and Playback. The first GTNET card with PMU protocol is used to transmit Synchrophasor data and the second card with GOOSE protocol is used to exchange IEC-61850 GOOSE signals with the RAS Logic Controller.

5.3.2 The Phasor Measurement Units (PMUs)

GPS-synchronized phasor measurements are most often considered for wide-area control [78]. PMUs generate voltage and current phasors (magnitude and angles) from direct time-domain analog signals. The PMUs used in this system are SEL-421 relays and GTNET-PMU card. The SEL-421 relays serve two purposes. First, they act as line distance relays, and second they serve as PMU sources. An SEL-2407 satellite-synchronized clock provides time synchronization. Each relay can output up to 20 phasors, 16 analog values, and four 16-bit digital words at a maximum rate of either 50 or 60 samples per second [79]. Digital words within Synchrophasor data packets are used to transmit information such as line fault type, breaker status, and power-system configuration.

5.3.3 The Protocol Gateway

The protocol gateway was developed to provide power system state information in the form of Synchrophasor data to the MATLAB-based TSA and RAS Determination Tool. SEL-3530 Real-Time Automation Controller (RTAC) is the protocol gateway. The RTAC is a powerful automation controller with a real-time operating system, an IEC 61131 logic engine, and protocol conversion capabilities [80]. It receives Synchrophasor data from the external PMUs via an Ethernet port. The time-aligned Synchrophasors are packaged in a high-speed GOOSE message and transmitted to the RAS logic controller. Since high-speed GOOSE messages are transmitted every few milliseconds, the integrity of the time-aligned Synchrophasors are not compromised during the protocol conversion process.

5.3.4 The MATLAB Based TSA and RAS Determination Tool

The MATLAB-based TSA and RAS Determination Tool is the brain behind the dynamic RAS. It reads power system state information in real-time from the RAS Logic Controller using Telnet protocol. It is also provided with a list of harmful and potentially harmful contingencies and with the dynamic model of the power system. Using SIME, the tool computes stability margin for each contingency. For an unstable contingency, an OPF-based generator shedding remedial actions are designed and tested using time-domain simulations. The list of all RAS control actions are then uploaded to the RAS logic controller, and constantly updated to capture changes in system configurations, operating conditions, and cost functions.

This tool is developed using the Power System Toolbox (PST), which a MATLAB based software package for power system computation, analysis and control [81]. A MATLAB script is written which reads the power system state information from the RAS logic controller and calls PST to execute time-domain simulation for each contingency. At the end of the simulation, the script computes stability margins using

equal-area criteria. For an unstable system, generation shedding remedial actions are determined using MATPOWER [82]. Critical generators with minimum generation shedding cost are selected for generation shedding RAS.

5.3.5 RAS Logic Controller

The RAS Logic Controller stores remedial action information for each unstable contingency. Whenever it detects a severe contingency, it executes a pre-assigned control action to stabilize the system. The SEL 421 relay, which has high speed communication and versatile logic programming capabilities, is used as the RAS Logic Controller. It receives a list of remedial actions for each unstable contingency from the MATLAB-based TSA and RAS determination tool. Whenever a critical contingency occurs, this information is passed to the RAS Logic Controller from the RTAC. The RAS Logic Controller then sends the pre-assigned RAS control actions to he RTDS via GTNET-GSE card to execute the control action in RTDS. It also receives information about the power system states and system configuration from the RTAC and passes this information to the MATLAB-based TSA and RAS determination tool.

5.4 Capabilities of the Real-Time Test Platform

The real-time test platform can serve as a test bed for extensive future research on wide range of power system studies and testing. Inclusion of multiple hardware in the test platform allows researchers to focus on different aspects of wide-area controller design. Some of the key capabilities of the test platform are listed below.

- The test platform facilitates the design, testing, and validation of wide-area continuous controllers [31].
- The test platform includes all necessary hardware to design, test, and validate wide-area discontinuous controllers and wide-area protection and control algorithms [28, 30].

- The RTAC, which is used as a protocol gateway, supports multiple communication protocols like IEEE C37.118, IEC 61850 GOOSE and MMS, DNP3, Modbus, FTP, Telnet, and various SEL protocols. This enables the test platform to use wide range of real-time controllers depending upon the communication protocol it uses.

- Three RTDS racks provide the capability to simulate a power system with a maximum of 90 three-phase nodes in real-time. Six SEL-421 relays and a GTNET-PMU card can generate Synchrophasor data for 30 nodes. Using the real-time platform, various Synchrophasor based monitoring, visualization, and control application can be developed.

- The test platform includes a GPS clock, PMUs and communication hardware. The effect of communication latency, loss of time synchronization, and other practical issues on the WACS can be studied in details.

CHAPTER 6: TEST CASES AND RESULTS

6.1 Overview

This chapter describes the test cases and results for the proposed TSC-OPF solution technique and the proposed OPF-based generation shedding RAS. The proposed methods are tested on three IEEE bus systems, i.e., IEEE 9-bus system, IEEE 39-bus system, and IEEE 145-bus system. In Section 6.1, the test results which demonstrate the effectiveness of the proposed TSC-OPF technique are presented. The comparison of TSC-OPF costs calculated using the proposed technique and other methods found in the literature is presented. The test cases and results for the proposed OPF-based generation shedding RAS are discussed in Section 6.2.

6.2 Test Cases For TSC-OPF

The proposed TSC-OPF solution technique is discussed in Section 3.4. The effectiveness of the proposed technique is demonstrated by simulations on the IEEE 9-bus, 3-machine system, the IEEE 39-bus, 10-machine system, and the IEEE 145-bus, 50-machine system. The time-domain simulation is carried out using PST software [81] and the SIME calculation is done using a MATLAB script. Since SIME uses time-domain simulations for transient stability assessment, any power-system modeling and stability scenarios can be considered in the proposed TSC-OPF technique. Integration time step is 0.001 second is used for transient stability simulation. For an unstable system, the time-domain simulation is run slightly longer than the time to instability t_u. In order to check against multi-swing instability condition, the simulation period is set to 5 seconds for a stable system. The OPF with the proposed transient stability constraint is solved using MATPOWER [82]. For the IEEE 9-bus,

3-machine system, and the IEEE 39-bus, 10 machine system, minimization of total generator fuel cost (3.36) is considered as the objective function. Minimization of total cost associated with generator power adjustment (3.37) is selected as the objective function for the IEEE 145-bus, 50-generator system.

6.2.1 IEEE 9-Bus, 3-Machine System

IEEE 9-bus, 3-machine test power system is shown in Fig. A.1. The power system, generator, and exciter data are taken from [35]. Note, the use of SIME technique enables the proposed method to consider any power-system modeling and stability scenario. However, to compare the results with other TSC-OPF methods found in the literature, the classical generator model is used i.e. only X'_d, H, and D generator parameters are considered. Table 6.1 lists the generator cost data and ratings for this system [53]. We use the proposed technique as a dispatching TSC-OPF; thus the objective function to minimize total generator fuel cost (3.36) is used in the OPF algorithm. The lower and upper limits of all bus voltage magnitudes are set at 0.95 p.u. and 1.05 p.u., respectively.

Table 6.1: Cost function and optimal loading for IEEE 9-bus system

Gen.	**Rating (MW)**	**Cost Function ($/h)**	**Base Case (MVA)**
G1	200	$0.0060P^2+2.0P+140$	105.94+j17.29
G2	150	$0.0075P^2+1.5P+120$	113.05+j4.77
G3	100	$0.0070P^2+1.8P+80$	99.23-j15.56

6.2.1.1 IEEE 9-Bus System - Case A: Fault On Bus 7

In Case A, a three-phase-to-ground fault is applied on Bus 7 and is cleared by tripping Line 7-5 after 0.35 s. Following the line trip, the system becomes unstable. Fig.6.1 shows the generator rotor angles and the OMIB $P-\delta$ curves for the base case. The SIME method identifies generators G2 and G3 as critical machines and computes

the OMIB equivalent parameters and the stability margin. The OMIB parameters at $t = 0$ s for the base case are shown in the first row (Sim. #1) of Table 6.2.

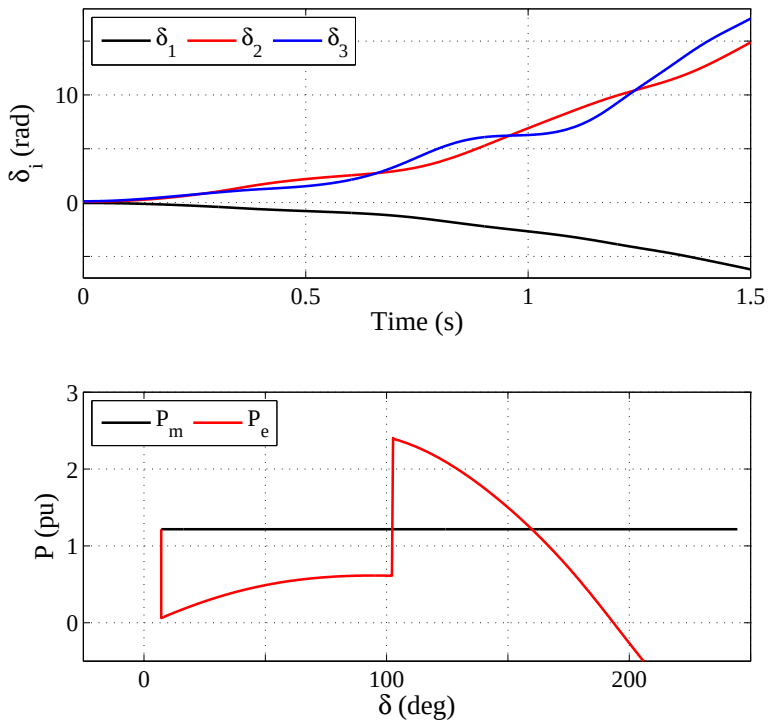

Figure 6.1: IEEE 9-bus system - Case A. Generator rotor angles and OMIB $P-\delta$ curves for the base case.

Table 6.2: TSC-OPF calculations for IEEE 9-bus system - Case A

Sim. #	P_{eC} **(MW)**	δ **(deg)**	δ_r **(deg)**	δ_u **(deg)**	η **(pu.rad)**	η_{max} **(pu.rad)**	**Cost ($/h)**
1	151.84	7.12	-	159.76	-0.535	0.253	1132.176
2	149.56	6.54	-	160.66	-0.380	0.239	1132.279
3	143.09	4.92	149.49	161.12	0.039	0.205	1133.690

Since the system is unstable, P_{eC} is decreased by λ=1.5%. The transient stability constraint is then added to the OPF problem using (3.40). Next, the OPF problem is solved with the stability constraint and the SIME calculation is carried out. The OMIB equivalent parameters and stability margin for this step is listed in the second

row (Sim. #2) of Table 6.2.

Once two data points for η and P_{eC} are available, the value of P_{eC*} is estimated using linear extrapolation (3.28) for $\eta_{ST} = 0.05{*}A_{acc}$ pu.rad, where A_{acc} is the accelerating area of the second iteration. The transient stability constraint is updated using (3.40) and the estimated value of P_{eC*}. The OPF and SIME calculations are repeated. With the estimated stability constraint, the stability margin is positive and within $\eta_{max} > \eta > \eta_{min}$, where $\eta_{max} = 0.205$ pu.rad ($0.2{*}A_{acc}$) and $\eta_{min} = 0$ pu.rad. The OMIB equivalent parameters, stability margin, and total cost for this step is listed in the third row (Sim. #3) of Table 6.2. Fig. 6.2 shows the system is stable against the first and multi-swings.

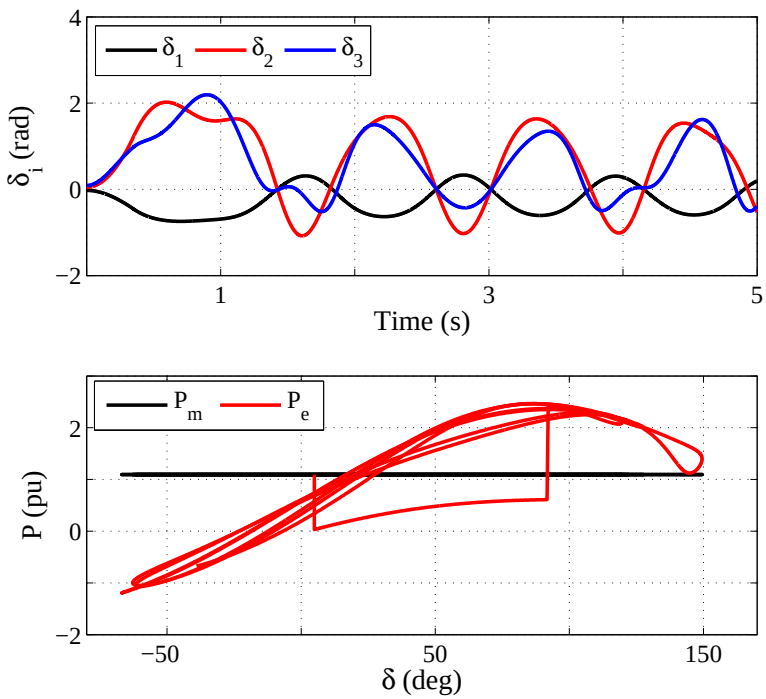

Figure 6.2: IEEE 9-bus system - Case A. Stable rotor angles and OMIB P-δ curves for the third iteration.

6.2.1.2 IEEE 9-Bus System - Case B: Fault On Bus 9

A three-phase-to-ground fault is applied on Bus 9 for 0.30 s and the fault is cleared by tripping Line 9-6. Fig. 6.3 shows the unstable base case and the SIME method

identifies generator G3 as the critical machine. The OMIB parameters for the base case are P_{eC}=90.19 MW, δ=7.59 deg, δ_u=164.64 deg, and η=-1.9713 pu.rad. Next, the proposed TSC-OPF algorithm is applied to this case. After six iterations, Case B stabilizes. For this test case, multi-swing instability is observed for small positive first swing stability margins. Therefore, the upper stability margin (η_{max}) limit is increased to 0.35 pu.rad. The rotor swing curves and OMIB $P-\delta$ curves for the stable system are shown in Fig. 6.4. The OMIB parameters for the sixth iteration are P_{eC}=69.92 MW, δ=2.61 deg, δ_r=161.34 deg, and η=0.329 pu.rad.

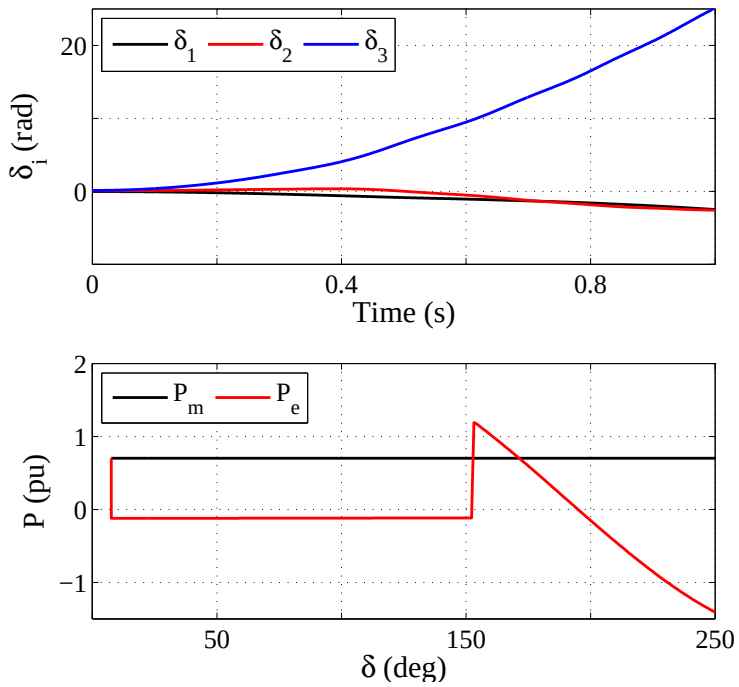

Figure 6.3: IEEE 9-bus system - Case B. Generator rotor angles and OMIB $P-\delta$ curves for the base case.

The TSC-OPF costs computed for Case A and Case B with the proposed method are shown in Table 6.3. The calculated cost is slightly lower to other methods found in the literature. Note, the calculated costs depend upon the dynamic model of the power system as well as the stability margin limits (η_{max} and η_{min}) selected to define a stable system. The optimal generator output and voltage magnitude for the IEEE 9-bus system base case, Case A, and Case B are listed in Table 6.4.

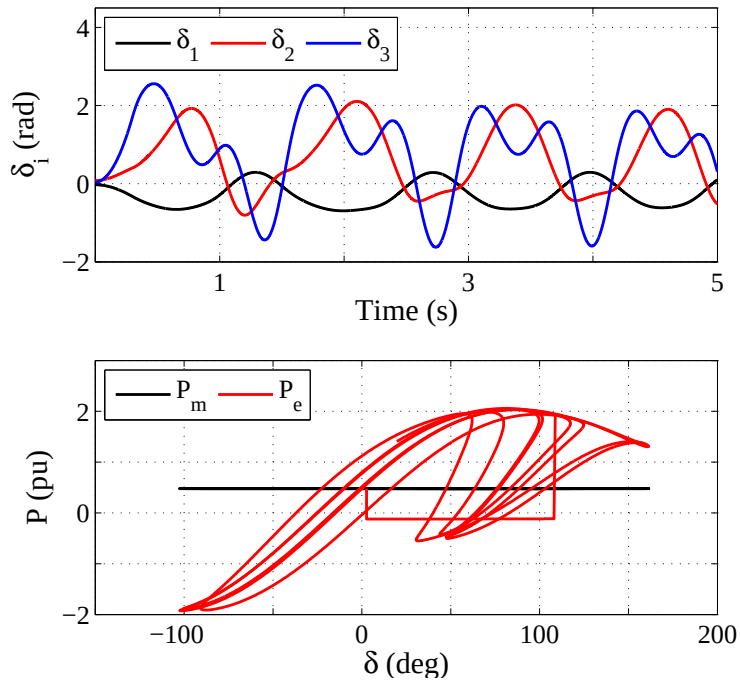

Figure 6.4: IEEE 9-bus system - Case B. Stable rotor angles and OMIB $P-\delta$ curves obtained for the sixth iteration.

Table 6.3: TSC-OPF costs comparison for IEEE 9-bus system

	Base Case ($/h)	**Case A ($/h)**	**Case B ($/h)**
Proposed	1,132.18	1,133.69	1,137.56
Ref. [9]	1,132.18	1,134.01	1,137.82
Ref. [14]	1,132.18	1,134.71	- - -
Ref. [53]	1,132.59	1,191.56	1,179.95
Ref. [12]	1,132.30	1,140.06	1,147.77

Table 6.4: Optimal solutions for IEEE 9-bus system

Gen.	**Base Case**		**Case A**		**Case B**	
	P (MW)	**V (pu)**	**P (MW)**	**V (pu)**	**P (MW)**	**V (pu)**
G1	105.94	1.050	117.91	1.050	117.91	1.050
G2	113.05	1.050	107.10	1.050	123.14	1.050
G3	99.23	1.040	92.95	1.040	76.92	1.040

6.2.2 IEEE 39-Bus, 10-Machine System

Fig. A.3 shows the IEEE 39-bus, 10-machine test power system. The power system, generator, and exciter data are taken from [36]. Table 6.5 lists the generator cost data and ratings for the test power system, taken from [53]. In order to compare results with other TSC-OPF methods found in the literature, we use the proposed technique as a dispatching TSC-OPF; thus, (3.36) is used as objective function. The steady-state voltage magnitude limit for all buses are set to $0.95 \leq V_i \leq 1.05$. The following two contingency cases are studied for this system.

Table 6.5: Cost function and optimal loading for IEEE 39-bus system

Gen.	**Rating (MW)**	**Cost Function ($/h)**	**Base Case (MVA)**
G1	350	$0.0193P^2+6.9P$	242.39-j57.25
G2	650	$0.0111P^2+3.7P$	566.94+j359.90
G3	800	$0.0104P^2+2.8P$	642.73+j254.25
G4	750	$0.0088P^2+4.7P$	629.50+j115.13
G5	650	$0.0128P^2+2.8P$	507.90+j141.28
G6	750	$0.0094P^2+3.7P$	650.39+j222.09
G7	750	$0.0099P^2+4.8P$	557.99+j59.87
G8	700	$0.0113P^2+3.6P$	534.77+j47.18
G9	900	$0.0071P^2+3.7P$	829.36+j28.70
G10	1200	$0.0064P^2+3.9P$	977.56+j68.07

6.2.2.1 IEEE 39-Bus System - Case A: Fault On Bus 4

In Case A, a three-phase-to-ground fault is applied on Bus 4 and is cleared by tripping Line 5-4 after 0.25 s. The system is unstable after the occurrence of the contingency and the following fault clearance for the base case. Fig. 6.5 shows the generator rotor angles and $P-\delta$ curves for the base case. The SIME method identifies generators G1 through G9 as critical machines. The OMIB parameters for the Case C base case are P_{eC}=3297.50 MW, δ=46.52 deg, δ_u=163.17 deg, and η=-2.864 pu.rad.

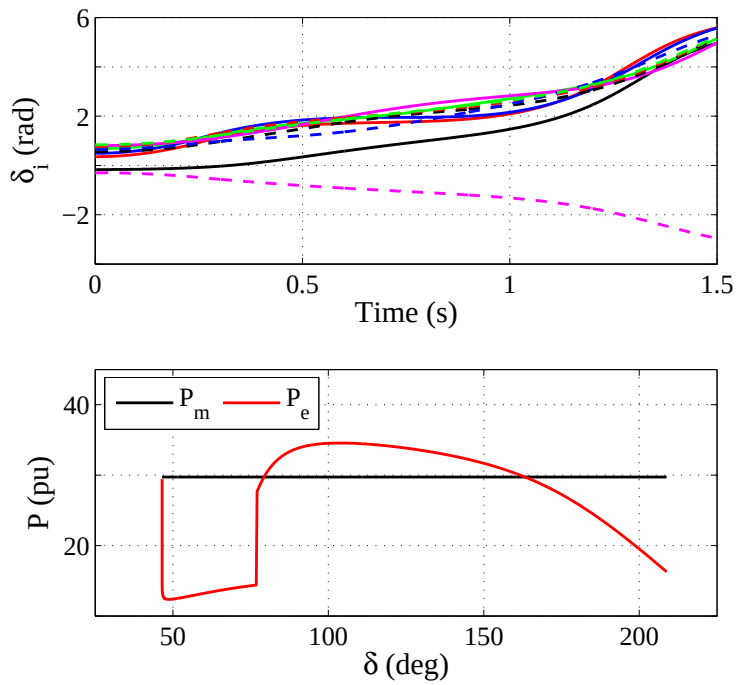

Figure 6.5: IEEE 39-bus system - Case A. Generator rotor angles and OMIB $P-\delta$ curves for the base case.

To compensate for large OMIB inertia coefficient M, the upper stability margin limit (η_{max}) is set to 0.25 pu.rad. Next, the proposed TSC-OPF algorithm is applied to this case. The proposed technique stabilizes the system in four iterations. Fig. 6.6 shows the generator rotor angles and the OMIB P-δ curves for the stable Case A. The OMIB parameters for the fourth iteration are P_{eC}=3248.20 MW, δ=43.85 deg, δ_r=168.62 deg, and η=0.213 pu.rad.

6.2.2.2 IEEE 39-Bus System Case B: Fault On Bus 21

A three-phase-to-ground fault is applied on Bus 21 and is cleared by tripping Line 21-22 after 0.16 s. Following the line trip, the system becomes unstable and the SIME method identifies generators G6 and G7 as critical machines. The OMIB parameters at $t = 0$ s for the base case are shown in the first row (Sim. #1) of Table 6.6. The proposed TSC-OPF method stabilizes Case B in four iterations. The stable rotor angles and the OMIB $P-\delta$ curves for Case B are shown in Fig. 6.8. The OMIB

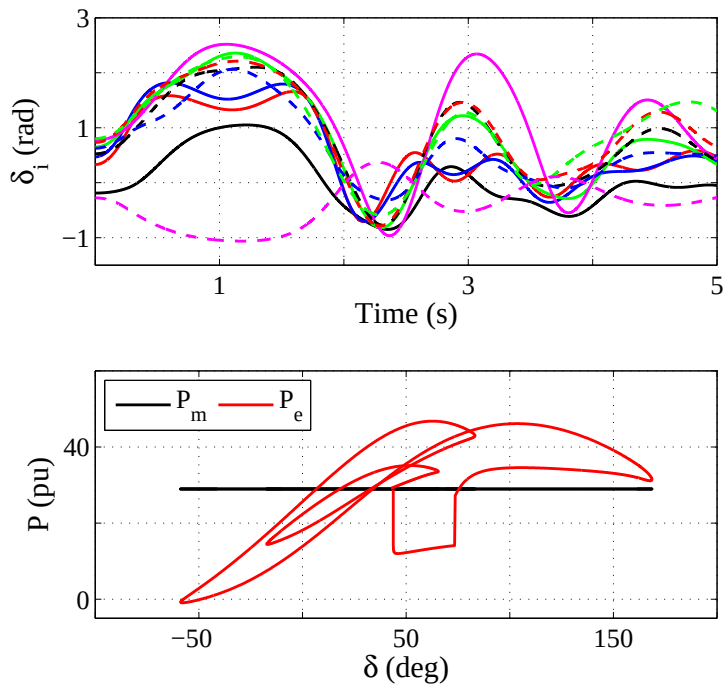

Figure 6.6: IEEE 39-bus system - Case A. Stable rotor angles and OMIB P-δ curves obtained for the fourth iteration.

parameters for the stable system are P_{eC}=1071.30 MW, δ=38.46 deg, δ_r=149.66 deg, and η=0.203 pu.rad (Sim. #4).

Table 6.6: TSC-OPF calculations for IEEE 39-bus system - Case B

Sim. #	P_{eC} **(MW)**	δ **(deg)**	δ_r **(deg)**	δ_u **(deg)**	η **(pu.rad)**	η_{max} **(pu.rad)**	**Cost ($/h)**
1	1113.90	40.44	-	165.37	-0.593	0.449	60918.77
2	1097.20	39.67	-	169.98	-0.125	0.431	60920.86
3	1088.73	38.92	-	173.98	-0.024	0.415	60923.16
4	1071.30	38.46	149.66	167.97	0.203	0.404	60932.41

Table 6.7 shows the cost comparison for the IEEE 39-bus system between the proposed TSC-OPF method and other methods found in the literature. The TSC-OPF cost for Case C is slightly higher than the cost calculated in [9]. In comparison to other methods, the proposed TSC-OPF cost is either cheaper or comparable. Note, the TSC-OPF costs depend upon multiple factors like power system dynamic model

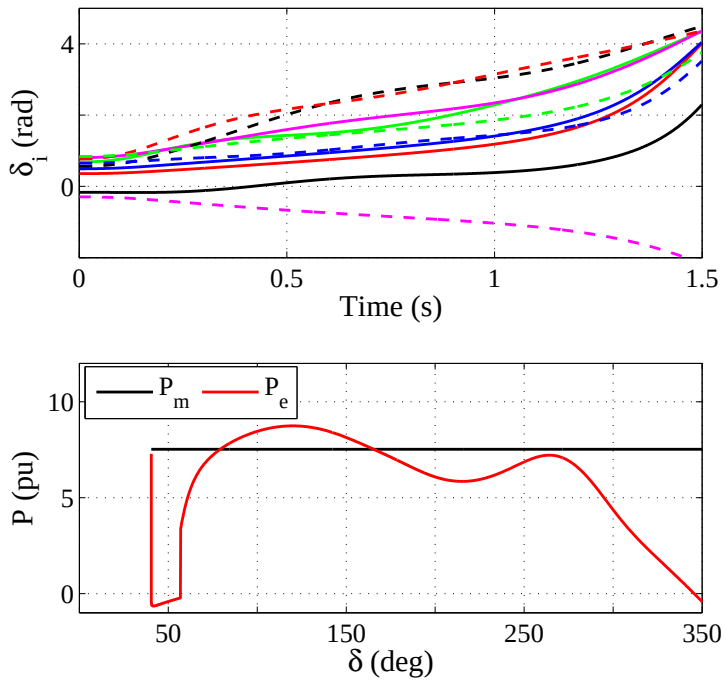

Figure 6.7: IEEE 39-bus system - Case B. Generator rotor angles and OMIB P-δ curves for the base case.

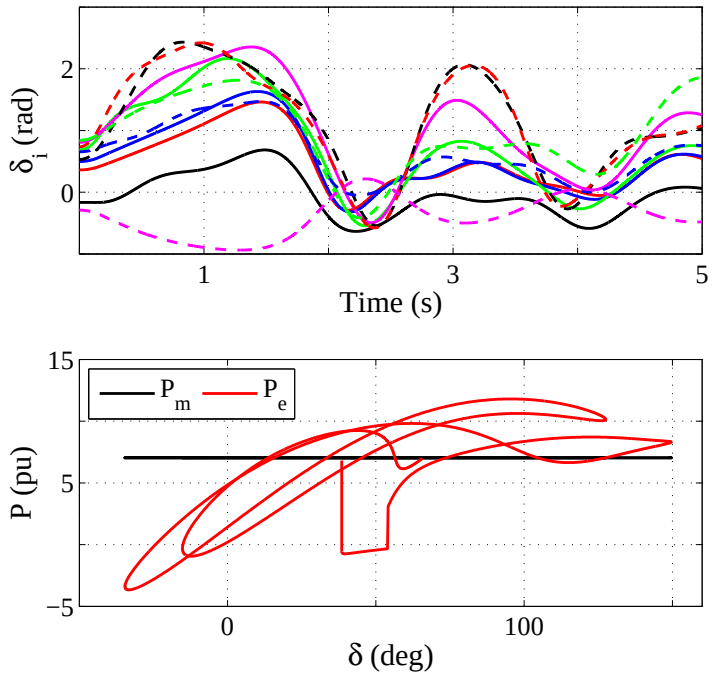

Figure 6.8: IEEE 39-bus system - Case B. Stable rotor angles and OMIB $P-\delta$ curves obtained for the fourth iteration.

used, transient stability limits, simulation step size etc. The optimal loading of generators for the base case, Case A, and Case B are tabulated in Table 6.8.

Table 6.7: Comparison of total costs for IEEE 39-bus system

	Base Case ($/h)	**Case A ($/h)**	**Case B ($/h)**
Proposed	60,918.77	60,964.30	60,932.41
Ref. [9]	60,918.66	60,934.82	60,937.85
Ref. [53]	60,992.88	61,826.53	- - -
Ref. [12]	60,936.51	61,021.04	60,988.25

Table 6.8: Optimal solutions for IEEE 39-bus system

Gen.	**Base Case**		**Case A**		**Case B**	
	P (MW)	**V (pu)**	**P (MW)**	**V (pu)**	**P (MW)**	**V (pu)**
G1	242.39	0.998	237.55	0.997	245.41	0.997
G2	566.94	1.050	558.80	1.050	572.16	1.050
G3	642.73	1.023	633.95	1.022	648.30	1.023
G4	629.50	0.998	619.54	0.998	636.31	0.998
G5	507.90	1.005	501.16	1.004	512.55	1.005
G6	650.39	1.050	641.30	1.050	626.56	1.050
G7	557.99	1.050	549.21	1.050	535.56	1.050
G8	534.77	1.030	526.79	1.029	539.53	1.030
G9	829.36	1.027	816.53	1.027	836.68	1.028
G10	977.56	1.033	1052.34	1.034	986.28	1.033

6.2.3 IEEE 145-Bus, 50-Machine System

IEEE 145-bus, 50-machine test power system was originally developed to test direct stability techniques for transient stability assessment [83]. The test system consists of 50 machines, out of which six machines are represented by the two-axis model, and the remaining machines by classical model. The detailed machine models are equipped with Type AC-4 exciters. The test power system is shown in Fig. A.5. The power system, generator, and exciter data are taken from [83]. The base case power

flow solution is assumed as the result of a market clearing procedure that does not include transient stability constraints. For this test system, the proposed technique is used as a redispatching tool, i.e., (3.37) is used as the objective function. This way, the TSC-OPF problem minimizes the cost of shifting generation with respect to the base case operating point. The lower and upper limits of all bus voltage magnitudes are set at 95% and 105% of the base power flow solution, respectively. r_{Gi}^{up} and r_{Gi}^{down}, the prices offered by the generator to increase or decrease its power dispatch, are both fixed at \$10/MW. The generator active and reactive power limits, and the lines thermal limits are taken from MATPOWER test file [82].

6.2.3.1 IEEE 145-Bus - Case A: Fault On Bus 7

A three-phase-to-ground fault is applied on Bus 7 and is cleared by tripping Line 7-6 after 0.140 s. Following the fault and the line trip, the system becomes unstable. Fig. 6.9 shows the generator rotor angles and the OMIB $P-\delta$ curves for the base case. The SIME method identifies generators at Bus 104 and Bus 111 as critical machines and computes the OMIB equivalent parameters and the stability margin. The OMIB parameters at $t = 0$ s for the base case are shown in the first row (Sim. #1) of Table 6.9.

Table 6.9: TSC-OPF calculations for IEEE 145-bus system - Case A

Sim. #	P_{eC} **(MW)**	δ **(deg)**	δ_r **(deg)**	δ_u **(deg)**	η **(pu.rad)**	η_{max} **(pu.rad)**	**Cost (\$/h)**
1	3969.31	34.29	-	139.17	-7.336	2.109	0.00
2	3770.84	30.78	-	152.19	-4.124	1.956	2005.60
3	3482.30	27.39	150.90	194.99	0.851	1.819	3911.93

The proposed TSC-OPF technique stabilizes the system in three iterations. The OMIB equivalent parameters, stability margin, and total cost for the stable system is listed in the third row (Sim. #3) of Table 6.9. Fig. 6.10 shows the system is stable against the first and multi-swings.

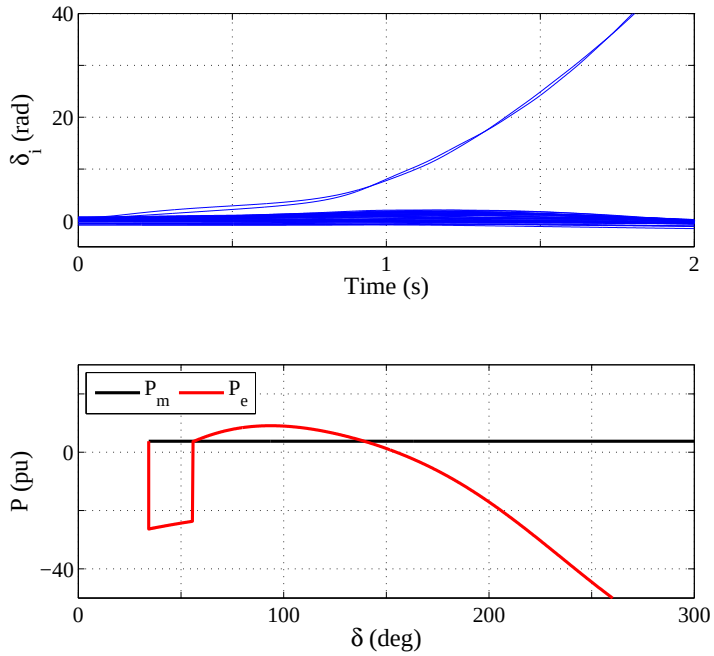

Figure 6.9: IEEE 145-bus system - Case A. Generator rotor angles and OMIB $P-\delta$ curves for the base case.

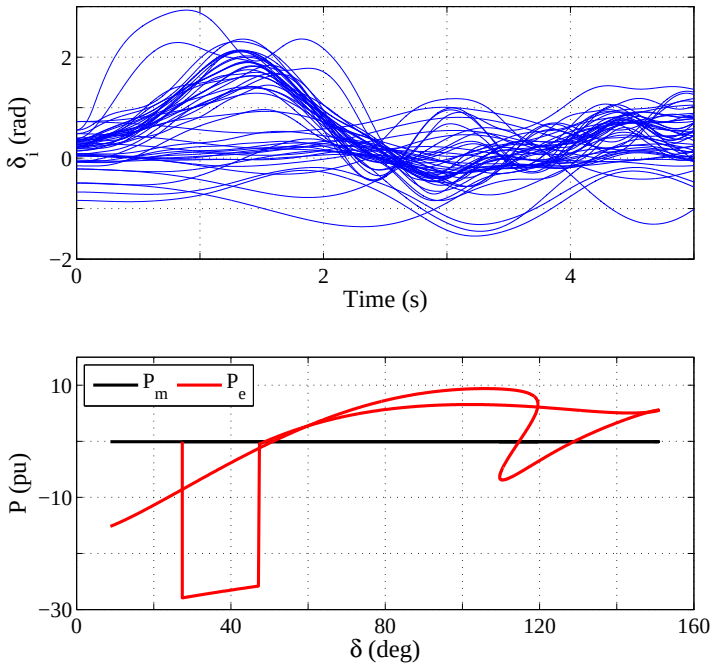

Figure 6.10: IEEE 145-bus system - Case A. Stable rotor angles and OMIB $P-\delta$ curves obtained for the third iteration.

6.2.3.2 IEEE 145-Bus System - Case B: Fault On Bus 25

In Case B, a three-phase-to-ground fault is applied on Bus 25 and is cleared by tripping Line 25-27 after 0.240 s. The base case OMIB equivalent is unstable and the machine rotor angles are shown in Fig. 6.11. For the given contingency, SIME identifies 29 machines, machines at Bus 60, 67, 79, 80, 82, 89, 90, 91, 93, 94, 95, 96, 97, 98, 99, 100, 101, 103, 104, 105, 106, 108, 109, 110, 111, 112, 121, 122, and 124, as critical machines and rest as non-critical machines. The OMIB parameters at $t = 0$ s for the base case are shown in the first row (Sim. #1) of Table 6.10.

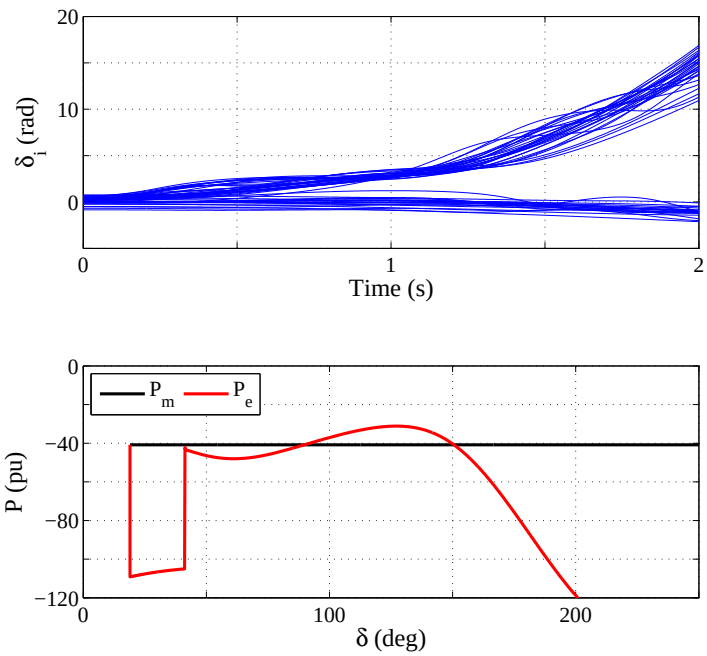

Figure 6.11: IEEE 145-bus system - Case B. Generator rotor angles and OMIB $P-\delta$ curves for the base case.

The proposed TSC-OPF method stabilizes Case B in three iterations. The OMIB parameters and the total cost of shifting generation for the stable system is tabulated in the third row (Sim. #3) of Table 6.10. Fig. 6.12 shows the stable rotor angles and the OMIB $P-\delta$ curves for Case B, stabilized by the proposed technique.

Table 6.10: TSC-OPF calculations for IEEE 145-bus Case B

Sim. #	P_{eC} **(MW)**	δ **(deg)**	δ_r **(deg)**	δ_u **(deg)**	η **(pu.rad)**	η_{max} **(pu.rad)**	**Cost ($/h)**
1	19361.43	18.99	-	150.46	-23.097	5.06	0.00
2	18393.36	11.42	-	164.92	-5.346	4.89	10415.47
3	17723.25	5.63	133.85	152.28	4.301	4.77	17957.69

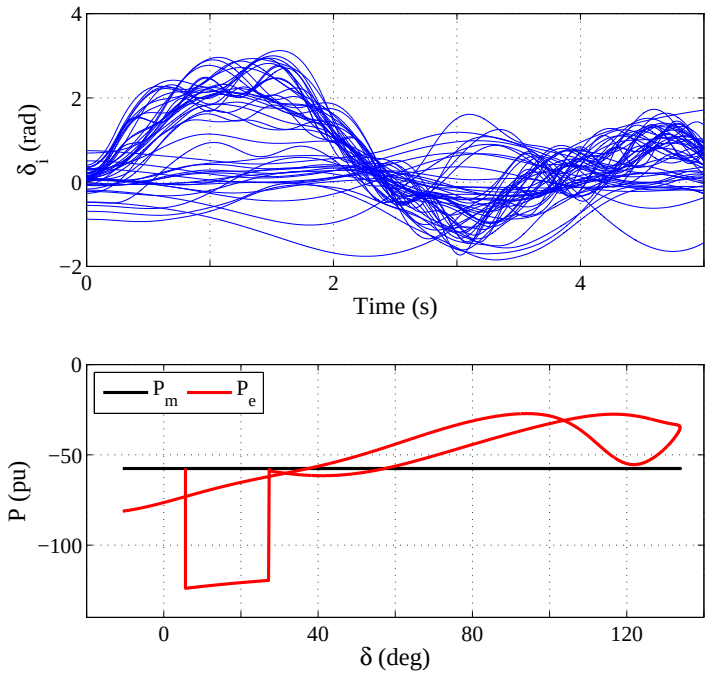

Figure 6.12: IEEE 145-bus system - Case B. Stable rotor angles and OMIB P-δ curves obtained for the third iteration.

6.2.4 Summary Of Results And Observations

An improved, yet relatively simple, technique for solving TSC-OPF problem is developed in this dissertation. The proposed method uses SIME to transform dynamic and transient stability constraints of the multi-machine power system into a single stability constraint. The quasi-linear relationship between critical machines power and stability margin is explored to develop a systematic approach to stabilize an unstable system. The use of critical machines power as a transient stability constraint enables the use of conventional OPF tools without any modification. The use of SIME

and of a conventional OPF tool imply that robust commercial tools can be used to implement the proposed method. This makes the proposed TSC-OPF technique ideal for real-time application.

Various test cases discussed in the chapter show the robustness of the proposed method. The TSC-OPF costs calculated are economical as compared to other methods found in the literature. The proposed TSC-OPF technique can be used as a dispatching and redispatching tool is demonstrated with the test cases.

6.3 Test Cases For Generation Shedding Dynamic RAS

This section provides the test cases and results for the proposed OPF-based generation-shedding RAS discussed in Section 4.3. The simulation results on the IEEE 9-bus, 8-machine system, the IEEE 39-bus, 16-machine system, and the IEEE 145-bus, 50-machine system demonstrate the robustness of the proposed generation shedding scheme. The IEEE 9-bus, 8-machine system, the IEEE 39-bus, 16-machine system are tested on the real-time Hardware-In-the-Loop (HIL) simulation platform described in Section 5. SIME calculations are carried out using PST software [81] and a MATLAB script. All loads are modeled as constant impedance in the time-domain simulation and as constant power in the OPF calculation. OPF algorithm for computing generation-shedding cost is solved using MATPOWER [82].

6.3.1 IEEE 9-Bus, 8-Machine System

To demonstrate the importance of online transient stability analysis on RAS, generation shedding dynamic RAS is tested on the IEEE 9-bus, 8-machine test industrial power system shown in Fig. A.2. The test system consists of 7 generators, 3 load buses, and is connected to the utility through two transmission lines. The generator and power system data are taken from [35]. Generators Gen21-Gen24 and Gen31-Gen33 are identical in construction and have the same parameters. All generators use the IEEE DC1 exciter and IEEE TGOV1 governor models, which are listed in Appendix

A.1 and Appendix A.2 respectively. Gen1 is operated as the swing generator. The test system is implemented in the real-time test platform, and power-system state information (generator voltage, active and reactive power, load active and reactive power, system configuration) is sent to the MATLAB based TSA and RAS determination tool, which computes remedial actions and updates the RAS logic controller. The cost associated with generation shedding is not considered for this test system. When the RAS logic controller detects unstable contingencies, it trips pre-assigned generator(s) to stabilize the system. For stable contingencies, no remedial action is taken. The contingency of interest is a 3-phase fault on Bus 7 and is cleared by tripping the Line 7-5 after 0.1s. The generation-tripping RAS action is applied 0.1s after the Line 7-5 opens. As noted previously, typical static RAS action can be overly conservative in some cases depending upon the actual operating conditions within the system. To demonstrate this, and the effectiveness of online updates, several test cases have been considered. These test cases are as follows:

- Static RAS Base Case (Case A)
- RAS Sensitivity to Generator Active Power (P)
  - 5% increase in Gen21-Gen24 P (Case B)
  - 5% decrease in Gen21-Gen24 P (Case C)
- RAS Sensitivity to Generator Voltage Magnitude ($|V|$)
  - 5% decrease in Gen1 $|V|$ (Case D)
  - 3% decrease in Gen21-Gen24 $|V|$ (Case E)

Since the proposed dynamic RAS is based on online computation of stability margins, remedial action can change from a two-generators trip, to one generator trip, to no control action, as a result of a change in power system conditions.

6.3.1.1 IEEE 9-Bus System - Case A: Static RAS Base Case

This case represents a base static RAS scenario in response to a 3-phase fault applied on Line 7-5. This contingency drives the test system to instability if no remedial action is taken. Fig. 6.13 shows the OMIB $P - \delta$ curve with negative stability margin and diverging rotor speed curves for this unstable contingency. In a static RAS scenario, the Gen21 tripping RAS action would be determined offline for this contingency. With Gen21 tripped, the stability margin becomes positive and machine rotor speeds stabilize (except for the tripped generator, ω_{21}), as shown in Fig. 6.14.

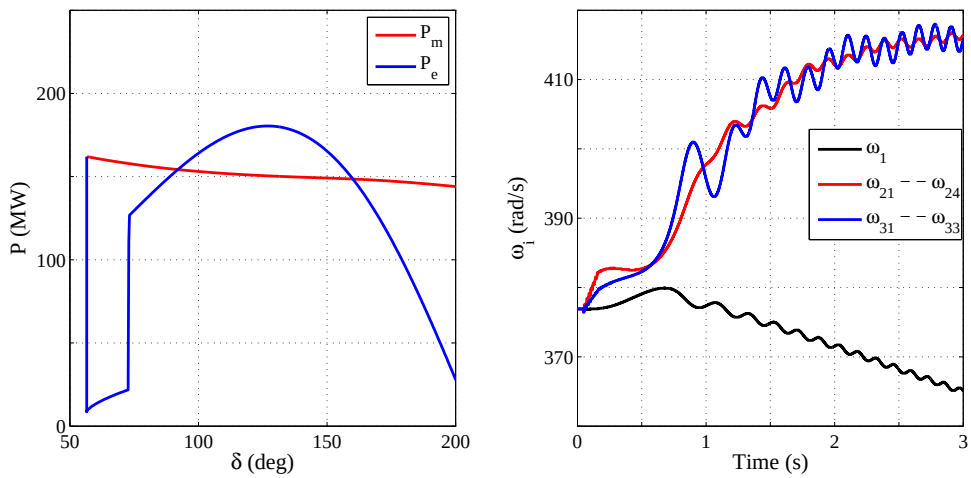

Figure 6.13: OMIB $P - \delta$ curve and generator speed curves for Test Case A without remedial action. The contingency drives the system to instability.

6.3.1.2 IEEE 9-Bus System - Case B And C: RAS Sensitivity To Generator P

In Case B, the P of Gen21-Gen24 is increased by 5% from the base case and the generator voltage and loads are kept the same. As the system operating condition changes, stability margin and RAS control actions are affected. The TSA tool detects the change in power system states and computes stability margin. With a 5% increase in Gen21-Gen24 P, stress in the system increases. As a result, the Gen21 tripping remedial action is no longer enough to stabilize the system. This is indicated by

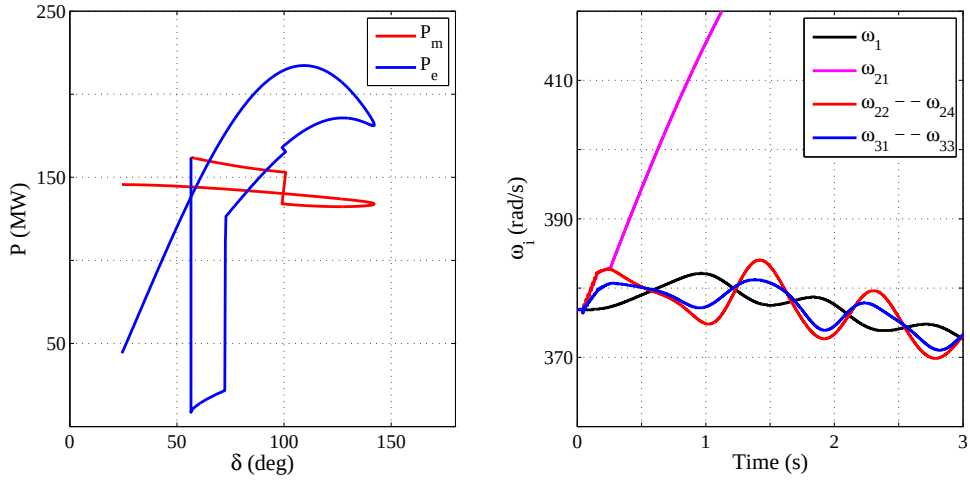

Figure 6.14: OMIB $P - \delta$ curve and generator speed curves for Test Case A with Gen21 trip remedial action. The remedial action stabilizes the system.

the negative stability margin and diverging rotor speeds in Fig. 6.15. With a few time-domain simulation and the stability margin calculations, the tool determines the remedial action of Gen21 and Gen22 trip to stabilize the system. Fig. 6.16 shows the OMIB $P - \delta$ curve and rotor speed curves with Gen21 and Gen22 trip remedial action. Hence, a 5% increase in Gen21-Gen24 P from Case A requires additional generator tripping to stabilize the system.

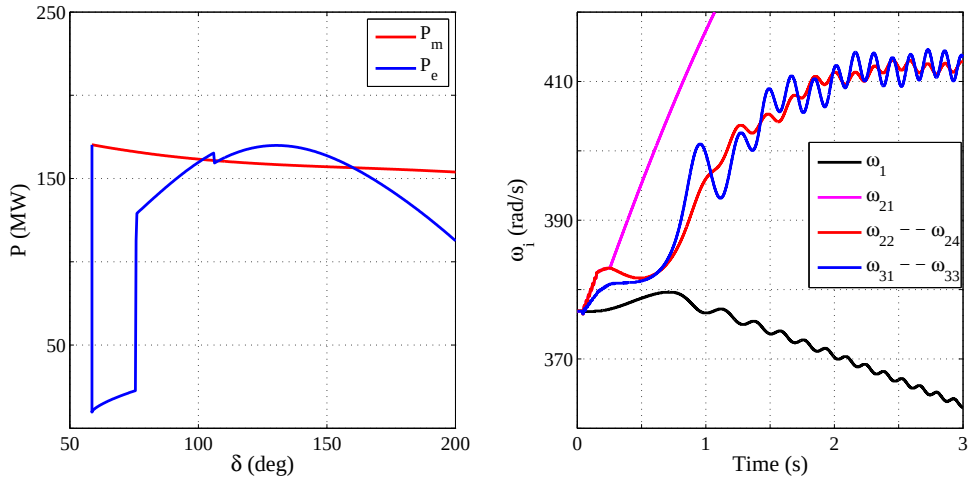

Figure 6.15: OMIB $P - \delta$ curve and generator speed curves for Test Case B (5% increase in Gen21-Gen24 P) with Gen21 trip remedial action.

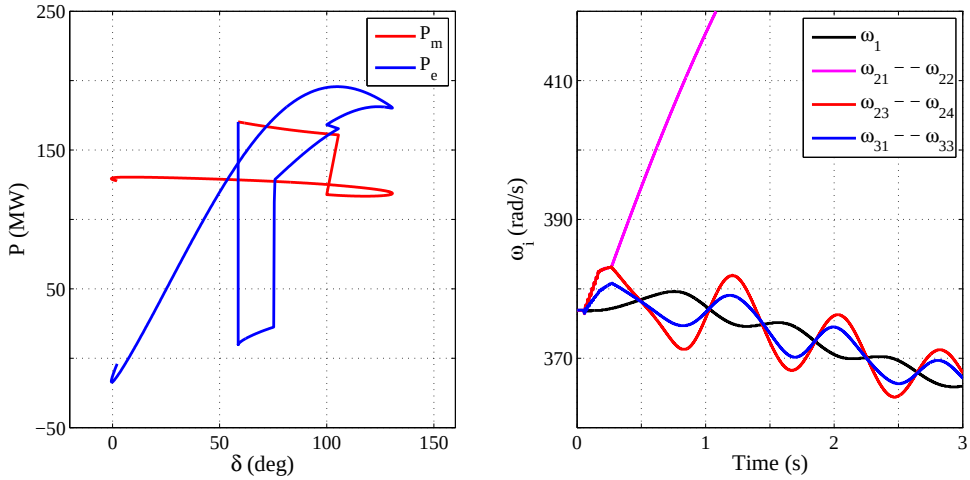

Figure 6.16: OMIB $P - \delta$ curve and generator speed curves for Test Case B (5% increase in Gen21-Gen24 P) with Gen21-Gen22 trip remedial action. Additional generator trip is needed to stabilize the system.

In Case C, the system is operated with Gen21-Gen24 active power decreased by 5% from Case A. Gen1 increases its P to balance the deficit. This change in operating condition reduces stress from the system. As a result, for the same contingency, the stability margin changes from negative to positive without any remedial action. The OMIB $P - \delta$ curve and rotor speed curves are shown in Fig. 6.17. Test Cases B and C demonstrate the stability margins sensitivity to P.

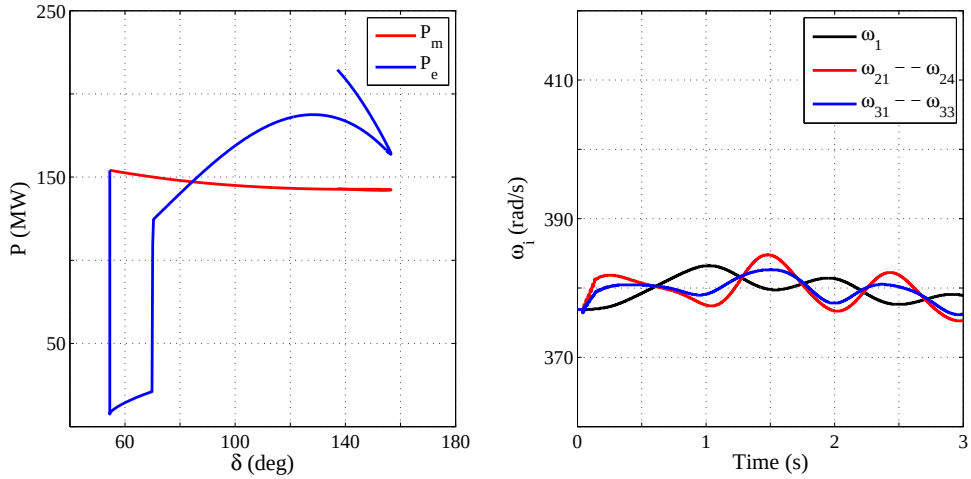

Figure 6.17: OMIB $P - \delta$ curve and generator speed curves for Case C (5% decrease in Gen21-Gen24 P). The system is stable and no remedial action is needed.

6.3.1.3 IEEE 9-Bus System - Case D And E: RAS Sensitivity To Generator $|V|$

In Case D, Gen1 |V| is reduced by 5% from Test Case A. Reduction in $|V|$ reduces the system stress. For the same contingency, the system is stable and no remedial action is needed. This is indicated by the positive stability margin in the $P-\delta$ curve and stable rotor speed plots in Fig. 6.18. In Case E, Gen21-Gen24 $|V|$ is reduced by 3% from Case A. With reduced voltage support at Gen21-Gen24 buses, the system is further stressed. Remedial action of Gen21 trip, which stabilized Case A, is no longer enough for system stability (Fig. 6.19). The negative stability margin and diverging rotor speed curves show loss of stability for the given contingency followed by Gen21 trip.

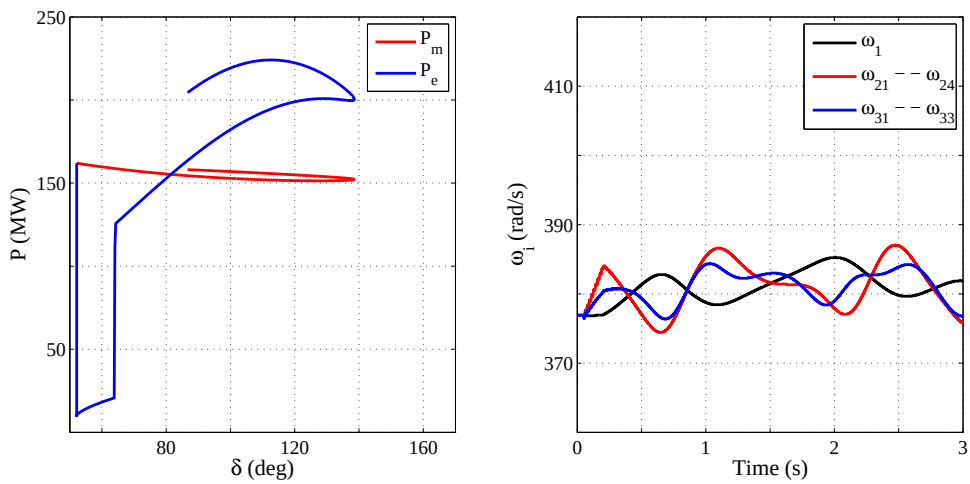

Figure 6.18: OMIB $P-\delta$ curve and generator speed curves for Case D (5% decrease in Gen1 $|V|$). The system is stable and no remedial action is needed.

6.3.2 IEEE 39-Bus, 16-Machine System

Fig. A.4 shows the modified IEEE 39-bus, 16 machine test power system used for testing the proposed OPF-based generation shedding RAS. The test system consists of 10 power plants. Generators connected at Bus 19, 20, 22, and 23 are split into smaller units of equal rating. The parameters for the test system are taken from [84]. Each generator is equipped with IEEE TGOV1 governor model, IEEE type ST1

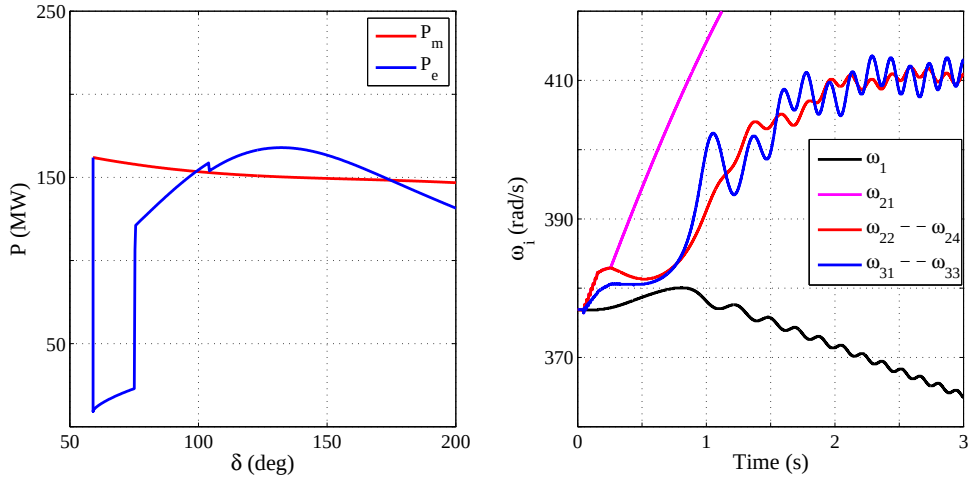

Figure 6.19: OMIB $P-\delta$ curve and generator speed curves for Case E (3% decrease in Gen21-Gen24 $|V|$). The system is unstable even with Gen21 tripping.

excitation system, and IEEE type 2 PSS, which are tabulated in Appendix A.4. The test power system is stressed by increasing the loads at Bus 18, 25, 26, 27, 28, and 29 by 45% from the base case. This system is implemented in the real-time Hardware-In-the-Loop (HIL) simulation platform developed in the Duke Energy Smart Grid Laboratory at UNC Charlotte [30]. The OPF problem is solved using MATPOWER software package [82]. For this test system, a single-element contingency is modeled as a 3-phase fault on a single line between Bus 16-17 near Bus 16. For a multiple-element contingency, a 3-phase fault on both lines between Bus 16-17 is considered. For both contingencies, the fault is cleared after 0.1s and the RAS actions are applied 0.1s after the line opens. The selection of generator(s) to shed for two test cases with different generator cost functions and the same multiple element contingency is shown in the next subsection.

6.3.2.1 IEEE 39-Bus System - Case A: Generator Cost Function I

The power plant MW rating and generator fuel cost for Case A are shown in Table 6.11. The maximum and minimum reactive power output of each power plant are fixed at ± 750 MVAr. The maximum and minimum voltage magnitude of each

bus are fixed at 1.05 and 0.95 p.u. respectively. Similarly, the MVA rating of all transmission lines and transformers are set to 1000 MVA. The optimal loading of each generator and total pre-RAS OPF cost for Case A are also included in Table 6.11.

Table 6.11: Plant cost function I and optimal loading for IEEE 39-bus system - Case A

Power Plant	**Rating (MW)**	**Cost Function ($/h)**	**OPF Result (MVA)**
1	1000	$0.0193P^2+6.9P$	271.63-j4.79
2	1000	$0.0111P^2+3.7P$	616.09+j367.22
3	1000	$0.0104P^2+2.8P$	694.84+j273.15
4	1000	$0.0088P^2+4.7P$	(229.68+j47.18)x3
5	1000	$0.0128P^2+2.8P$	(182.60+j52.08)x3
6	1000	$0.0094P^2+3.7P$	(354.01+j123.84)x2
7	1000	$0.0099P^2+4.8P$	(305.91+j39.44)x2
8	1000	$0.0113P^2+3.6P$	595.31+j104.11
9	1000	$0.0071P^2+3.7P$	929.17+j96.98
10	1200	$0.0064P^2+3.9P$	1060.41+j49.76
Pre-RAS OPF Cost ($/h)			**70,571.50**

Using the OPF result, the test power system is initialized and time-domain simulations of the single-element and the multiple element contingencies discussed above are conducted. Fig. 6.20 shows the generator rotor angles for both contingencies. The system is stable for loss of a single line, but is unstable for loss of both lines. For the unstable case, the rotor angle plot shows that the system separates into the group of critical and non-critical generators. The SIME tool identifies 10 generators G41-G43, G51-G53, G61-G62, and G71-G72 as critical generators. It is assumed that all critical generators are capable of executing generation-shedding remedial actions. To stabilize the system, some of the critical generators should be shed. Identification of the critical generators greatly aids in the development of the generation-shedding RAS.

Table 6.12 lists 10 practical generation-shedding RAS choices based on the critical

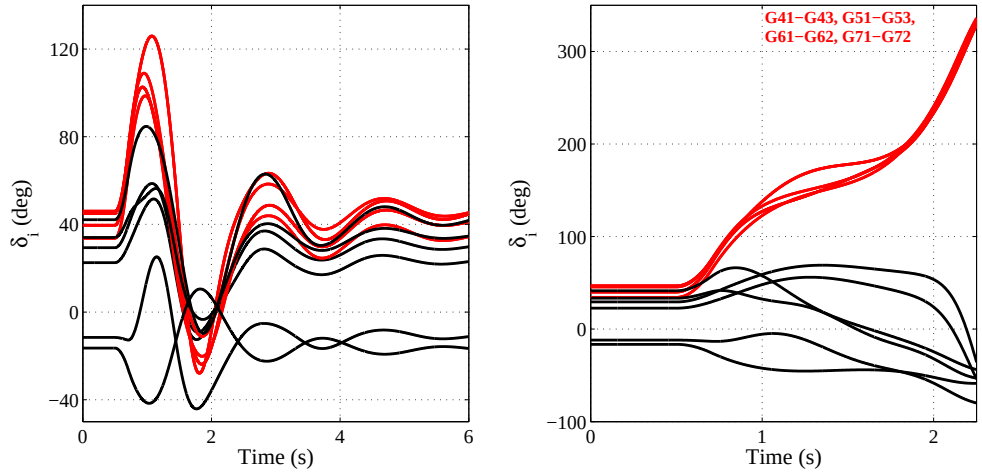

Figure 6.20: (a) Generator rotor angles for 3-phase fault on a single line between Bus 16-17. (b) Generator rotor angles for 3-phase fault on both lines. The system is stable for the first case and is unstable for the second case.

generators identified by the SIME tool. Next, the post-RAS OPF cost is calculated by removing both lines from the system, shedding the generator(s) from the RAS choice, and running OPF calculation. Post-RAS OPF cost and generation-shedding cost for Case A are tabulated in ascending order in Table 6.12. From Table 6.12, it can be seen that the minimum-cost RAS action is to shed G51. Therefore, the tool would next compute the stability margin of the unstable contingency followed by G51 generation-shedding RAS action.

Fig. 6.21 shows the OMIB P-δ and rotor angles for G51 RAS choice. The stability margin is positive and none of the stability limits are violated. Similarly, Fig. 6.22 shows the OMIB $P - \delta$ and rotor angles for G41 RAS choice. Shedding of generator G41 does not stabilize the system. Since the selected G51 RAS choice is stable, it is not necessary to conduct transient stability assessment of other RAS choices. The 'Transient Stability' results in Table 6.12 are tabulated just for reference. It is noted that for Case A, G51 generation-shedding RAS choice corresponds to the minimum generation-shedding cost as well as minimum amount of generation to shed for stable operation. For the same contingency, the RAS choice is updated upon change in

Table 6.12: Generation-shedding cost For IEEE 39-bus system - Case A ($/h)

RAS Choice	MW Shed (MW)	Post-RAS OPF Cost ($/h)	Gen Shed Cost ($/h)	Transient Stability
G51	**182.60**	**72,065.60**	**1494.10**	**Stable**
G41	229.68	72,193.10	1621.60	Unstable
G71	305.91	72,680.40	2108.90	Stable
G61	354.01	73,198.40	2626.90	Stable
G51, G52	365.20	73,446.20	2874.7	Stable
G41, G42	459.36	73,765.70	3194.20	Unstable
G71, G72	611.82	74,885.00	4313.50	Unstable
G51, G52, G53	547.80	74,942.10	4370.60	Stable
G41, G42, G43	689.04	75,544.70	4973.20	Unstable
G61, G62	708.02	76,040.70	5469.20	Unstable

system operating point and generator cost functions.

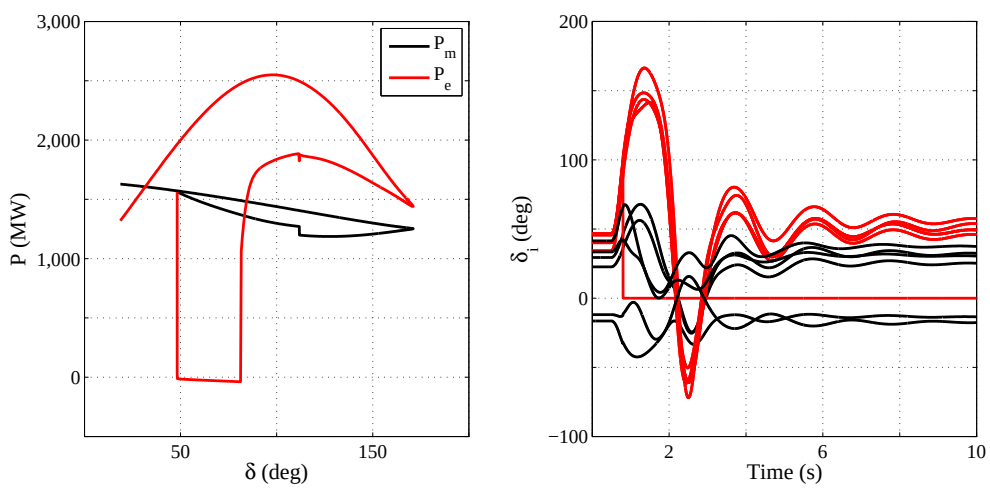

Figure 6.21: OMIB $P - \delta$ curve and generator rotor angles for G51 RAS choice. Shedding generator G51 stabilizes the system.

6.3.2.2 IEEE 39-Bus System - Case B: Generator Cost Function II

In Case B, the generator cost functions from Case A are slightly modified. All other parameters remain unchanged. The generator cost functions, optimal loading of generators, and pre-RAS OPF cost for Test Case B are shown in Table 6.13.

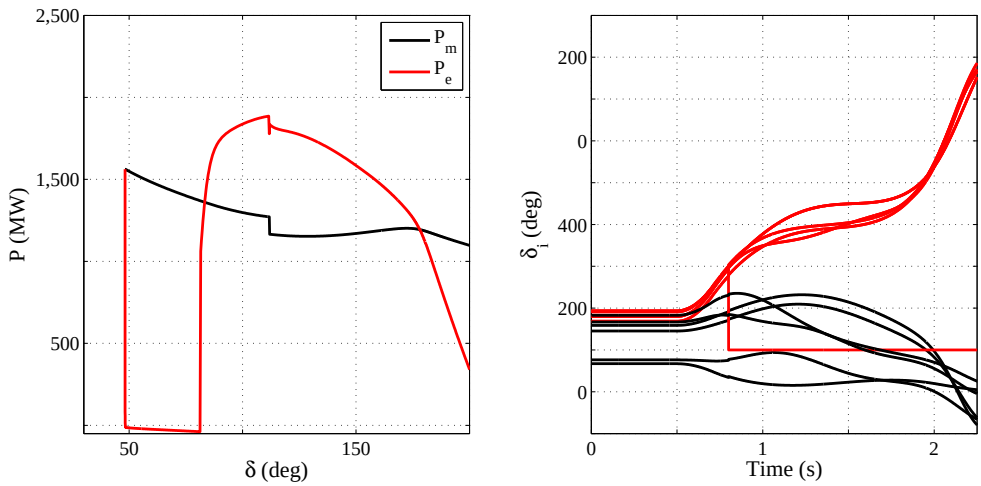

Figure 6.22: OMIB $P - \delta$ curve and generator rotor angles for G41 RAS choice. Shedding generator G41 does not stabilize the system.

Fig. 6.23 shows the OMIB $P - \delta$ curve for both contingencies. The system is stable for loss of a single line, but unstable for loss of both lines.

Table 6.13: Plant cost function II and optimal loading for IEEE 39-bus system - Case B

Power Plant	**Rating (MW)**	**Cost Function ($/h)**	**OPF Result (MVA)**
1	1000	$0.0153P^2+5.9P$	346.31+j14.72
2	1000	$0.0101P^2+2.7P$	681.78+j381.09
3	1000	$0.0094P^2+1.8P$	773.80+j303.94
4	1000	$0.0108P^2+1.7P$	(220.92+j43.93)x3
5	1000	$0.0108P^2+3.2P$	(197.43+j56.42)x3
6	1000	$0.0080P^2+2.8P$	(418.52+j129.24)x2
7	1000	$0.0104P^2+6.7P$	(227.18+j27.93)x2
8	1000	$0.0093P^2+3.6P$	680.11+j127.79
9	1000	$0.0091P^2+3.7P$	700.78+j49.16
10	1200	$0.0064P^2+3.9P$	993.35+j49.51
Pre-RAS OPF Cost ($/h)			**66,130.60**

The RAS choice, MW shed, post-RAS OPF cost, and generation-shedding cost for Case B are tabulated in Table 6.14. Fig. 6.24 shows the OMIB $P - \delta$ and generator

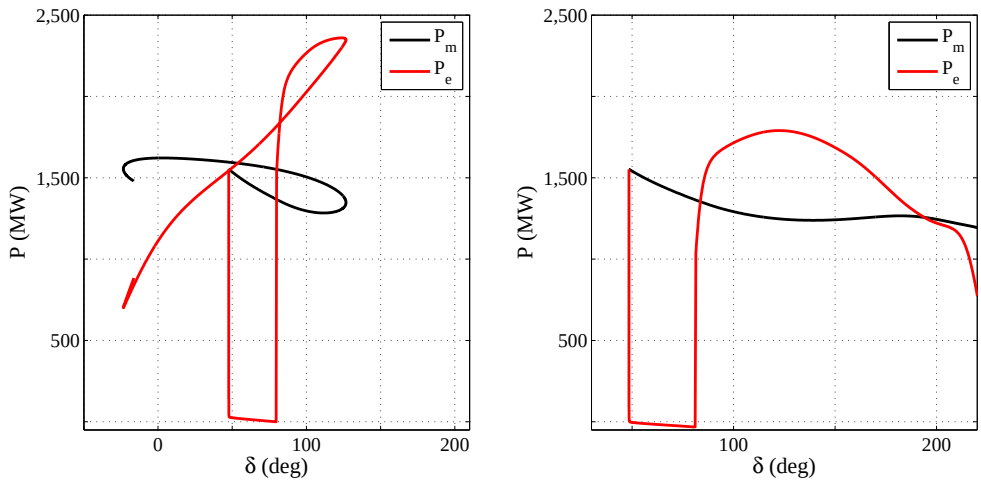

Figure 6.23: OMIB $P-\delta$ curves for 3-phase fault on a single and double lines between Bus 16-17. The system is stable for the first case and is unstable for the second case.

rotor angles for the G71 RAS choice. The RAS choice of G71 results in a stable system with minimum generation-shedding cost. It is noted that the MW shed during G71 generation shedding is greater than the G51. This shows that shedding minimum generation for system stability might not always be the most economical choice.

Table 6.14: Generation-shedding cost For IEEE 39-bus System - Case B ($/h)

RAS Choice	**MW Shed (MW)**	**Post-RAS OPF Cost ($/h)**	**Gen Shed Cost ($/h)**	**Transient Stability**
G71	**227.18**	**67,452.70**	**1322.10**	**Stable**
G51	197.43	67,646.50	1515.90	Stable
G41	220.92	67,969.10	1838.50	Unstable
G71, G72	454.36	68,674.60	2544.00	Unstable
G51, G52	394.86	69,021.70	2891.10	Stable
G61	418.52	69,275.20	3144.60	Stable
G41, G42	441.84	69,695.60	3565.00	Unstable
G51, G52, G53	592.29	70,524.80	4394.20	Stable
G41, G42, G43	662.76	71,582.80	5452.20	Unstable
G61, G62	837.04	72,729.10	6598.50	Unstable

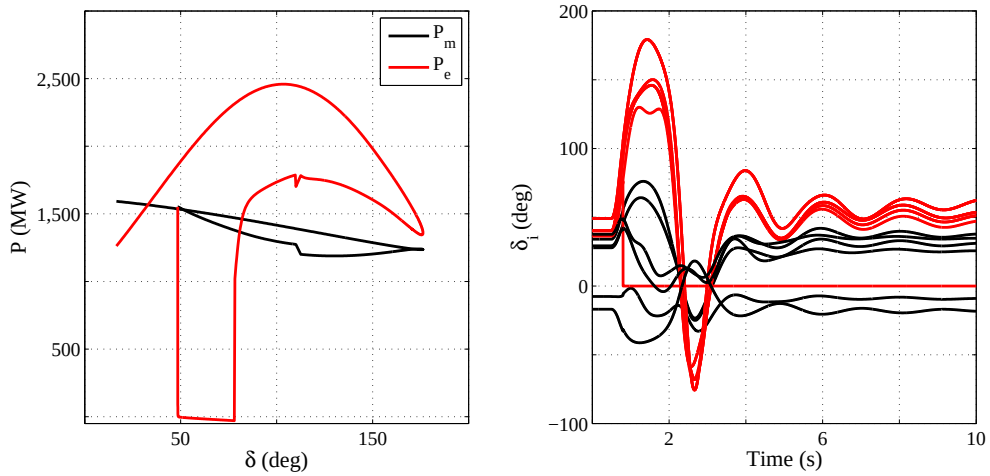

Figure 6.24: OMIB P-δ curve and generator rotor angles for G71 RAS choice. Shedding generators G71 stabilizes the system.

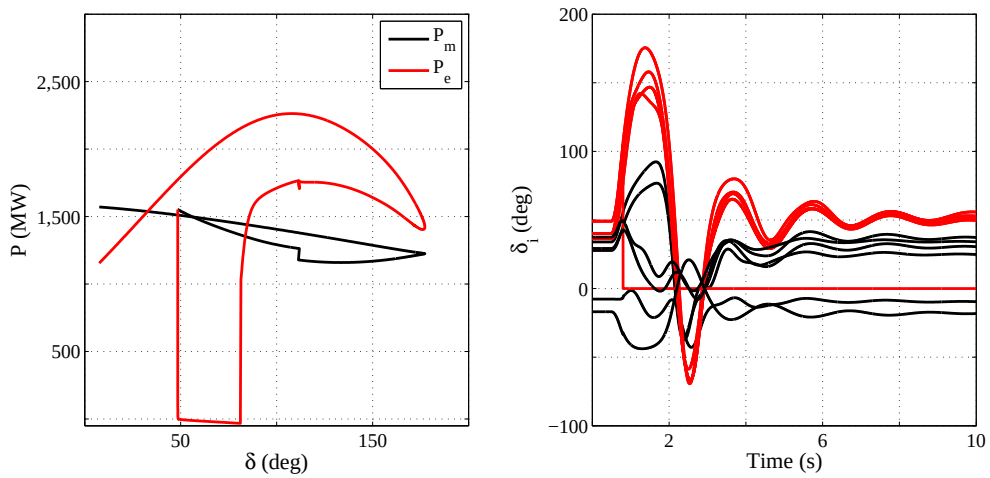

Figure 6.25: OMIB P-δ curve and generator rotor angles for G51 RAS choice. Shedding generators G51 stabilizes the system.

6.3.3 IEEE 145-Bus, 50-Machine System

The proposed OPF-based generation shedding RAS is also tested on IEEE 145-bus, 50-machine system. The power system model and the parameters for the test system is shown in Appendix A.5. Due to the size of the test power system and the physical limitation of the real-time Hardware-In-The-Loop (HIL) simulation platform, the test system is tested using offline simulation. The time-domain simulation is carried

out using the PST toolbox and the OPF problem is solved using the MATPOWER package.

The base case power flow solution is assumed as the result of a market clearing procedure. The generation-shedding cost is calculated using (XX). The prices offered by the generator to increase or decrease its active power, r_{Gi}^{up} and r_{Gi}^{down}, are assumed to be \$10/MW. The lower and upper limits of all bus voltage magnitudes are set at 95% and 105% of the base power flow solution, respectively. The generator active and reactive power limits, and the lines thermal limit are taken from MATPOWER test file [82].

For IEEE 50 Generator 145 Bus System Test Case 3 (fault on Bus 25, and and both lines removed between Bus 25 and Bus 12 after 0.205 seconds), the Critical Generators are: G1-G17, G19-G27, G33-G35.

6.3.3.1 IEEE 145-Bus System - Case A

In Case A, a single-element contingency is modeled as a 3-phase fault on the Bus 25 and the fault is cleared by opening a single line between Bus 25-12. Similarly, for a multiple-element contingency, a 3-phase fault on the Bus 25, followed by tripping of both lines between Bus 25-12 is considered. For both contingencies, the fault is cleared after 0.205s and the RAS actions are applied 0.1s after the line opens. The generator rotor angles for the single- and multiple-element contingency is shown in Fig. 6.26. The test system is stable for the loss of one line between Bus 25-12, and unstable for the loss of both lines. To stabilized the system against loss of two lines, a generation shedding remedial action is needed.

For the unstable contingency, the SIME tool identified 29 generators as critical machines. These critical machines are the machines at Bus 60 (G1), 67 (G2), 79 (G3), 80 (G4), 82 (G5), 89 (G6), 90 (G7), 91 (G8), 93 (G9), 94 (G10), 95 (G11), 96 (G12), 97 (G13), 98 (G14), 99 (G15), 100 (G16), 101 (G17), 103 (G18), 104 (G19), 105 (G20), 106 (G21), 108 (G22), 109 (G23), 110 (G24), 111 (G25), 112 (G26), 121 (G27), 122

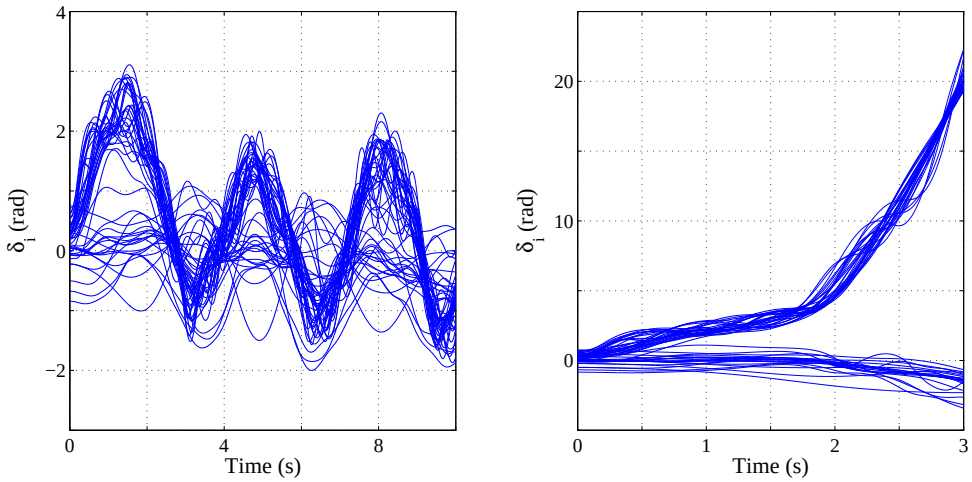

Figure 6.26: (a) Generator rotor angles for 3-phase fault on a single line between Bus 25-12. (b) Generator rotor angles for 3-phase fault on both lines. The system is stable for the first case and is unstable for the second case

(G28), and 124 (G29). Out of 29 critical machines, we assume the generators G2, G9, G13, G15, G20, G21, G22, G23, G25, G26, G27, G33, G34, and G35 are equipped with control system for generation shedding RAS. Using the proposed generation-shedding RAS technique, the cost associated with tripping each critical generator with generation shedding capability is calculated. Table. 6.15 tabulates the generation shedding cost and MW shed associated with each generation shedding RAS choice.

Fig. 6.27 shows the OMIB $P - \delta$ curve and generator rotor angles for G15 RAS choice. G15 RAS choice results in the minimum generation-shedding cost. However, the G15 RAS choice is unable to stabilize the system. Similarly, the next two RAS choices, G13 and G23, also result in unstable system.

Fig. 6.28 shows the OMIB $P-\delta$ and generator rotor angles for the G34 RAS choice. Similarly, the OMIB $P-\delta$ and generator rotor angles for the G9 RAS choice is shown in Fig. 6.29. Both RAS choices result in stable system. The generation shedding cost associated with G34 RAS choice is the minimum among RAS choices that results in the stable system. It is noted that the MW shed during G34 generation shedding is greater than the G9. This shows that shedding minimum generation for system

Table 6.15: Generation shedding cost For IEEE 145-bus system ($/h)

RAS Choice	MW Shed (MW)	Gen Shed Cost ($1000/h)	Transient Stability
G15	200	3.6	Unstable
G13	140	32.4	Unstable
G23	800	33.1	Unstable
G34	**1009**	**33.4**	**Stable**
G2	1486	49.6	Stable
G27	300	65.8	Unstable
G9	700	71.1	Stable
G20	2005	102.5	Stable
G22	1080	112.5	Stable
G35	3005	176.8	Unstable
G33	2997	214.9	Unstable
G21	1620	635.1	Stable
G25	700	865.8	Unstable
G26	2005	3960.6	Stable

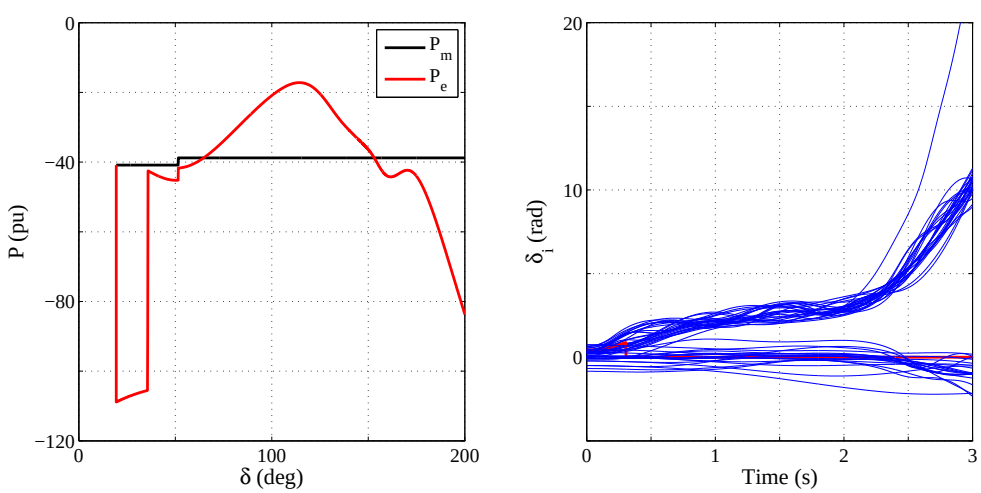

Figure 6.27: OMIB P-δ curve and generator rotor angles for G15 RAS choice. Shedding generator G15 does not stabilize the system.

stability might not always be the most economical choice.

Next, the G34 RAS choice is uploaded to the RAS logic controller. If the multiple-element contingency described above occurs, the RAS logic controller trips generator

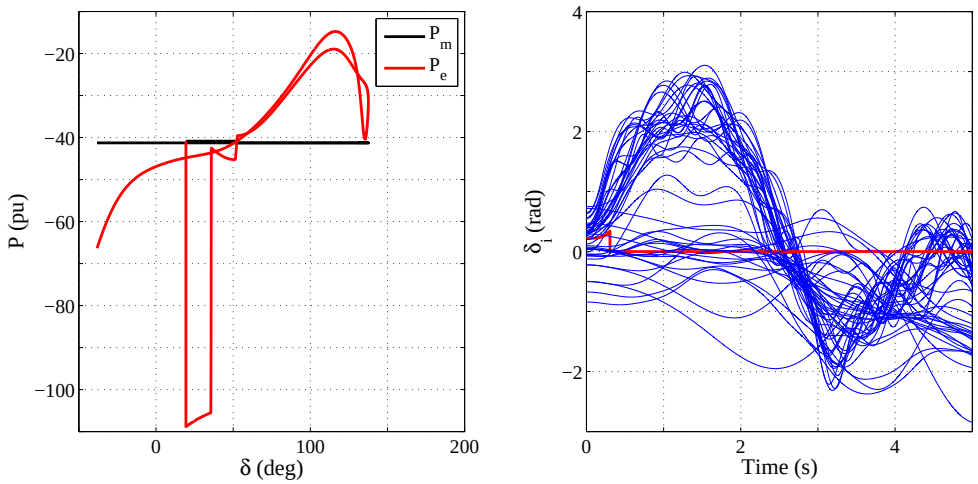

Figure 6.28: OMIB P-δ curve and generator rotor angles for G34 RAS choice. Shedding generator G34 stabilizes the system.

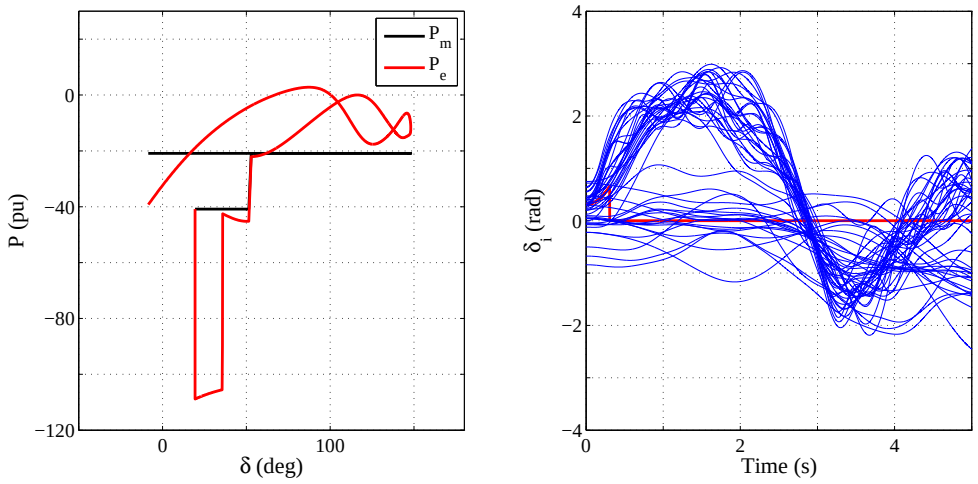

Figure 6.29: OMIB P-δ curve and generator rotor angles for G9 RAS choice. Shedding generator G9 stabilizes the system.

G34 to stabilize the system. The RAS choice is recalculated upon the change in generator market clearing price and change in power system states.

6.3.4 Summary Of Results And Observations

The test results from IEEE 9-bus, 8-machine system demonstrate the need for online transient stability calculations to determine remedial actions. Test results show the variability of the generation shedding RAS choice with power system operating

condition for the same unstable contingency. Dynamic RAS which combines wide-area monitoring system and fast transient stability analysis can adapt to any change in power system operating condition and system configuration.

The effectiveness of the proposed OPF-based generation shedding RAS is demonstrated by the test results of IEEE 39-bus and IEEE 145-bus system. The criteria for selecting generators to trip is based on the minimum cost rather than minimum amount of generation to shed. For an unstable Category C contingency, the RAS control action that results in stable system with minimum generation shedding cost is selected among possible candidate solutions. Selection of generators to shed based on cost can be particularly attractive in the deregulated power industry, where economics dictate both the operation and control of the power system. The RAS control actions update whenever there is a change in operating condition, system configuration, or cost functions.

CHAPTER 7: CONCLUSIONS

This chapter summarizes the research conducted in this thesis and presents the concluding remarks. The main contributions of this work are listed and several opportunities for future research are suggested.

7.1 Concluding Remarks

In North America, the power systems are planned and operated to withstand the loss of any single or multiple elements without violating North American Electric Reliability Corporation (NERC) system performance criteria. For a contingency resulting in the loss of a single element (Category B), the power system must remain stable with all equipment loaded to within its normal operating limits. Similarly, for a contingency resulting in the loss of multiple elements (Category C), emergency transient stability controls like load shedding, generation shedding, or curtailment of contracted power may be necessary to stabilize the power system. In this thesis, procedures to assist system operators to overcome problems related to NERC Category B and Category C contingencies are developed. A new TSC-OPF technique is proposed to withstand Category B contingency and a dynamic generation shedding RAS is developed to withstand Category C contingency.

An improved, yet relatively simple, method for solving TSC-OPF problem is proposed. Using SIngle Machine Equivalent (SIME) technique, the multi-machine power system model is reduced to a One-Machine Infinite Bus (OMIB) equivalent to compute stability margin. Use of SIME technique allows to consider complex power system models in the stability study. The quasi-linear behavior of the OMIB stability margin and critical machine(s) active power is explored to formulate the transient

stability constraint. Since the stability constraint is based on the OMIB equivalent, the multi-machine system's dynamic and stability constraints are reduced to a single, time independent constraint. This single stability constraint is formulated as a limit on the sum of critical machines' active power, as opposed to on the OMIB rotor angle, avoiding the addition of the generator stator algebraic equations in the OPF formulation and enabling the use of conventional OPF. The proposed method shifts critical machines active power based on generator costs using an OPF algorithm. Moreover, the transient stability limit is based on stability margin, and not on a heuristically set limit on OMIB rotor angle. As a result, the proposed TSC-OPF solution is more economical and transparent. The proposed technique enables the use of fast and robust commercial OPF tool and time-domain simulation software for solving a large scale TSC-OPF problem, which makes the proposed method also suitable for real-time application. The effectiveness of the proposed technique is demonstrated by simulation on the IEEE 9-bus, 3-machine system, IEEE 39-bus, 10-machine system, and IEEE 145-bus, 50-machine system.

A new generation shedding technique based on the dynamic RAS is proposed. This scheme uses online stability calculations and generator cost functions to determine appropriate remedial actions. Unlike conventional RAS, which are designed using offline simulations, online stability calculations make the proposed technique dynamic and adapting to any power system configuration and operating state. The generation-shedding cost is calculated using pre-RAS and post-RAS OPF costs. The criteria for selecting generators to trip is based on the minimum cost rather than minimum amount of generation to shed. For an unstable Category C contingency, the RAS control action that results in stable system with minimum generation shedding cost is selected among possible candidate solutions. The RAS control actions update whenever there is a change in operating condition, system configuration, or cost functions. The robustness of the proposed technique is demonstrated by simulation

on the IEEE 9-bus, 8-machine system, IEEE 39-bus, 16-machine system, and IEEE 145-bus, 50-machine system.

A real-time hardware-in-the-loop test platform is designed and developed specifically for validation and testing of the proposed dynamic RAS. This setup allows one to include all of the necessary hardware for control, measurement, communications, and protection. The test platform consists of multiple Real Time Digital Simulators (RTDS), multiple PMUs, a protocol gateway, and a MATLAB-based controller. The real-time platform is suitable for the design, testing, and validation of both continuous and discontinuous wide-area controllers.

7.2 Summary of Research Contributions

The main contributions of this thesis are summarized below:

1. Formulation of an improved, yet relatively simple, technique for solving Transient Stability-Constrained Optimal Power Flow (TSC-OPF) problem for generation dispatch and redispatch procedures. The transient stability constraint is formulated by exploring the quasi-linear behavior of the OMIB stability margin and critical machine(s) active power. The propose technique can address both first-swing and multi-swing transient instability phenomena. Specifically,

   Sub-Problem 1: An optimization problem was formulated for security dispatch.

   - Given: an unstable contingency and generator fuel cost function,
   - Determine: transient security dispatch at minimum operation cost.

   Sub-Problem 2: An optimization problem was formulated for security redispatch.

   - Given: an unstable contingency and market-clearing or spot price,
   - Determine: transient security redispatch at minimum cost difference.

2. Identification and formulation of a dynamic generation shedding remedial action scheme problem by combining online transient stability analysis and generator cost function. Specifically,

   Sub-Problem 1: An optimization problem was formulated for a vertically integrated utility.

   - Given: a list of credible contingencies and generator fuel cost function,
   - Determine: generation-shedding RAS choice with minimum generation-shedding cost.

   Sub-Problem 2: An optimization problem was formulated for a deregulated energy market.

   - Given: a list of credible contingencies and market-clearing or spot price,
   - Determine: generation-shedding RAS choice with minimum generation-shedding cost.

3. Development of the real-time hardware-in-the-loop test platform specifically for validation and testing of the proposed dynamic RAS. The real-time platform is useful for the design, testing, and validation of both continuous and discontinuous wide-area controllers.

4. Development of a fast solution for converting synchrophasor data (IEEE C37.118 format) into analog values that are readable by any controller. This allows one to thoroughly test any control solution using the most realistic system possible.

7.3 Future Work

Several suggestions and considerations for future research work are listed below.

1. In this research, generation dispatch and redispatch problems with a single contingency are considered. The proposed TSC-OPF method can be easily extended to incorporate multiple contingencies.

2. The proposed TSC-OPF technique enables the use of fast and robust commercial OPF tool and time-domain simulation software for solving large scale TSC-OPF problem, making it suitable for real-time application. Analysis of a real-world TSC-OPF problem using a commercial time-domain simulation software (e.g. DSATools) and an OPF tool (e.g. GAMS) can be investigated.

3. Minimization of total generation cost is the only objective function considered in both dynamic RAS and TSC-OPF formulation. Alternative objective functions such as maximization of available transfer capacity, minimization of active power losses, minimization of both active and reactive costs etc. can be investigated.

4. In this thesis, only generation shedding remedial actions are investigated for the proposed dynamic RAS technique. Future research could expand the remedial actions to include several wide-area controls such as load-shedding, capacitor/reactor bank switching, SVC switching, HVDC modulation etc.

5. For an unstable contingency which requires shedding of multiple generators for stability, the current method might require several time-domain simulations to select the appropriate RAS choice. As part of the future work, methods described for example in [25,60] can be used in parallel to determine generation-shedding amount to reduce the number of time-domain simulations.

REFERENCES

[1] G. Andersson, P. Donalek, R. Farmer, N. Hatziargyriou, I. Kamwa, P. Kundur, N. Martins, J. Paserba, P. Pourbeik, J. Sanchez-Gasca *et al.*, "Causes of the 2003 major grid blackouts in North America and Europe, and recommended means to improve system dynamic performance," *Power Systems, IEEE Transactions on*, vol. 20, no. 4, pp. 1922–1928, 2005.

[2] Report on the grid disturbance on 30th July 2012 and grid disturbance on 31st July 2012. [Online]. Available: http://www.cercind.gov.in/2012/orders/Final_Report_Grid_Disturbance.pdf

[3] Western systems Coordinating Council (WSCC), Disturbance Report for the Power System Outage that Occcurred on the Western Interconnection on August 10th, 1996 at 15:48 PAST. [Online]. Available: https://www.wscc.com

[4] NERC Reliability Concepts. [Online]. Available: http://www.nerc.com/files/concepts_v1.0.2.pdf

[5] Standard TPL-003-2a: System performance following loss of two or more BES elements (Category C). [Online]. Available: http://www.nerc.com/files/TPL-003-2a.pdf

[6] D. Ruiz-Vega and M. Pavella, "A comprehensive approach to transient stability control - Part I: Near optimal preventive control," *Power Systems, IEEE Transactions on*, vol. 18, no. 4, pp. 1446–1453, Nov 2003.

[7] D. Gan, R. J. Thomas, and R. D. Zimmerman, "Stability-constrained optimal power flow," *Power Systems, IEEE Transactions on*, vol. 15, no. 2, pp. 535–540, May 2000.

[8] M. La Scala, M. Trovato, and C. Antonelli, "On-line dynamic preventive control: an algorithm for transient security dispatch," *Power Systems, IEEE Transactions on*, vol. 13, no. 2, pp. 601–610, 1998.

[9] R. Zarate-Minano, T. Van Cutsem, F. Milano, and A. J. Conejo, "Securing transient stability using time-domain simulations within an optimal power flow," *Power Systems, IEEE Transactions on*, vol. 25, no. 1, pp. 243–253, Feb. 2010.

[10] A. L. Bettiol, L. Wehenkel, and M. Pavella, "Transient stability-constrained maximum allowable transfer," *Power Systems, IEEE Transactions on*, vol. 14, no. 2, pp. 654–659, May 1999.

[11] D. Ernst, A. L. Bettiol, D. Ruiz-Vega, L. Wehenkel, and M. Pavella, "Compensation schemes for transient stability assessment and control," in *LESCOPE'98*, 1998.

[12] H. R. Cai, C. Y. Chung, and K. P. Wong, "Application of differential evolution algorithm for transient stability constrained optimal power flow," *Power Systems, IEEE Transactions on*, vol. 23, no. 2, pp. 719–728, May 2008.

[13] Y. Xu, Z. Y. Dong, K. Meng, J. H. Zhao, and K. P. Wong, "A hybrid method for transient stability-constrained optimal power flow computation," *Power Systems, IEEE Transactions on*, vol. 27, no. 4, pp. 1769–1777, 2012.

[14] A. Pizano-Martinez, C. R. Fuerte-Esquivel, and D. Ruiz-Vega, "A new practical approach to transient stability-constrained optimal power flow," *Power Systems, IEEE Transactions on*, vol. 26, no. 3, pp. 1686–1696, Aug. 2011.

[15] ——, "Global transient stability-constrained optimal power flow using an OMIB reference trajectory," *Power Systems, IEEE Transactions on*, vol. 25, no. 1, pp. 392–403, Feb. 2010.

[16] M. Pavella, D. Ernst, and D. Ruiz-Vega, *Transient Stability of Power Systems: A Unified Approach to Assessment and Control.* Norwell, MA: Kluwer, 2000.

[17] W. Ongsakul and D. N. Vo, *Artificial Intelligence in Power System Optimization.* New York: CRC Press, 2013.

[18] V. Madani, D. Novosel, S. Horowitz, M. Adamiak, J. Amantegui, D. Karlsson, S. Imai, and A. Apostolov, "IEEE PSRC report on global industry experiences with system integrity protection schemes (SIPS)," *Power Delivery, IEEE Transactions on*, vol. 25, no. 4, pp. 2143–2155, Oct 2010.

[19] P. Cholley, P. Crossley, V. Van Acker, T. Van Cutsem, W. Fu, J. Soto Idia Oez, F. Ilar, D. Karlsson, Y. Kojima, J. McCalley *et al.*, "System protection schemes in power networks," *CIGRE Technical Brochure*, 2001.

[20] WECC guideline: Remedial action scheme design guide. [Online]. Available: https://www.wecc.biz/Reliability/Remedial%20Action%20Scheme%20Design%20Guide.pdf

[21] K. Baskin, M. Thompson, and L. Lawhead, "Design and testing of a system to classify faults for a generation-shedding RAS," in *62nd Annual Conference for Protective Relay Engineers*, March 2009, pp. 140–149.

[22] M. Vaughn, R. Schloss, S. Manson, S. Raghupathula, and T. Maier, "Idaho power RAS: A dynamic remedial action case study," in *13th Annual Georgia Tech Protective Relaying Conference*, May 2010.

[23] S. M. S. R. D. Miller, R. Schloss and T. Maier, "Pacificorp's jim bridger RAS: A dual triple modular redundant case study," in *11th Annual Western Power Delivery Automation Conference*, April 2009.

[24] Savu C. Savulescu, *Real-Time Stability Assessment in Modern Power System Control Centers.* New Jersey, John Wiley & Sons, 2009.

[25] A. Fouad, A. Ghafurian, K. Nodehi, and Y. Mansour, "Calculation of generation-shedding requirements of the B. C. hydro system using transient energy functions," *Power Systems, IEEE Transactions on*, vol. 1, no. 2, pp. 17–23, May 1986.

[26] A. Shrestha, V. Cecchi, and R. W. Cox, "Transient stability-constrained optimal power flow using quasi-linear behavior of critical machines," *under review IEEE Transactions on Power Systems.*

[27] A. Shrestha, V. Cecchi, and R. W. Cox, "Minimum-cost generation-shedding for dynamic remedial action scheme," in *Power and Energy Society General Meeting, 2015 IEEE*, 26-30 July 2015, pp. 1–5.

[28] A. Shrestha, V. Cecchi, and R. W. Cox, "Optimal power flow-based generation shedding for dynamic remedial action scheme," in *Transmission and Distribution Conference and Exhibition, 2016 IEEE PES*, 1-5 May 2016, pp. 1–6.

[29] A. Shrestha, V. Cecchi, and R. W. Cox, "Dynamic generation shedding remedial action scheme using online transient stability analysis," *In preparation.*

[30] A. Shrestha, V. Cecchi, and R. W. Cox, "Dynamic remedial action scheme using online transient stability analysis," in *North American Power Symposium (NAPS)*, 7-9 Sept 2014, pp. 1–6.

[31] A. Shrestha, V. Cecchi, and R. W. Cox, "A real-time platform for validating continuous wide-area control systems," in *Innovative Smart Grid Technologies (ISGT), 2013 IEEE PES*, 2013, pp. 1–6.

[32] D. Ruiz-Vega and M. Pavella, "A comprehensive approach to transient stability control - Part II: Open loop emergency control," *Power Systems, IEEE Transactions on*, vol. 18, no. 4, pp. 1454–1460, Nov 2003.

[33] P. Kundur, *Power System Stability and Control.* New York: McGraw-Hill, 1994.

[34] P. Kundur, J. Paserba, V. Ajjarapu, G. Andersson, A. Bose, C. Canizares, N. Hatziargyriou, D. Hill, A. Stankovic, C. Taylor *et al.*, "Definition and classification of power system stability IEEE/CIGRE joint task force on stability terms and definitions," *Power Systems, IEEE Transactions on*, vol. 19, no. 3, pp. 1387–1401, 2004.

[35] P. W. Sauer and M. A. Pai, *Power System Dynamics and Stability.* Upper Saddle River, NJ: Prentice Hall, 1998.

[36] M. A. Pai, *Energy Function Analysis for Power System Stability.* Norwell, MA: Kluwer, 1989.

[37] A. A. Fouad and V. Vittal, *Power System Transient Stability Analysis Using the Transient Energy Function Method.* Englewood Cliffs, NJ: Prentice-Hall, 1992.

[38] A. H. El-Abiad and K. Nagappan, "Transient stability regions of multimachine power systems," *Power Apparatus and Systems, IEEE Transactions on*, vol. PAS-85, no. 2, pp. 169–179, Feb 1966.

[39] H.-D. Chiang, F. F. Wu, and P. Varaiya, "Foundations of the potential energy boundary surface method for power system transient stability analysis," *Circuits and Systems, IEEE Transactions on*, vol. 35, no. 6, pp. 712–728, 1988.

[40] T. Athay, R. Podmore, and S. Virmani, "A practical method for the direct analysis of transient stability," *Power Apparatus and Systems, IEEE Transactions on*, no. 2, pp. 573–584, 1979.

[41] H.-D. Chiang, F. F. Wu, and P. P. Varaiya, "A BCU method for direct analysis of power system transient stability," *Power Systems, IEEE Transactions on*, vol. 9, no. 3, pp. 1194–1208, 1994.

[42] Hsiao-Dong Chiang, *Direct Methods for Stability Analysis of Electric Power Systems: Theoretical Foundation, BCU Methodologies, and Applications.* John Wiley & Sons, 2011.

[43] G. Maria, C. Tang, and J. Kim, "Hybrid transient stability analysis," *Power Systems, IEEE Transactions on*, vol. 5, no. 2, pp. 384–393, 1990.

[44] H.-D. Chiang, J. Tong, and Y. Tada, "On-line transient stability screening of 14,000-bus models using TEPCO-BCU: Evaluations and methods," in *Power and Energy Society General Meeting, 2010 IEEE*, July 2010, pp. 1–8.

[45] H. Ota, Y. Kitayama, H. Ito, N. Fukushima, K. Omata, K. Morita, and Y. Kokai, "Development of transient stability control system (TSC system) based on on-line stability calculation," *Power Systems, IEEE Transactions on*, vol. 11, no. 3, pp. 1463–1472, Aug 1996.

[46] M. Koaizawa, M. Nakane, K. Omata, and Y. Kokai, "Actual operating experience of on-line transient stability control systems (TSC systems)," in *Power Engineering Society Winter Meeting, 2000. IEEE*, vol. 1, 2000, pp. 84–89.

[47] K. Morison, L. Wang, P. Kundur, X. Lin, W. Gao, C. He, F. Xue, J. Xu, T. Xu, and Y. Xue, "Critical requirements for successful on-line security assessment," in *Power Systems Conference and Exposition, 2004. IEEE PES*, Oct 2004, pp. 1676–1680 vol.3.

[48] J. Tong and L. Wang, "Design of a DSA tool for real time system operations," in *Power System Technology, 2006. PowerCon 2006. International Conference on.* IEEE, 2006, pp. 1–5.

[49] A. J. Wood, B. F. Wollenberg, and G. B. Sheble, *Power Generation, Operation, and Control.* New York: McGraw-Hill, 2014.

[50] J. Zhu, *Optimization of Power System Operations.* New Jersey: John Wiley & Sons, Inc., 2009.

[51] J. Condren and T. Gedra, "Expected-security-cost optimal power flow with small-signal stability constraints," *Power Systems, IEEE Transactions on*, vol. 21, no. 4, pp. 1736–1743, Nov 2006.

[52] C. Canizares, W. Rosehart, A. Berizzi, and C. Bovo, "Comparison of voltage security constrained optimal power flow techniques," in *Power Engineering Society Summer Meeting, 2001*, vol. 3, July 2001, pp. 1680–1685.

[53] T. B. Nguyen and M. A. Pai, "Dynamic security-constrained rescheduling of power systems using trajectory sensitivities," *Power Systems, IEEE Transactions on*, vol. 18, no. 2, pp. 848–854, May 2003.

[54] D. H. Kuo and A. Bose, "A generation rescheduling method to increase the dynamic security of power systems," *Power Systems, IEEE Transactions on*, vol. 10, no. 1, pp. 68–76, 1995.

[55] H. D. Chiang, F. F. Wu, and P. P. Varaiya, "Foundations of the potential energy boundary surface method for power system transient stability analysis," *Circuits and Systems, IEEE Transactions on*, vol. 35, no. 6, pp. 712–728, Jun 1988.

[56] ——, "A BCU method for direct analysis of power system transient stability," *Power Systems, IEEE Transactions on*, vol. 9, no. 3, pp. 1194–1208, Aug 1994.

[57] M. Yin, C. Y. Chung, K. P. Wong, Y. Xue, and Y. Zou, "An improved iterative method for assessment of multi-swing transient stability limit," *IEEE Transactions on Power Systems*, vol. 26, no. 4, pp. 2023–2030, Nov 2011.

[58] P. Anderson and B. LeReverend, "Industry experience with special protection schemes," *Power Systems, IEEE Transactions on*, vol. 11, no. 3, pp. 1166–1179, Aug 1996.

[59] Special protection systems (SPS) / remedial action schemes (RAS): Assessment of definition, regional practices, and application of related standards. [Online]. Available: http://www.nerc.com/docs/pc/Agenda%203.7_SPS%20Assessment%20Report_20120910.pdf

[60] H.-C. Chang and H. Chen, "Fast determination of generation-shedding in transient-emergency state," *Energy Conversion, IEEE Transactions on*, vol. 8, no. 2, pp. 178–183, Jun 1993.

[61] G. G. Karady and J. Gu, "A hybrid method for generator tripping," *Power Systems, IEEE Transactions on*, vol. 17, no. 4, pp. 1102–1107, 2002.

[62] C. R. Chen, W. T. Tsai, C. Y. Lee, and Z. F. Lin, "Sps generator tripping planning using immune algorithm," in *Intelligent System Application to Power Systems (ISAP), 2011 16th International Conference on*, Sept 2011, pp. 1–4.

[63] *User Manual: TSAT Transient Security Assessment Tool.* Powertech Labs Inc., April, 2012.

[64] A. J. Conejo, F. Milano, and R. Garcia-Bertrand, "Congestion management ensuring voltage stability," *IEEE Transactions on Power Systems*, vol. 21, no. 1, pp. 357–364, Feb 2006.

[65] Daniel Kirschen and Goran Strbac, *Fundamentals of Power System Economics.* New Jersey, John Wiley & Sons, 2004.

[66] C. W. Taylor, D. C. Erickson, K. E. Martin, R. E. Wilson, and V. Venkatasubramanian, "WACS-wide-area stability and voltage control system: R&D and online demonstration," *Proceedings of the IEEE*, vol. 93, no. 5, pp. 892–906, 2005.

[67] E. O. Schweitzer and D. E. Whitehead, "Real-world synchrophasor solutions," in *62nd Annual Conference for Protective Relay Engineers.* IEEE, 2009, pp. 536–547.

[68] E. O. Schweitzer III, D. Whitehead, A. Guzman, Y. Gong, and M. Donolo, "Advanced real-time synchrophasor applications," in *proceedings of the 35th Annual Western Protective Relay Conference, Spokane, WA*, 2008.

[69] R. Cresap, W. Mittelstadt, N. Scott, and C. Taylor, "Operating experience with modulation of the pacific HVDC intertie," *Power Apparatus and Systems, IEEE Transactions on*, no. 4, pp. 1053–1059, 1978.

[70] I. Kamwa, R. Grondin, and Y. Hébert, "Wide-area measurement based stabilizing control of large power systems-a decentralized/hierarchical approach," *Power Systems, IEEE Transactions on*, vol. 16, no. 1, pp. 136–153, 2001.

[71] C. Lu, X. Wu, J. Wu, P. Li, Y. Han, and L. Li, "Implementations and experiences of wide-area HVDC damping control in China Southern Power Grid," in *Power and Energy Society General Meeting, 2012 IEEE*, July 2012, pp. 1–7.

[72] J. He, C. Lu, X. Wu, P. Li, and J. Wu, "Design and experiment of wide area HVDC supplementary damping controller considering time delay in China southern power grid," *IET Generation, Transmission Distribution*, vol. 3, no. 1, pp. 17–25, January 2009.

[73] J. Malcón, N. Yedrzejewski, A. Balasubramanian, R. Syed, and S. K. Raghupathula, "Implementing a country-wide modular remedial action scheme in Uruguay," in *42nd Annual Western Protective Relaying Conference*, October 2015.

[74] J. V. Espinoza, A. Guzmán, F. Calero, M. V. Mynam, and E. Palma, "Wide-area protection and control scheme maintains Central America's power system," in *40nd Annual Western Protective Relaying Conference*, October 2012.

[75] B. C. G. Shin, P. F. Gibson, B. R. Wangen, and L. A. Perez, "Wide-area dts implementation in the western electricity coordinating council," in *Power and Energy Society General Meeting, 2011 IEEE*, July 2011, pp. 1–8.

[76] S.-T. Cha, T.-K. Kim, C.-K. Lee, J.-H. Shin, J.-H. Choi, and S.-C. Nam, "Development of a training simulator for power system operation," Dec 2005, pp. 1–6.

[77] RTDS Manual. [Online]. Available: http://www.rtds.com

[78] A. G. Phadke and J. S. Thorp, *Synchronized phasor measurements and their applications*. Springer Science & Business Media, 2008.

[79] SEL-421 Protection, Automation, and Control System Instruction Manual. [Online]. Available: http://www.selinc.com

[80] SEL-3530 Real-Time Automation Controller (RTAC) Instruction Manual. [Online]. Available: http://www.selinc.com

[81] Power System Toolbox. [Online]. Available: http://www.ecse.rpi.edu/pst/PST.html

[82] R. D. Zimmerman, C. E. Murillo-Sanchez, and R. J. Thomas, "MATPOWER: Steady-state operations, planning, and analysis tools for power systems research and education," *Power Systems, IEEE Transactions on*, vol. 26, no. 1, pp. 12–19, Feb 2011.

[83] V. Vittal, D. Martin, R. Chu, J. Fish, J. C. Giri, C. K. Tang, F. E. Villaseca, and R. Farmer, "Transient stability test systems for direct stability methods," *IEEE Transactions on Power Systems*, vol. 7, no. 1, p. 37, 1992.

[84] IEEE 39 Bus System. [Online]. Available: http://www.sel.eesc.usp.br/ieee/index.htm

APPENDIX A: IEEE TEST POWER SYSTEMS

This appendix contains the data for the test power systems used for testing throughout this thesis. A short description of each test power system is shown below.

1. IEEE 9-bus, 3-machine test power system

   The network data and the dynamic data (generator and exciter parameters) for this test power system are taken from [35].

2. IEEE 9-bus, 8-machine test power system

   This test power system is developed by modifying the IEEE 9-bus, 3-machine system. Generators G2 and G3 from the original system are divided into Gen21-Gen24 and Gen31-Gen33 of equal ratings. Similarly, the transmission lines between Bus 7 and 8, and Bus 8 and 9, are split into parallel lines. The network data, the generator and exciter parameters match the original system. The IEEE TGOV1 governor parameters are taken from [81].

3. IEEE 39-bus, 10-machine test power system

   The network, generator, and exciter parameters for this test system are taken from [36].

4. IEEE 39-bus, 16-machine test power system

   This test power system is developed from IEEE 39-bus, 10-machine test power system by splitting the generators connected at Bus 19, 20, 22, and 23 into smaller units of equal rating. The network data and the dynamic data (generator, exciter, governor, PSS parameters) are taken from [84].

5. IEEE 145-bus, 50-machine test power system

   This test power system was originally developed to test direct stability techniques for transient stability assessment. The network data and dynamic parameters are taken from [83].

A.1 IEEE 9-Bus, 3-Machine System

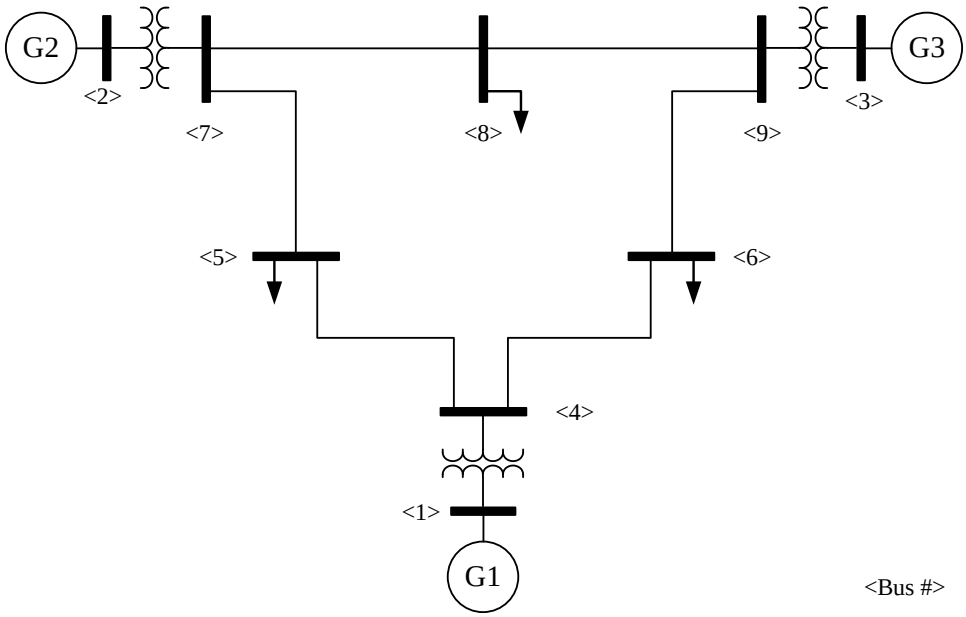

Figure A.1: IEEE 9-bus, 3-machine test power system.

Table A.1: OPF result for IEEE 9-bus system base case

Bus #	**Voltage**		**Generation**		**Load**	
	Mag (pu)	**Angle (deg)**	**P (MW)**	**Q (Mvar)**	**P (MW)**	**Q (Mvar)**
1	1.050	0.000	105.94	17.29	0.00	0.00
2	1.050	2.611	113.05	4.77	0.00	0.00
3	1.040	2.536	99.23	-15.56	0.00	0.00
4	1.042	-3.197	0.00	0.00	0.00	0.00
5	1.018	-6.105	0.00	0.00	125.00	50.00
6	1.031	-5.099	0.00	0.00	90.00	30.00
7	1.049	-1.065	0.00	0.00	0.00	0.00
8	1.038	-3.006	0.00	0.00	100.00	35.00
9	1.050	-0.517	0.00	0.00	0.00	0.00

Table A.2: Branch data for IEEE 9-bus system in 100 MVA base

Line Data					**Transformer Tap**	
From Bus	**To Bus**	**R (pu)**	**X (pu)**	**B (pu)**	**Mag (pu)**	**Angle (deg)**
1	4	0.0000	0.0576	0.0000	1.0	0.0
4	5	0.0100	0.0850	0.1760	0.0	0.0
5	7	0.0320	0.1610	0.3060	0.0	0.0
4	6	0.0170	0.0920	0.1580	0.0	0.0
6	9	0.0390	0.1700	0.3580	0.0	0.0
7	8	0.0085	0.0720	0.1490	0.0	0.0
3	9	0.0000	0.0586	0.0000	1.0	0.0
8	9	0.0119	0.1008	0.2090	0.0	0.0
2	7	0.0000	0.0625	0.0000	1.0	0.0

Table A.3: Generator data for IEEE 9-bus system

Parameters	**G1**	**G2**	**G3**
x_l	0	0	0
r_a	0	0	0
x_d	0.1460	0.8958	1.3125
x'_d	0.0608	0.1198	0.1813
x''_d	0	0	0
τ'_{d0}	8.96	6.00	5.89
τ''_{d0}	0	0	0
x_q	0.0969	0.8645	1.2578
x'_q	0.0969	0.1969	0.2500
x''_q	0	0	0
τ'_{q0}	0.310	0.535	0.600
τ''_{q0}	0	0	0
H	23.64	6.40	3.01
D	1.254	0.679	0.479

Table A.4: Exciter data for IEEE 9-bus system

Parameters	**G1**	**G2**	**G3**
τ_R	0	0	0
K_A	20	20	20
τ_A	0.2	0.2	0.2
V_{Rmax}	99	99	99
V_{Rmin}	-0.9	-0.9	-0.9
K_E	1	1	1
τ_E	0.314	0.314	0.314
EX_1	3.1	3.1	3.1
SE_1	0.4836	0.4836	0.4836
EX_2	2.3	2.3	2.3
SE_2	0.138	0.138	0.138
K_F	0.063	0.063	0.063
τ_F	0.35	0.35	0.35

A.2 IEEE 9-Bus, 8-Machine System

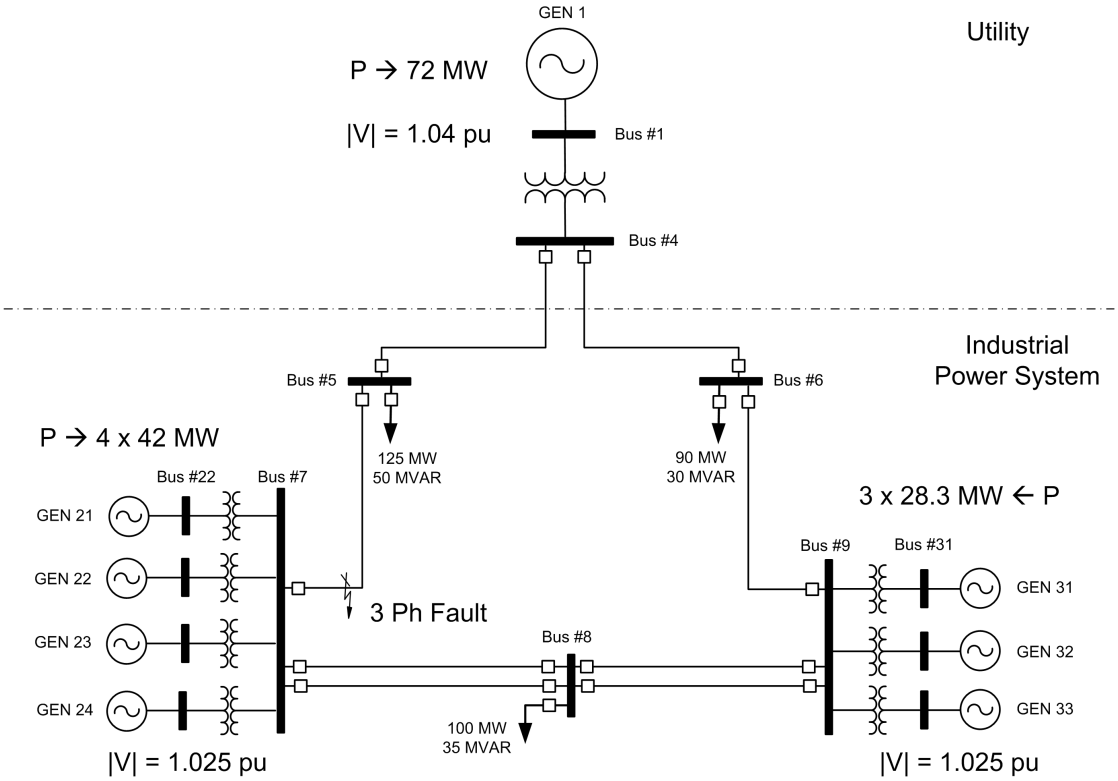

Figure A.2: IEEE 9-bus, 8-machine test power system.

Table A.5: Turbine-governor data for IEEE 9-bus, 8-machine system

Parameters	**G1**	**G21-G24**	**G31-G33**
ω_f	1	1	1
$1/r$	25	25	25
T_{max}	2	2	2
τ_s	0.1	0.1	0.1
τ_c	0.005	0.005	0.005
τ_3	0	0	0
τ_4	1.25	1.25	1.25
τ_5	5.0	5.0	5.0

A.3 IEEE 39-Bus, 10-Machine System

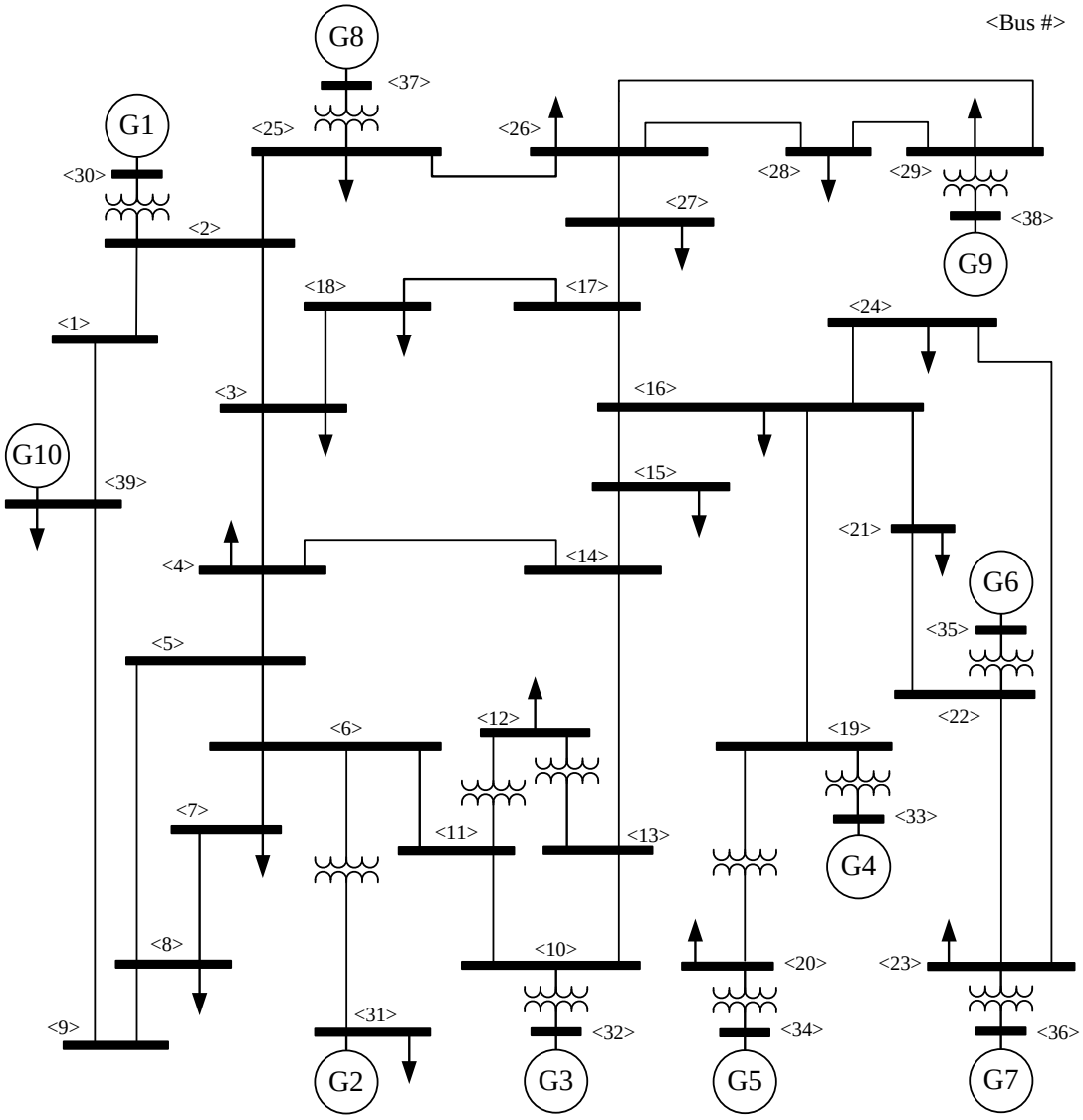

Figure A.3: IEEE 39-bus test power system.

Table A.6: OPF result for IEEE 39-bus system base case

Bus #	Voltage		Generation		Load	
	Mag (pu)	**Angle (deg)**	**P (MW)**	**Q (Mvar)**	**P (MW)**	**Q (Mvar)**
1	1.044	-8.632	0.00	0.00	0.00	0.00
2	1.034	-5.737	0.00	0.00	0.00	0.00
3	1.031	-8.601	0.00	0.00	322.00	2.40
4	1.026	-9.492	0.00	0.00	500.00	184.00
5	1.038	-8.473	0.00	0.00	0.00	0.00
6	1.043	-7.832	0.00	0.00	0.00	0.00
7	1.030	-9.909	0.00	0.00	233.80	84.00
8	1.028	-10.390	0.00	0.00	522.00	176.00
9	1.043	-10.390	0.00	0.00	0.00	0.00
10	1.050	-5.544	0.00	0.00	0.00	0.00
11	1.046	-6.323	0.00	0.00	0.00	0.00
12	1.033	-6.297	0.00	0.00	7.50	88.00
13	1.044	-6.171	0.00	0.00	0.00	0.00
14	1.035	-7.646	0.00	0.00	0.00	0.00
15	1.025	-7.750	0.00	0.00	320.00	153.00
16	1.035	-6.229	0.00	0.00	329.00	32.30
17	1.036	-7.348	0.00	0.00	0.00	0.00
18	1.033	-8.252	0.00	0.00	158.00	30.00
19	1.050	-1.094	0.00	0.00	0.00	0.00
20	0.988	-2.079	0.00	0.00	628.00	103.00
21	1.033	-3.830	0.00	0.00	274.00	115.00
22	1.049	0.619	0.00	0.00	0.00	0.00
23	1.042	0.424	0.00	0.00	247.50	84.60
24	1.040	-6.112	0.00	0.00	308.60	-92.20
25	1.049	-4.564	0.00	0.00	224.00	47.20
26	1.050	-5.667	0.00	0.00	139.00	17.00
27	1.038	-7.596	0.00	0.00	281.00	75.50
28	1.049	-2.159	0.00	0.00	206.00	27.60
29	1.050	0.598	0.00	0.00	283.50	26.90
30	0.998	-3.240	242.39	-57.25	0.00	0.00
31	1.050	0.000	566.94	359.90	9.20	4.60
32	1.023	1.814	642.73	254.25	0.00	0.00
33	0.998	4.096	629.50	115.13	0.00	0.00
34	1.005	3.177	507.90	141.28	0.00	0.00
35	1.050	5.583	650.39	222.09	0.00	0.00
36	1.050	8.383	557.99	59.87	0.00	0.00
37	1.030	2.177	534.77	47.18	0.00	0.00
38	1.027	7.651	829.36	28.70	0.00	0.00
39	1.033	-10.330	977.56	68.07	1104.00	250.00

Table A.7: Branch data for IEEE 39-bus system in 100 MVA base

Line Data					Transformer Tap	
From Bus	**To Bus**	**R (pu)**	**X (pu)**	**B (pu)**	**Mag (pu)**	**Angle (deg)**
1	2	0.0035	0.0411	0.6987	0.000	0.0
1	39	0.0010	0.0250	0.7500	0.000	0.0
2	3	0.0013	0.0151	0.2572	0.000	0.0
2	25	0.0070	0.0086	0.1460	0.000	0.0
2	30	0.0000	0.0181	0.0000	1.025	0.0
3	4	0.0013	0.0213	0.2214	0.000	0.0
3	18	0.0011	0.0133	0.2138	0.000	0.0
4	5	0.0008	0.0128	0.1342	0.000	0.0
4	14	0.0008	0.0129	0.1382	0.000	0.0
5	8	0.0008	0.0112	0.1476	0.000	0.0
6	5	0.0002	0.0026	0.0434	0.000	0.0
6	7	0.0006	0.0092	0.1130	0.000	0.0
6	11	0.0007	0.0082	0.1389	0.000	0.0
6	31	0.0000	0.0250	0.0000	1.070	0.0
7	8	0.0004	0.0046	0.0780	0.000	0.0
8	9	0.0023	0.0363	0.3804	0.000	0.0
9	39	0.0010	0.0250	1.2000	0.000	0.0
10	11	0.0004	0.0043	0.0729	0.000	0.0
10	13	0.0004	0.0043	0.0729	0.000	0.0
10	32	0.0000	0.0200	0.0000	1.070	0.0
12	11	0.0016	0.0435	0.0000	1.006	0.0
12	13	0.0016	0.0435	0.0000	1.006	0.0
13	14	0.0009	0.0101	0.1723	0.000	0.0
14	15	0.0018	0.0217	0.3660	0.000	0.0
15	16	0.0009	0.0094	0.1710	0.000	0.0
16	17	0.0007	0.0089	0.1342	0.000	0.0
16	19	0.0016	0.0195	0.3040	0.000	0.0
16	21	0.0008	0.0135	0.2548	0.000	0.0
16	24	0.0003	0.0059	0.0680	0.000	0.0
17	18	0.0007	0.0082	0.1319	0.000	0.0
17	27	0.0013	0.0173	0.3216	0.000	0.0
19	33	0.0007	0.0142	0.0000	1.070	0.0
19	20	0.0000	0.0138	0.0000	1.060	0.0
20	34	0.0009	0.0180	0.0000	1.009	0.0
21	22	0.0008	0.0140	0.2565	0.000	0.0
22	23	0.0006	0.0096	0.1846	0.000	0.0
22	35	0.0000	0.0143	0.0000	1.025	0.0
23	24	0.0022	0.0350	0.3610	0.000	0.0
23	36	0.0005	0.0272	0.0000	1.000	0.0
25	26	0.0032	0.0323	0.5130	0.000	0.0
25	37	0.0006	0.0232	0.0000	1.025	0.0

Table A.7 (continued)

Line Data					Transformer Tap	
From Bus	**To Bus**	**R (pu)**	**X (pu)**	**B (pu)**	**Mag (pu)**	**Angle (deg)**
26	27	0.0014	0.0147	0.2396	0.000	0.0
26	28	0.0043	0.0474	0.7802	0.000	0.0
26	29	0.0057	0.0625	1.0290	0.000	0.0
28	29	0.0014	0.0151	0.2490	0.000	0.0
29	38	0.0008	0.0156	0.0000	1.025	0.0

Table A.8: Generator data for IEEE 39-bus system

Para.	**G1**	**G2**	**G3**	**G4**	**G5**	**G6**	**G7**	**G8**	**G9**	**G10**
x_l	0.1	0.4	0.3	0.295	0.54	0.224	0.322	0.28	0.298	0.03
r_a	0.0	0.0	0.0	0.0	0.0	0.0	0.0	0.0	0.0	0.0
x_d	1.0000	2.9500	2.4950	2.62	6.7	2.54	2.95	2.9	2.106	0.2
x'_d	0.31	0.697	0.531	0.436	1.32	0.5	0.49	0.57	0.57	0.06
x''_d	0.2	0.2	0.2	0.2	0.2	0.2	0.2	0.2	0.2	0.02
τ'_{d0}	10.20	6.56	5.70	5.69	5.4	7.3	5.66	6.7	4.79	7
τ''_{d0}	0.0	0.0	0.0	0.03	0.03	0.03	0.03	0.03	0.03	0.03
x_q	0.69	2.82	2.37	2.58	6.2	2.41	2.92	2.8	2.05	0.19
x'_q	0.3100	0.6970	0.5310	0.436	1.32	0.5	0.49	0.57	0.57	0.06
x''_q	0.2	0.2	0.2	0.2	0.2	0.2	0.2	0.2	0.2	0.02
τ'_{q0}	1.500	1.500	1.500	1.5	0.44	0.4	1.5	0.41	1.96	0.7
τ''_{q0}	0.0	0.0	0.0	0.04	0.04	0.04	0.04	0.04	0.04	0.04
H	4.20	3.03	3.58	2.86	2.6	3.48	2.64	2.43	3.45	50
D	0	0	0	0	0	0	0	0	0	0

Table A.9: Exciter data for IEEE 39-bus system

Para.	G1	G2	G3	G4	G5	G6	G7	G8	G9	G10
τ_R	0	0	0	0	0	0	0	0	0	0.01
K_A	5	6.2	5	5	40	5	40	5	40	200
τ_A	0.06	0.05	0.06	0.06	0.02	0.02	0.02	0.02	0.02	0.015
V_{Rmax}	99	99	99	99	99	99	99	99	99	99
V_{Rmin}	-0.9	-0.9	-0.9	-0.9	-0.9	-0.9	-0.9	-0.9	-0.9	-0.9
K_E	-0.05	0.63	-0.02	-0.05	-0.04	1	1	-0.05	1	0.1
τ_E	0.25	0.41	0.5	0.5	0.785	0.471	0.73	0.528	1.4	0.5
EX_1	1.7	3	3	3	3	3	3	3	3	2.8
SE_1	0.4998	0.66	0.129	0.081	0.03	0.081	0.03	0.09	0.03	0.0812
EX_2	3	4	4	4	4	4	4	4	4	3.7
SE_2	2.001	0.88	0.34	0.312	0.912	0.252	0.74	0.28	0.852	0.3293
K_F	0.04	0.06	0.08	0.08	0.03	0.08	0.03	0.09	0.03	0.05
τ_F	1	0.5	1	1	1	1.25	1	1.26	1	0.7

A.4 IEEE 39-Bus, 16-Machine System

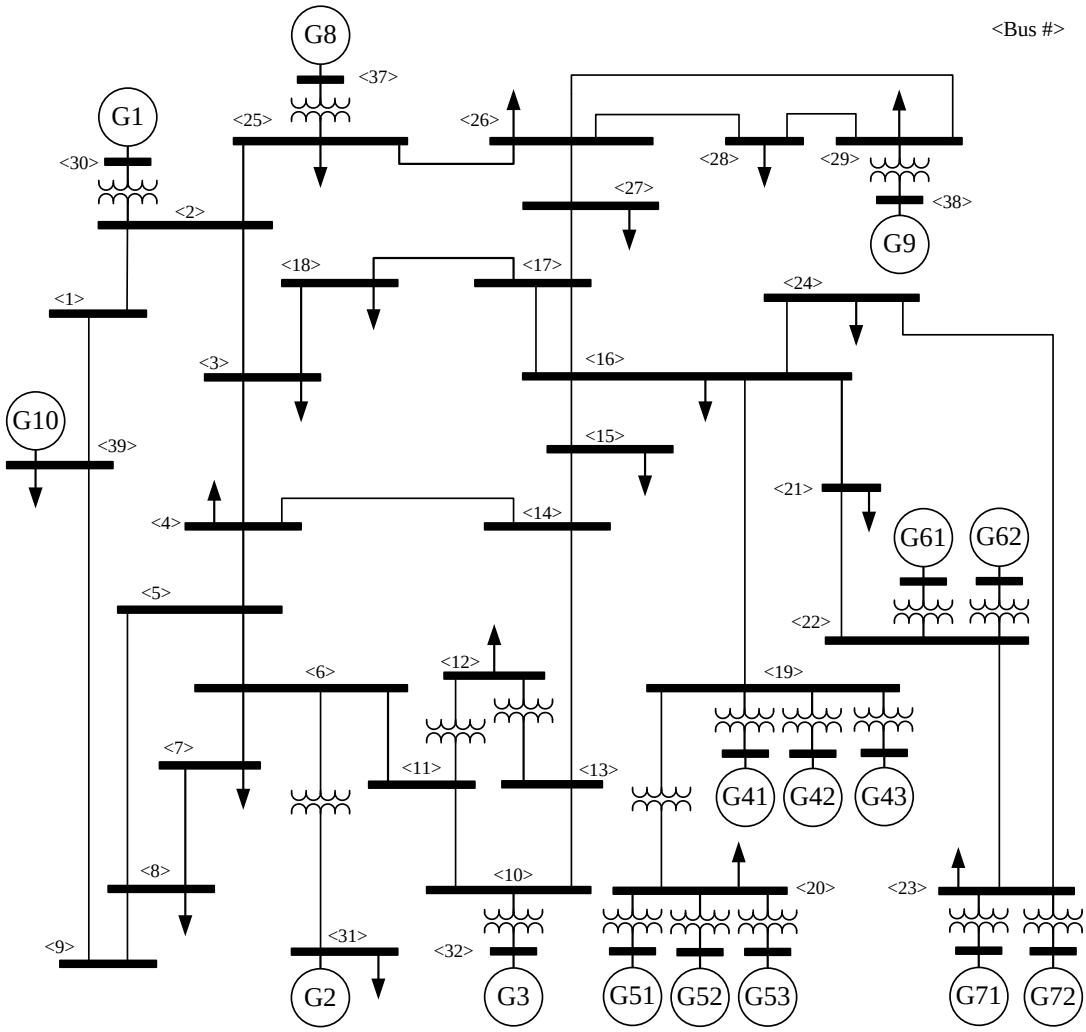

Figure A.4: IEEE 39-bus 16-machine test power system.

Table A.10: Exciter data for IEEE 39-bus, 16-machine system

Parameters	**G**n
τ_R	0.01
K_A	200
τ_A	0.015
τ_B	10
τ_C	1
V_{Rmax}	5
V_{Rmin}	-5

Table A.11: Turbine-governor data for IEEE 39-bus, 16-machine system

Parameters	**G**n
ω_f	1
$1/r$	25
T_{max}	2
τ_s	0.1
τ_c	0.005
τ_3	0
τ_4	1.25
τ_5	5.0

Table A.12: PSS data for IEEE 39-bus, 16-machine system

Parameters	**G**n
$Type$	1
G_{pss}	1
τ_w	10
τ_{n1}	1
τ_{d1}	0.05
τ_{n2}	3.0
τ_{d2}	0.5
y_{max}	0.2
y_{min}	-0.2

A.5 IEEE 145-Bus, 50-Machine System

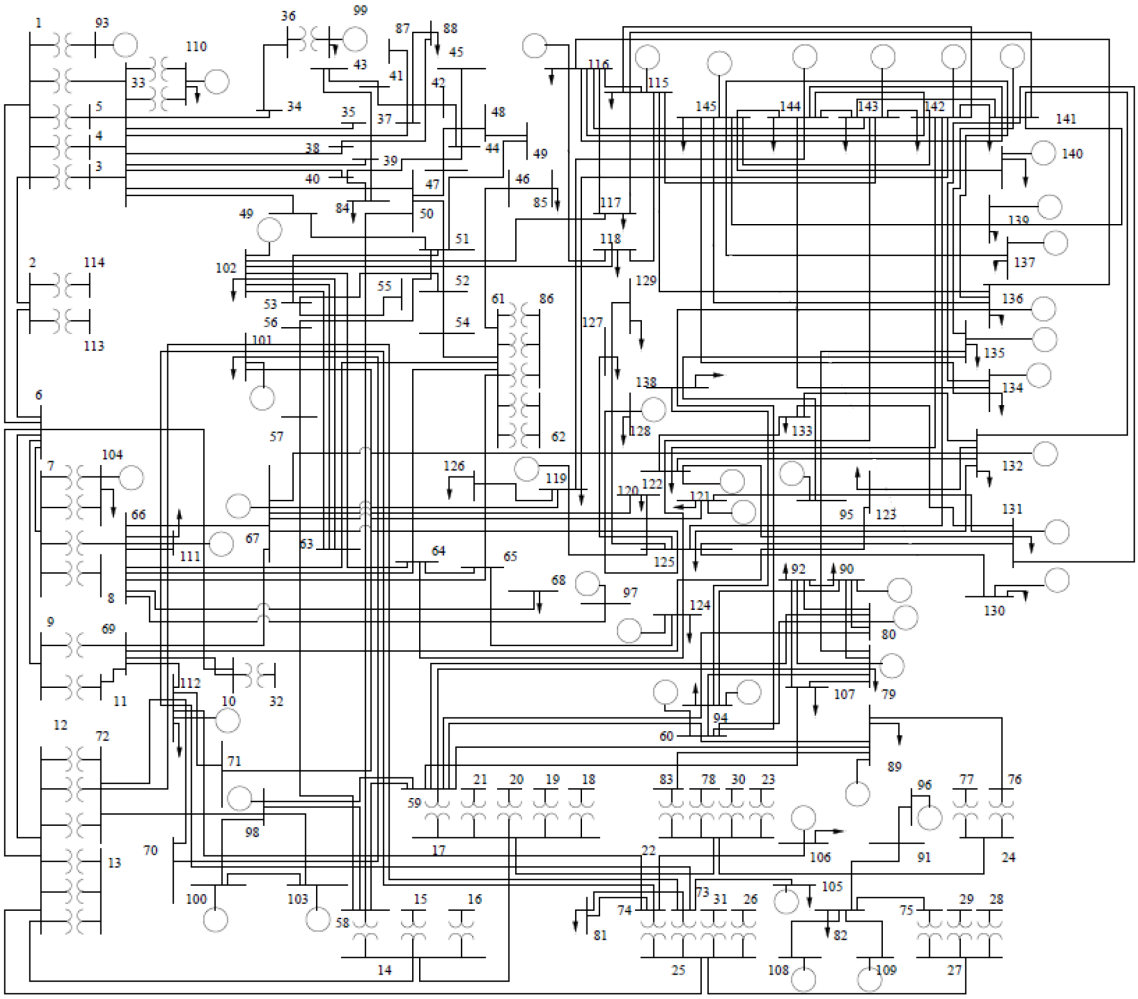

Figure A.5: IEEE 145-bus, 50-machine test power system.

Table A.13: Loadflow result for IEEE 145-bus system

Bus	Voltage		Generation		Load		GS	BS
	Mag	Angle	P	Q	P	Q		
#	(pu)	(deg)	(MW)	(Mvar)	(MW)	(Mvar)	(MW)	(Mvar)
1	1.081	-4.321	0.0	0.0	0.0	0.0	0.0	0.0
2	1.081	-4.388	0.0	0.0	0.0	0.0	0.0	0.0
3	1.102	-4.024	0.0	0.0	0.0	0.0	0.0	-126.0
4	1.102	-4.024	0.0	0.0	0.0	0.0	0.0	-126.0
5	1.102	-4.024	0.0	0.0	0.0	0.0	0.0	-126.0
6	1.043	-7.837	0.0	0.0	0.0	0.0	0.0	0.0
7	1.076	3.210	0.0	0.0	0.0	0.0	0.0	0.0
8	1.114	1.149	0.0	0.0	0.0	0.0	0.0	0.0
9	1.040	-8.052	0.0	0.0	0.0	0.0	0.0	0.0
10	1.040	-8.052	0.0	0.0	0.0	0.0	0.0	0.0
11	1.094	-10.657	0.0	0.0	0.0	0.0	0.0	0.0
12	1.039	-8.769	0.0	0.0	0.0	0.0	0.0	0.0
13	1.098	-11.430	0.0	0.0	0.0	0.0	0.0	0.0
14	1.039	-9.177	0.0	0.0	0.0	0.0	0.0	0.0
15	1.068	-9.811	0.0	0.0	0.0	0.0	0.0	-126.0
16	1.069	-9.865	0.0	0.0	0.0	0.0	0.0	-126.0
17	1.001	-9.441	0.0	0.0	0.0	0.0	0.0	-250.0
18	1.075	-10.880	0.0	0.0	0.0	0.0	0.0	-126.0
19	1.071	-10.960	0.0	0.0	0.0	0.0	0.0	-58.0
20	1.113	-10.959	0.0	0.0	0.0	0.0	0.0	0.0
21	1.109	-11.242	0.0	0.0	0.0	0.0	0.0	0.0
22	1.031	-3.884	0.0	0.0	0.0	0.0	0.0	0.0
23	1.098	-5.509	0.0	0.0	0.0	0.0	0.0	0.0
24	1.027	2.305	0.0	0.0	0.0	0.0	0.0	0.0
25	1.038	-9.871	0.0	0.0	0.0	0.0	0.0	0.0
26	1.089	-11.374	0.0	0.0	0.0	0.0	0.0	0.0
27	1.039	-13.074	0.0	0.0	0.0	0.0	0.0	0.0
28	1.076	-15.279	0.0	0.0	0.0	0.0	0.0	-126.0
29	1.075	-15.442	0.0	0.0	0.0	0.0	0.0	-126.0
30	1.073	-5.350	0.0	0.0	0.0	0.0	0.0	0.0
31	1.091	-11.814	0.0	0.0	0.0	0.0	0.0	0.0
32	1.094	-10.665	0.0	0.0	0.0	0.0	0.0	0.0
33	1.139	-4.062	0.0	0.0	0.0	0.0	0.0	0.0
34	1.139	-4.002	0.0	0.0	45.1	46.6	0.0	0.0
35	1.139	-4.080	0.0	0.0	49.2	27.5	0.0	0.0
36	1.139	-3.815	0.0	0.0	0.0	0.0	0.0	0.0
37	1.124	-6.232	0.0	0.0	0.0	0.0	0.0	0.0
38	1.131	-5.293	0.0	0.0	0.0	0.0	0.0	0.0
39	1.127	-7.916	0.0	0.0	0.0	0.0	0.0	0.0
40	1.127	-7.920	0.0	0.0	0.0	0.0	0.0	0.0

Table A.13 (continued)

Bus	Voltage		Generation		Load		GS	BS
#	Mag (pu)	Angle (deg)	P (MW)	Q (Mvar)	P (MW)	Q (Mvar)	(MW)	(Mvar)
41	1.119	-10.432	0.0	0.0	0.0	0.0	54.0	-10.0
42	1.119	-10.446	0.0	0.0	0.0	0.0	54.8	-10.0
43	1.119	-10.404	0.0	0.0	0.0	0.0	0.0	0.0
44	1.119	-10.418	0.0	0.0	0.0	0.0	0.0	0.0
45	1.117	-11.415	0.0	0.0	0.0	0.0	0.0	0.0
46	1.117	-11.410	0.0	0.0	0.0	0.0	0.0	0.0
47	1.128	-6.725	0.0	0.0	0.0	0.0	15.2	5.4
48	1.128	-6.706	0.0	0.0	0.0	0.0	13.8	5.2
49	1.128	-6.697	0.0	0.0	0.0	0.0	0.0	0.0
50	1.128	-6.715	0.0	0.0	0.0	0.0	0.0	0.0
51	1.112	-10.159	0.0	0.0	58.5	28.4	0.0	0.0
52	1.112	-11.132	0.0	0.0	0.0	0.0	23.0	-9.7
53	1.112	-11.134	0.0	0.0	0.0	0.0	23.2	-9.7
54	1.113	-11.786	0.0	0.0	0.0	0.0	18.8	-9.3
55	1.113	-11.786	0.0	0.0	0.0	0.0	18.7	-9.2
56	1.107	-9.943	0.0	0.0	0.0	0.0	18.6	-7.5
57	1.107	-9.944	0.0	0.0	0.0	0.0	18.8	-7.0
58	1.107	-9.764	0.0	0.0	76.3	-10.8	121.0	140.0
59	1.116	-10.843	0.0	0.0	0.0	0.0	508.0	8.6
60	1.137	-6.367	51.0	32.9	0.0	0.0	201.0	165.0
61	1.114	-11.891	0.0	0.0	0.0	0.0	0.0	149.0
62	1.057	-14.469	0.0	0.0	0.0	0.0	0.0	0.0
63	1.111	-13.980	0.0	0.0	0.0	0.0	823.0	525.0
64	1.098	-9.288	0.0	0.0	0.0	0.0	123.0	-26.0
65	1.098	-9.289	0.0	0.0	0.0	0.0	124.0	-26.0
66	1.113	1.318	0.0	0.0	102.2	26.7	216.0	1897.0
67	1.090	-5.657	1486.0	285.2	0.0	0.0	1821.0	1280.0
68	1.209	-30.985	0.0	0.0	0.0	-7.4	56.3	-25.0
69	1.097	-10.417	0.0	0.0	0.0	0.0	971.0	-144.0
70	1.000	-14.167	0.0	0.0	0.0	56.6	103.0	-86.0
71	1.027	-14.260	0.0	0.0	0.0	-21.2	106.0	-122.0
72	1.101	-11.194	0.0	0.0	0.0	0.0	1019.0	24.6
73	1.098	-11.060	0.0	0.0	0.0	0.0	1222.0	841.0
74	1.097	-11.461	0.0	0.0	81.9	43.7	857.0	574.0
75	1.118	-15.188	0.0	0.0	0.0	0.0	387.0	199.0
76	1.021	5.536	0.0	0.0	0.0	0.0	-667.0	-185.0
77	0.988	6.721	0.0	0.0	0.0	0.0	0.0	-125.0
78	1.074	-5.189	0.0	0.0	89.0	26.8	0.0	0.0
79	1.052	-9.511	250.2	-16.0	9.1	3.0	238.0	27.1
80	1.069	-8.210	47.0	-15.1	17.1	5.0	-0.1	29.9
81	1.130	-25.865	0.0	0.0	82.2	-93.1	70.0	-47.0

Table A.13 (continued)

Bus	Voltage		Generation		Load		GS	BS
#	Mag (pu)	Angle (deg)	P (MW)	Q (Mvar)	P (MW)	Q (Mvar)	(MW)	(Mvar)
82	0.975	-18.663	70.0	17.2	2.1	1.1	111.0	-28.0
83	1.098	-5.381	0.0	0.0	0.0	0.0	105.0	-0.4
84	1.116	-9.439	0.0	0.0	24.3	8.2	0.0	0.0
85	1.116	-13.046	0.0	0.0	27.4	0.3	0.0	0.0
86	1.057	-14.010	0.0	0.0	0.0	0.0	292.0	-22.0
87	1.065	-7.171	0.0	0.0	0.0	0.0	37.7	-47.0
88	1.109	-8.345	0.0	0.0	69.0	20.9	0.0	0.0
89	1.066	3.684	673.0	136.4	0.6	0.2	678.0	71.1
90	0.950	-7.354	22.0	-3.9	4.6	1.5	29.5	-19.0
91	1.000	-9.277	64.0	-1.5	0.0	0.0	19.3	-27.0
92	0.956	-12.752	0.0	0.0	0.0	31.0	43.4	-43.0
93	1.000	-1.918	700.0	373.8	100.4	73.2	0.0	0.0
94	1.020	-0.742	300.0	19.1	15.4	7.6	140.0	-141.0
95	0.920	18.882	131.0	10.1	6.7	2.2	27.2	-58.0
96	1.000	-8.977	60.0	21.1	0.0	0.0	47.8	-45.0
97	0.967	-4.345	140.0	45.6	0.0	0.0	129.0	-177.0
98	0.970	5.186	426.0	-32.7	0.0	0.0	82.1	-121.0
99	1.000	1.098	200.0	-8.3	10.5	5.2	0.0	0.0
100	1.014	0.702	170.0	58.7	0.0	0.0	59.1	-101.0
101	1.039	-6.090	310.9	148.7	17.8	4.5	64.7	-238.0
102	1.019	-4.764	2040.0	488.9	37.6	9.2	458.0	-619.0
103	1.000	1.514	135.0	5.0	0.0	0.0	62.4	-45.0
104	1.006	13.677	2000.0	499.9	30.2	7.6	0.0	0.0
105	1.007	-2.795	1620.0	388.4	96.0	167.4	24.2	-999.0
106	1.005	-2.750	1080.0	209.4	64.0	16.0	36.9	-719.0
107	1.021	-13.574	0.0	0.0	-17.5	-12.8	28.8	-22.0
108	1.014	-14.031	800.0	77.3	0.0	0.0	520.0	-244.0
109	0.915	-18.455	52.0	-15.6	0.0	0.0	84.5	-47.0
110	1.000	-1.307	700.0	519.8	100.4	73.2	0.0	0.0
111	1.000	7.971	2000.0	563.8	60.4	1166.0	23.3	-999.0
112	1.037	-6.264	300.0	140.1	18.6	4.6	64.3	-236.0
113	0.978	-4.388	0.0	0.0	0.0	0.0	0.0	0.0
114	0.978	-4.388	0.0	0.0	0.0	0.0	0.0	0.0
115	1.049	-15.611	2493.0	142.7	683.5	184.7	2856.0	9.4
116	1.043	-16.862	2713.0	631.8	792.6	315.5	1930.0	-195.0
117	1.030	-15.324	2627.0	258.6	485.3	71.4	2410.0	-54.0
118	1.010	-17.793	4220.0	660.4	651.9	328.4	4788.0	-979.0
119	1.013	-59.412	8954.0	4748.5	2094.0	3774.0	9999.0	-999.0
120	1.033	-51.605	0.0	0.0	-408.0	175.1	2026.0	855.0
121	1.046	-20.196	2997.0	-160.2	237.7	-17.3	306.0	1055.0
122	1.000	-2.789	1009.0	174.0	29.2	7.0	397.0	-61.0

Table A.13 (continued)

Bus	Voltage		Generation		Load		GS	BS
#	Mag (pu)	Angle (deg)	P (MW)	Q (Mvar)	P (MW)	Q (Mvar)	(MW)	(Mvar)
123	1.017	-33.122	0.0	0.0	-84.0	-19.0	118.0	1.4
124	1.000	-1.886	3005.0	569.2	94.1	780.3	766.0	-999.0
125	1.008	-32.594	0.0	0.0	-712.0	-319.0	2831.0	-71.0
126	1.052	-73.900	0.0	0.0	-333.0	-160.0	1604.0	347.0
127	1.007	-36.399	0.0	0.0	-546.0	-72.0	305.0	-51.0
128	1.025	-39.706	12963.0	2610.8	4075.0	703.5	5252.0	-472.0
129	0.980	-73.073	0.0	0.0	-482.0	-122.0	3855.0	387.0
130	1.057	-51.865	5937.0	1835.0	4328.0	944.3	3830.0	-91.0
131	1.042	-24.317	28300.0	7473.1	21840.0	4320.0	5145.0	-780.0
132	1.042	-7.241	3095.0	633.4	491.9	110.2	1239.0	-226.0
133	1.092	-11.599	0.0	0.0	-83.0	-36.3	103.0	-5.9
134	1.044	-10.821	20626.0	7402.2	22309.0	7402.0	-141.0	-78.0
135	1.107	29.045	5982.0	1564.8	4298.0	1264.0	-999.0	835.0
136	1.083	4.388	51950.0	14453.5	52951.0	13552.0	-999.0	375.0
137	1.064	-72.731	12068.0	3450.8	12946.0	2608.0	499.0	-219.0
138	1.114	12.011	0.0	0.0	-363.0	-188.0	433.0	-81.0
139	1.040	-10.557	56834.0	15849.7	57718.0	13936.0	1609.0	-999.0
140	1.050	-26.164	23123.0	6710.5	24775.0	6676.0	-289.0	-77.0
141	1.053	-9.120	37911.0	11669.5	32799.0	11361.0	5212.0	-999.0
142	1.155	-10.732	24449.0	5496.1	17737.0	3934.0	4323.0	2210.0
143	1.031	-13.664	5254.0	2158.6	4672.0	1709.0	586.0	-999.0
144	0.997	-8.577	11397.0	2686.9	9602.0	2203.0	-436.0	-999.0
145	1.052	5.020	14118.6	2987.2	9173.0	1555.0	-999.0	457.0

Table A.14: Branch data for IEEE 145-bus system in 100 MVA base

Line Data					Transformer Tap	
From Bus	**To Bus**	**R (pu)**	**X (pu)**	**B (pu)**	**Mag (pu)**	**Angle (deg)**
1	2	0.0000	0.0008	0.0632	0.000	0
1	2	0.0000	0.0008	0.0632	0.000	0
1	3	-0.0090	-0.1718	0.0000	0.935	0
1	4	-0.0090	-0.1718	0.0000	0.935	0
1	5	-0.0089	-0.1697	0.0000	0.935	0
1	6	0.0019	0.0209	2.3792	0.000	0
1	33	0.0001	0.0060	0.0000	0.935	0
1	93	0.0002	0.0138	0.0000	1.104	0
1	93	0.0002	0.0138	0.0000	1.104	0
2	6	0.0019	0.0209	2.3792	0.000	0
2	113	0.0000	0.0148	0.0000	1.105	0
2	114	0.0002	0.0145	0.0000	1.105	0
3	33	0.0002	0.0221	0.0000	0.000	0
4	33	0.0002	0.0221	0.0000	0.000	0
5	33	0.0002	0.0219	0.0000	0.000	0
6	7	0.0013	0.0139	1.4652	0.000	0
6	9	0.0002	0.0017	0.1752	0.000	0
6	10	0.0002	0.0017	0.1752	0.000	0
6	12	0.0002	0.0021	0.8776	0.000	0
6	12	0.0002	0.0021	0.8776	0.000	0
7	8	-0.0112	-0.1516	0.0000	0.972	0
7	66	0.0001	0.0097	0.0000	0.972	0
7	104	0.0004	0.0190	0.0000	1.105	0
7	104	0.0004	0.0174	0.0000	1.105	0
8	66	0.0002	0.0299	0.0000	0.000	0
8	66	0.0002	0.0221	0.0000	0.000	0
9	11	-0.0217	-0.3062	0.0000	0.917	0
9	69	0.0004	0.0188	0.0000	0.917	0
10	32	-0.0270	-0.3041	0.0000	0.917	0
10	69	0.0004	0.0187	0.0000	0.917	0
11	69	0.0002	0.0262	0.0000	0.000	0
12	13	-0.0223	-0.3099	0.0000	0.917	0
12	13	-0.0237	-0.3160	0.0000	0.917	0
12	13	-0.0237	-0.3160	0.0000	0.917	0
12	14	0.0010	0.0091	0.8556	0.000	0
12	14	0.0010	0.0091	0.8556	0.000	0
12	25	0.0005	0.0055	0.6250	0.000	0
12	25	0.0005	0.0055	0.6250	0.000	0
12	72	0.0003	0.0189	0.0000	0.917	0
12	72	0.0003	0.0190	0.0000	0.917	0
12	72	0.0003	0.0190	0.0000	0.917	0

Table A.14 (continued)

Line Data					Transformer Tap	
From Bus	**To Bus**	**R (pu)**	**X (pu)**	**B (pu)**	**Mag (pu)**	**Angle (deg)**
13	72	0.0002	0.0260	0.0000	0.000	0
13	72	0.0003	0.0262	0.0000	0.000	0
13	72	0.0002	0.0260	0.0000	0.000	0
14	15	-0.0415	-0.3996	0.0000	0.916	0
14	16	-0.0100	-0.1669	0.0000	0.916	0
14	17	0.0034	0.0367	3.4582	0.000	0
14	17	0.0035	0.0367	3.4516	0.000	0
14	58	0.0002	0.0097	0.0000	0.916	0
15	58	0.0002	0.0255	0.0000	0.000	0
16	58	0.0002	0.0220	0.0000	0.000	0
17	18	-0.3181	-1.3150	0.0000	0.871	0
17	19	0.0000	-0.8470	0.0000	0.863	0
17	20	0.0000	-0.8676	0.0000	0.863	0
17	21	-0.0095	-0.1615	0.0000	0.871	0
17	22	0.0023	0.0276	2.6204	0.000	0
17	59	0.0001	0.0071	0.0000	0.871	0
18	59	0.0002	0.0298	0.0000	0.000	0
19	59	0.0000	0.0629	0.0000	0.000	0
20	59	0.0000	0.0638	0.0000	0.000	0
21	59	0.0002	0.0329	0.0000	0.000	0
22	23	0.0000	-0.3787	0.0000	0.932	0
22	24	0.0017	0.0208	1.9648	0.000	0
22	30	0.0000	-0.3066	0.0000	0.953	0
22	78	0.0000	0.0268	0.0000	0.953	0
22	83	0.0000	0.0349	0.0000	0.932	0
23	83	0.0004	0.0595	0.0000	0.000	0
23	83	0.0003	0.0597	0.0000	0.000	0
24	76	0.0002	0.0088	0.0000	0.990	0
24	77	-0.0023	-0.0603	0.0000	0.990	0
25	26	-0.0060	-0.1375	0.0000	0.917	0
25	27	0.0023	0.0266	3.0508	0.000	0
25	27	0.0023	0.0266	3.0508	0.000	0
25	31	-0.0082	-0.1648	0.0000	0.917	0
25	73	0.0003	0.0172	0.0000	0.917	0
25	74	0.0004	0.0179	0.0000	0.917	0
26	73	0.0003	0.0267	0.0000	0.000	0
27	28	-0.1153	-0.7453	0.0000	0.907	0
27	29	-0.0163	-0.2618	0.0000	0.907	0
27	75	0.0002	0.0100	0.0000	0.907	0
28	75	0.0002	0.0290	0.0000	0.000	0
29	75	0.0002	0.0269	0.0000	0.000	0
30	78	0.0000	0.0335	0.0000	0.000	0

Table A.14 (continued)

Line Data					Transformer Tap	
From Bus	**To Bus**	**R (pu)**	**X (pu)**	**B (pu)**	**Mag (pu)**	**Angle (deg)**
31	74	0.0003	0.0279	0.0000	0.000	0
32	69	0.0002	0.0265	0.0000	0.000	0
33	34	0.0001	0.0009	0.0006	0.000	0
33	35	0.0001	0.0009	0.0006	0.000	0
33	37	0.0100	0.0707	0.1116	0.000	0
33	38	0.0100	0.0693	0.1110	0.000	0
33	39	0.0085	0.0699	0.1006	0.000	0
33	40	0.0085	0.0698	0.1004	0.000	0
33	49	0.0056	0.0493	0.0778	0.000	0
33	50	0.0056	0.0493	0.0778	0.000	0
33	110	0.0002	0.0157	0.0000	1.180	0
33	110	0.0002	0.0156	0.0000	1.180	0
34	36	0.0003	0.0022	0.0006	0.000	0
36	99	0.0008	0.0455	0.0000	1.129	0
37	87	0.0009	0.0442	0.0000	1.050	0
37	88	0.0031	0.1651	0.0000	0.000	0
38	88	0.0031	0.1638	0.0000	0.000	0
39	43	0.0060	0.0495	0.0712	0.000	0
39	84	0.0072	0.2786	0.0000	0.000	0
40	44	0.0060	0.0496	0.0714	0.000	0
40	84	0.0073	0.2756	0.0000	0.000	0
41	42	0.0005	0.1514	0.0000	0.000	0
41	43	0.0000	0.0009	0.0006	0.000	0
42	44	0.0000	0.0009	0.0006	0.000	0
43	46	0.0062	0.0508	0.0732	0.000	0
44	45	0.0062	0.0508	0.0732	0.000	0
45	61	0.0045	0.0366	0.0526	0.000	0
45	85	0.0000	0.2600	0.0000	0.000	0
46	61	0.0045	0.0366	0.0526	0.000	0
46	85	0.0000	0.2592	0.0000	0.000	0
47	48	-0.0100	0.2306	0.0000	0.000	0
47	50	0.0000	0.0009	0.0006	0.000	0
47	87	0.0831	0.4010	0.0000	0.000	0
48	49	0.0000	0.0009	0.0006	0.000	0
48	87	0.0998	0.4360	0.0000	0.000	0
49	51	0.0090	0.0790	0.1248	0.000	0
50	51	0.0090	0.0790	0.1248	0.000	0
51	52	0.0029	0.0279	0.0466	0.000	0
51	53	0.0029	0.0279	0.0466	0.000	0
51	56	0.0076	0.0483	0.0712	0.000	0
51	57	0.0076	0.0483	0.0712	0.000	0
52	53	-0.0067	0.3911	0.0000	0.000	0

Table A.14 (continued)

Line Data					Transformer Tap	
From Bus	**To Bus**	**R (pu)**	**X (pu)**	**B (pu)**	**Mag (pu)**	**Angle (deg)**
52	54	0.0047	0.0293	0.0462	0.000	0
53	55	0.0047	0.0293	0.0462	0.000	0
54	55	-0.0553	0.9289	0.0000	0.000	0
54	61	0.0014	0.0087	0.0138	0.000	0
55	61	0.0014	0.0087	0.0138	0.000	0
56	57	-0.0090	0.3895	0.0000	0.000	0
56	58	0.0019	0.0120	0.0178	0.000	0
57	58	0.0019	0.0120	0.0178	0.000	0
58	59	0.6674	2.2175	0.0000	0.000	0
58	72	0.0302	0.2364	0.0000	0.000	0
58	87	0.0863	0.3906	0.0000	0.000	0
58	98	0.0131	0.1765	0.0000	0.000	0
58	100	0.1193	1.2690	0.0000	0.000	0
58	103	0.8416	5.5383	0.0000	0.000	0
59	60	-0.1803	5.9659	0.0000	0.000	0
59	72	0.8613	3.0485	0.0000	0.000	0
59	79	0.0099	0.2644	0.0000	0.000	0
59	80	0.2876	2.3898	0.0000	0.000	0
59	89	0.3421	9.0571	0.0000	0.000	0
59	92	-0.0070	0.5678	0.0000	0.000	0
59	94	0.7041	5.9885	0.0000	0.000	0
59	98	0.1060	0.5845	0.0000	0.000	0
59	100	0.0183	0.2016	0.0000	0.000	0
59	103	0.0368	0.3341	0.0000	0.000	0
59	107	0.0372	0.8834	0.0000	0.000	0
60	135	-1.8310	9.7964	0.0000	0.000	0
60	79	-0.0375	1.1068	0.0000	0.000	0
60	80	0.0655	2.6441	0.0000	0.000	0
60	90	-0.0201	1.5135	0.0000	0.000	0
60	92	-0.2640	3.7139	0.0000	0.000	0
60	94	0.0012	0.0775	0.0000	0.000	0
60	95	-0.0855	0.9926	0.0000	0.000	0
60	138	-0.3639	1.7936	0.0000	0.000	0
61	62	-0.0362	-0.2608	0.0000	1.050	0
61	62	-0.0472	-0.5438	0.0000	1.050	0
61	63	0.0081	0.0782	0.1318	0.000	0
61	63	0.0081	0.0782	0.1318	0.000	0
61	64	0.0024	0.0318	0.0568	0.000	0
61	65	0.0024	0.0318	0.0568	0.000	0
61	86	0.0013	0.0320	0.0000	1.050	0
61	86	0.0011	0.0370	0.0000	1.050	0
61	86	0.0011	0.0370	0.0000	1.050	0

Table A.14 (continued)

Line Data					Transformer Tap	
From Bus	**To Bus**	**R (pu)**	**X (pu)**	**B (pu)**	**Mag (pu)**	**Angle (deg)**
62	86	0.0036	0.0501	0.0000	0.000	0
62	86	0.0013	0.0838	0.0000	0.000	0
63	64	0.0147	0.2825	0.0000	0.000	0
63	65	0.0147	0.2813	0.0000	0.000	0
63	66	0.0056	0.0900	0.0000	0.000	0
63	67	0.0321	0.2785	0.0000	0.000	0
63	69	0.0107	0.1571	0.0000	0.000	0
63	102	0.0106	0.1583	0.0000	0.000	0
63	102	0.0106	0.1576	0.0000	0.000	0
63	102	0.0107	0.1604	0.0000	0.000	0
63	102	0.0104	0.1542	0.0000	0.000	0
63	116	-0.3897	6.8588	0.0000	0.000	0
63	117	0.0030	0.0560	0.0000	0.000	0
63	118	-0.0125	0.2425	0.0000	0.000	0
63	124	-0.1265	2.0220	0.0000	0.000	0
64	65	0.0013	0.1674	0.0000	0.000	0
64	66	0.0039	0.0684	0.0000	0.000	0
64	67	0.0233	0.2120	0.0000	0.000	0
64	69	0.0075	0.1196	0.0000	0.000	0
64	97	-0.4336	8.2923	0.0000	0.000	0
64	124	-0.1041	1.5375	0.0000	0.000	0
65	66	0.0039	0.0682	0.0000	0.000	0
65	67	0.0233	0.2111	0.0000	0.000	0
65	69	0.0075	0.1191	0.0000	0.000	0
65	97	-0.4292	8.2582	0.0000	0.000	0
65	124	-0.1032	1.5312	0.0000	0.000	0
66	67	0.0081	0.0675	0.0000	0.000	0
66	68	-2.4730	2.4720	0.0000	0.000	0
66	69	0.0028	0.0381	0.0000	0.000	0
66	97	-0.1119	2.6432	0.0000	0.000	0
66	111	0.0000	0.0264	0.0000	0.000	0
66	111	0.0006	0.0266	0.0000	0.000	0
66	111	0.0000	0.0273	0.0000	0.000	0
66	111	0.0006	0.0264	0.0000	0.000	0
66	124	-0.0283	0.4902	0.0000	0.000	0
67	68	-3.4430	3.7172	0.0000	0.000	0
67	69	0.0061	0.0550	0.0000	0.000	0
67	97	0.0063	0.1166	0.0000	0.000	0
67	119	-0.2213	9.3918	0.0000	0.000	0
67	120	-0.0034	1.7847	0.0000	0.000	0
67	121	0.0082	1.1700	0.0000	0.000	0
67	122	-0.0047	0.4473	0.0000	0.000	0

Table A.14 (continued)

Line Data					Transformer Tap	
From Bus	**To Bus**	**R (pu)**	**X (pu)**	**B (pu)**	**Mag (pu)**	**Angle (deg)**
67	124	0.0003	0.0065	0.0000	0.000	0
67	125	0.0062	0.2519	0.0000	0.000	0
67	132	-0.3194	4.3566	0.0000	0.000	0
68	69	-0.6920	0.6984	0.0000	0.000	0
69	70	0.0085	0.3333	0.0000	0.000	0
69	71	0.0075	0.3120	0.0000	0.000	0
69	72	0.0013	0.0100	0.0000	0.000	0
69	73	0.0098	0.0747	0.0000	0.000	0
69	74	0.0135	0.0741	0.0000	0.000	0
69	97	-0.0674	1.5849	0.0000	0.000	0
69	101	0.0174	0.2188	0.0000	0.000	0
69	112	0.0175	0.2201	0.0000	0.000	0
69	124	-0.0267	0.3986	0.0000	0.000	0
70	71	-0.4891	2.6613	0.0000	0.000	0
70	72	-0.0062	0.1216	0.0000	0.000	0
70	73	-0.0424	0.9125	0.0000	0.000	0
70	74	0.0032	0.9138	0.0000	0.000	0
70	101	-0.1248	1.0409	0.0000	0.000	0
70	112	-0.1257	1.0471	0.0000	0.000	0
71	72	-0.0060	0.1138	0.0000	0.000	0
71	73	-0.0409	0.8541	0.0000	0.000	0
71	74	0.0018	0.8553	0.0000	0.000	0
71	101	-0.1592	1.2303	0.0000	0.000	0
71	112	-0.1603	1.2377	0.0000	0.000	0
72	73	0.0015	0.0275	0.0000	0.000	0
72	74	0.0028	0.0274	0.0000	0.000	0
72	98	0.0138	0.2417	0.0000	0.000	0
72	100	0.1337	1.7384	0.0000	0.000	0
72	101	0.0002	0.0802	0.0000	0.000	0
72	103	1.0224	7.5945	0.0000	0.000	0
72	112	0.0002	0.0806	0.0000	0.000	0
73	74	-0.0007	0.0393	0.0000	0.000	0
73	75	0.0147	0.2581	0.0000	0.000	0
73	81	-0.0122	0.3068	0.0000	0.000	0
73	82	0.0036	2.0169	0.0000	0.000	0
73	91	0.0271	0.5732	0.0000	0.000	0
73	96	0.0245	0.4805	0.0000	0.000	0
73	101	0.0044	0.6014	0.0000	0.000	0
73	105	0.0007	0.0325	0.0000	0.000	0
73	105	0.0007	0.0325	0.0000	0.000	0
73	105	0.0006	0.0295	0.0000	0.000	0
73	108	-0.0182	0.5832	0.0000	0.000	0

Table A.14 (continued)

Line Data					Transformer Tap	
From Bus	**To Bus**	**R (pu)**	**X (pu)**	**B (pu)**	**Mag (pu)**	**Angle (deg)**
73	109	0.0524	3.0059	0.0000	0.000	0
73	112	0.0043	0.6050	0.0000	0.000	0
73	121	-0.0268	1.7653	0.0000	0.000	0
74	75	0.0215	0.3277	0.0000	0.000	0
74	81	-0.0333	0.4631	0.0000	0.000	0
74	82	-0.0098	1.9859	0.0000	0.000	0
74	91	0.0413	0.7511	0.0000	0.000	0
74	96	0.4350	7.6901	0.0000	0.000	0
74	101	0.0344	0.6005	0.0000	0.000	0
74	106	0.0030	0.0335	0.0000	0.000	0
74	106	0.0005	0.0328	0.0000	0.000	0
74	108	-0.0187	0.4544	0.0000	0.000	0
74	109	0.1004	3.4697	0.0000	0.000	0
74	112	0.0345	0.6042	0.0000	0.000	0
74	121	-0.0348	1.3757	0.0000	0.000	0
75	82	0.0777	1.1250	0.0000	0.000	0
75	91	-0.2255	3.1442	0.0000	0.000	0
75	96	-0.4516	4.6310	0.0000	0.000	0
75	108	0.0042	0.1049	0.0000	0.000	0
75	109	0.1046	1.4465	0.0000	0.000	0
75	121	0.0178	0.3172	0.0000	0.000	0
76	77	0.0002	0.0160	0.0000	0.000	0
76	89	0.0011	0.0221	0.0000	0.000	0
79	80	0.0440	0.0991	0.0000	0.000	0
79	90	0.0506	2.4710	0.0000	0.000	0
79	92	0.0017	0.3032	0.0000	0.000	0
79	94	0.1275	1.1195	0.0000	0.000	0
79	95	0.3050	6.4154	0.0000	0.000	0
79	107	0.0786	1.4140	0.0000	0.000	0
80	90	0.4658	5.8756	0.0000	0.000	0
80	92	0.1192	1.5053	0.0000	0.000	0
80	94	0.4600	2.6475	0.0000	0.000	0
82	91	-0.2349	2.4188	0.0000	0.000	0
82	108	-0.0742	0.7278	0.0000	0.000	0
82	109	-0.0071	0.2634	0.0000	0.000	0
82	121	-0.1892	2.2054	0.0000	0.000	0
83	89	0.0582	0.3855	0.0000	0.000	0
89	103	-1.0730	4.1433	0.0000	0.000	0
90	92	-0.1380	8.2959	0.0000	0.000	0
90	94	0.0689	1.0717	0.0000	0.000	0
91	96	-0.1224	4.2463	0.0000	0.000	0
91	108	-0.1078	0.6994	0.0000	0.000	0

Table A.14 (continued)

Line Data					Transformer Tap	
From Bus	**To Bus**	**R (pu)**	**X (pu)**	**B (pu)**	**Mag (pu)**	**Angle (deg)**
91	109	-0.2699	4.2634	0.0000	0.000	0
91	121	-0.2924	2.1210	0.0000	0.000	0
92	94	0.2883	3.7717	0.0000	0.000	0
92	107	0.0176	3.0227	0.0000	0.000	0
94	95	0.0534	0.9960	0.0000	0.000	0
94	138	-0.1125	1.8385	0.0000	0.000	0
95	138	-0.0732	0.6389	0.0000	0.000	0
96	108	-0.8215	6.1143	0.0000	0.000	0
97	124	-0.3793	1.9557	0.0000	0.000	0
98	100	-0.0063	0.3269	0.0000	0.000	0
98	103	0.0544	1.4358	0.0000	0.000	0
100	103	-0.0249	0.4891	0.0000	0.000	0
101	112	-0.0138	0.3610	0.0000	0.000	0
102	117	-0.0003	0.0190	0.0000	0.000	0
102	118	-0.0267	0.3222	0.0000	0.000	0
108	109	-0.0825	1.2713	0.0000	0.000	0
108	121	-0.0009	0.0431	0.0000	0.000	0
109	121	-0.1881	3.8499	0.0000	0.000	0
115	116	0.0008	0.0291	0.0000	0.000	0
115	117	-0.0092	0.2222	0.0000	0.000	0
115	118	-0.0044	0.0677	0.0000	0.000	0
115	143	-0.1017	0.4924	0.0000	0.000	0
116	117	0.0019	0.0288	0.0000	0.000	0
116	118	-0.0010	0.0440	0.0000	0.000	0
116	143	-0.2187	1.2896	0.0000	0.000	0
117	118	0.0008	0.0081	0.0000	0.000	0
117	143	-0.0834	0.6854	0.0000	0.000	0
118	131	-0.8925	6.2385	0.0000	0.000	0
118	132	-0.6967	8.1430	0.0000	0.000	0
118	143	-0.0011	0.0231	0.0000	0.000	0
119	120	0.0010	0.0236	0.0000	0.000	0
119	121	-0.0110	0.2901	0.0000	0.000	0
119	122	-0.6013	5.8941	0.0000	0.000	0
119	124	-0.2618	3.3940	0.0000	0.000	0
119	125	-0.0082	0.2595	0.0000	0.000	0
119	126	0.0015	0.0179	0.0000	0.000	0
119	127	-0.1172	1.3932	0.0000	0.000	0
119	128	-0.0054	0.0516	0.0000	0.000	0
119	129	0.0034	0.0642	0.0000	0.000	0
119	130	-0.0022	0.0163	0.0000	0.000	0
119	131	-0.0044	0.0242	0.0000	0.000	0
119	132	-0.4137	2.4027	0.0000	0.000	0

Table A.14 (continued)

Line Data					Transformer Tap	
From Bus	**To Bus**	**R (pu)**	**X (pu)**	**B (pu)**	**Mag (pu)**	**Angle (deg)**
119	144	-0.8511	3.8358	0.0000	0.000	0
120	121	0.0009	0.0779	0.0000	0.000	0
120	122	-0.0610	0.9305	0.0000	0.000	0
120	123	-0.0466	0.5011	0.0000	0.000	0
120	124	-0.0259	0.4722	0.0000	0.000	0
120	125	-0.0002	0.0555	0.0000	0.000	0
120	127	0.0020	0.1818	0.0000	0.000	0
120	128	-0.0029	0.0743	0.0000	0.000	0
120	129	-0.0229	0.4911	0.0000	0.000	0
120	130	-0.1674	1.0675	0.0000	0.000	0
120	131	-0.0687	0.4516	0.0000	0.000	0
120	132	-0.0255	0.4566	0.0000	0.000	0
121	122	-0.0108	0.4830	0.0000	0.000	0
121	123	-0.1712	1.9482	0.0000	0.000	0
121	124	-0.0060	0.3494	0.0000	0.000	0
121	125	0.0000	0.0124	0.0000	0.000	0
121	127	-0.0204	0.8338	0.0000	0.000	0
121	128	-0.0278	0.3095	0.0000	0.000	0
121	129	-0.4545	4.2540	0.0000	0.000	0
121	131	-0.2183	1.5066	0.0000	0.000	0
121	132	-0.1308	1.3815	0.0000	0.000	0
122	123	-0.5840	4.8609	0.0000	0.000	0
122	124	-0.0009	0.0552	0.0000	0.000	0
122	125	-0.0069	0.1583	0.0000	0.000	0
122	131	-0.2433	1.9350	0.0000	0.000	0
122	132	-0.0187	0.2572	0.0000	0.000	0
122	133	-0.0980	0.9821	0.0000	0.000	0
122	143	-0.0312	0.4888	0.0000	0.000	0
123	124	-0.2230	1.9670	0.0000	0.000	0
123	125	-0.0821	0.6062	0.0000	0.000	0
123	131	-0.1783	1.2535	0.0000	0.000	0
123	132	-0.1355	1.2041	0.0000	0.000	0
124	125	-0.0017	0.0949	0.0000	0.000	0
124	128	-1.1530	8.2513	0.0000	0.000	0
124	131	-0.1062	0.8185	0.0000	0.000	0
124	132	-0.0094	0.1612	0.0000	0.000	0
124	133	-0.0342	1.1798	0.0000	0.000	0
124	143	-0.0078	0.7607	0.0000	0.000	0
125	127	-0.0791	0.9851	0.0000	0.000	0
125	128	-0.0620	0.5991	0.0000	0.000	0
125	129	-0.4217	3.9702	0.0000	0.000	0
125	130	-1.9740	8.4854	0.0000	0.000	0

Table A.14 (continued)

Line Data					Transformer Tap	
From Bus	**To Bus**	**R (pu)**	**X (pu)**	**B (pu)**	**Mag (pu)**	**Angle (deg)**
125	131	-0.1251	0.6939	0.0000	0.000	0
125	132	-0.0536	0.5086	0.0000	0.000	0
127	128	-0.0026	0.1240	0.0000	0.000	0
127	129	-0.0392	1.1082	0.0000	0.000	0
128	129	-0.0010	0.0207	0.0000	0.000	0
128	130	-1.1000	2.9924	0.0000	0.000	0
128	131	-1.5590	4.0869	0.0000	0.000	0
130	131	-0.0027	0.0154	0.0000	0.000	0
130	132	-0.6509	3.0310	0.0000	0.000	0
130	144	-0.7532	3.0664	0.0000	0.000	0
131	132	-0.0032	0.0411	0.0000	0.000	0
131	133	-1.0770	5.5285	0.0000	0.000	0
131	143	-0.0588	0.4055	0.0000	0.000	0
131	144	-0.0022	0.0151	0.0000	0.000	0
132	133	-0.0916	0.8229	0.0000	0.000	0
132	143	-0.0049	0.0965	0.0000	0.000	0
132	144	-0.1108	0.9827	0.0000	0.000	0
133	143	-0.3600	2.6309	0.0000	0.000	0
134	131	-0.4042	0.9144	0.0000	0.000	0
134	136	-0.0698	0.6428	0.0000	0.000	0
134	139	-0.0353	0.1660	0.0000	0.000	0
134	141	-0.0230	0.1179	0.0000	0.000	0
134	142	-0.0263	0.1167	0.0000	0.000	0
134	144	-0.0145	0.0435	0.0000	0.000	0
134	145	-0.0034	0.0216	0.0000	0.000	0
135	95	-0.3448	3.4845	0.0000	0.000	0
135	136	-0.0031	0.0178	0.0000	0.000	0
135	138	-0.0084	0.1729	0.0000	0.000	0
135	141	-0.1290	0.6993	0.0000	0.000	0
136	115	-0.0120	0.0855	0.0000	0.000	0
136	116	-1.2000	4.2655	0.0000	0.000	0
136	117	-2.9690	9.0875	0.0000	0.000	0
136	118	-0.5749	1.6206	0.0000	0.000	0
136	138	-0.1581	0.5485	0.0000	0.000	0
136	139	-0.0059	0.0293	0.0000	0.000	0
136	140	-2.4030	9.3780	0.0000	0.000	0
136	141	-0.0026	0.0175	0.0000	0.000	0
136	142	-0.0467	0.1709	0.0000	0.000	0
136	143	-1.7620	3.4549	0.0000	0.000	0
136	145	-0.0049	0.0539	0.0000	0.000	0
137	139	-0.0183	0.0936	0.0000	0.000	0
137	140	-2.2290	8.0228	0.0000	0.000	0

Table A.14 (continued)

Line Data					Transformer Tap	
From Bus	**To Bus**	**R (pu)**	**X (pu)**	**B (pu)**	**Mag (pu)**	**Angle (deg)**
137	145	-0.0852	0.4071	0.0000	0.000	0
139	140	-0.0054	0.0239	0.0000	0.000	0
139	141	-0.0083	0.0460	0.0000	0.000	0
139	142	-0.3102	1.2670	0.0000	0.000	0
139	145	-0.0009	0.0080	0.0000	0.000	0
140	145	-0.1088	0.4800	0.0000	0.000	0
141	115	-0.0007	0.0131	0.0000	0.000	0
141	116	-0.1568	0.7448	0.0000	0.000	0
141	117	-0.3702	1.3820	0.0000	0.000	0
141	118	-0.0414	0.1439	0.0000	0.000	0
141	131	-0.2331	0.8129	0.0000	0.000	0
141	132	-1.6280	7.0936	0.0000	0.000	0
141	142	-0.0018	0.0105	0.0000	0.000	0
141	143	-0.0702	0.1778	0.0000	0.000	0
141	144	-0.0756	0.2441	0.0000	0.000	0
141	145	-0.0038	0.0358	0.0000	0.000	0
142	115	-0.0166	0.1563	0.0000	0.000	0
142	116	-0.6916	2.6302	0.0000	0.000	0
142	117	-0.5596	2.2284	0.0000	0.000	0
142	118	-0.0185	0.1037	0.0000	0.000	0
142	119	-0.2742	1.8611	0.0000	0.000	0
142	120	-0.6043	7.3530	0.0000	0.000	0
142	122	-0.2589	2.1732	0.0000	0.000	0
142	124	-0.1736	2.1347	0.0000	0.000	0
142	125	-1.0900	8.6160	0.0000	0.000	0
142	130	-0.3608	1.8618	0.0000	0.000	0
142	131	-0.0013	0.0157	0.0000	0.000	0
142	132	-0.0055	0.0810	0.0000	0.000	0
142	133	-1.6360	9.1725	0.0000	0.000	0
142	143	-0.0038	0.0187	0.0000	0.000	0
142	144	-0.0020	0.0229	0.0000	0.000	0
142	145	-0.0738	0.4380	0.0000	0.000	0
143	144	-0.4863	2.3282	0.0000	0.000	0
144	145	-0.3835	1.2052	0.0000	0.000	0

Table A.15: Generator data for IEEE 145-bus system

Bus #	**H** (s)	x'_d (pu)	x'_q (pu)	x_d (pu)	x_q (pu)	x_l (pu)	**S(1.0)** (pu)	**S(1.2)** (pu)	τ'_{d0} (s)	τ'_{q0} (s)
93	115.04	0.024	0.037	0.098	0.097	0.012	0.07	0.57	8.50	1.24
104	73.85	0.012	0.014	0.102	0.098	0.008	0.21	0.55	10.00	1.50
105	84.39	0.021	0.031	0.114	0.109	0.011	0.13	0.41	6.61	1.50
106	56.26	0.031	0.047	0.172	0.164	0.017	0.13	0.00	6.61	1.50
110	115.05	0.024	0.037	0.098	0.097	0.012	0.07	0.57	8.50	1.24
111	73.85	0.012	0.014	0.102	0.098	0.008	0.21	0.55	10.00	1.50
60	1.41	0.477	0.0	0.0	0.0	0.0	0.0	0.0	0.0	0.0
67	52.18	0.021	0.0	0.0	0.0	0.0	0.0	0.0	0.0	0.0
79	6.65	0.129	0.0	0.0	0.0	0.0	0.0	0.0	0.0	0.0
80	1.29	0.665	0.0	0.0	0.0	0.0	0.0	0.0	0.0	0.0
82	2.12	0.529	0.0	0.0	0.0	0.0	0.0	0.0	0.0	0.0
89	20.56	0.059	0.0	0.0	0.0	0.0	0.0	0.0	0.0	0.0
90	0.76	1.600	0.0	0.0	0.0	0.0	0.0	0.0	0.0	0.0
91	1.68	0.372	0.0	0.0	0.0	0.0	0.0	0.0	0.0	0.0
94	17.34	0.084	0.0	0.0	0.0	0.0	0.0	0.0	0.0	0.0
95	5.47	0.162	0.0	0.0	0.0	0.0	0.0	0.0	0.0	0.0
96	2.12	0.482	0.0	0.0	0.0	0.0	0.0	0.0	0.0	0.0
97	5.49	0.213	0.0	0.0	0.0	0.0	0.0	0.0	0.0	0.0
98	13.96	0.080	0.0	0.0	0.0	0.0	0.0	0.0	0.0	0.0
99	17.11	0.115	0.0	0.0	0.0	0.0	0.0	0.0	0.0	0.0
100	7.56	0.139	0.0	0.0	0.0	0.0	0.0	0.0	0.0	0.0
101	12.28	0.092	0.0	0.0	0.0	0.0	0.0	0.0	0.0	0.0
102	78.44	0.014	0.0	0.0	0.0	0.0	0.0	0.0	0.0	0.0
103	8.16	0.106	0.0	0.0	0.0	0.0	0.0	0.0	0.0	0.0
108	30.43	0.025	0.0	0.0	0.0	0.0	0.0	0.0	0.0	0.0
109	2.66	0.203	0.0	0.0	0.0	0.0	0.0	0.0	0.0	0.0
112	12.28	0.092	0.0	0.0	0.0	0.0	0.0	0.0	0.0	0.0
115	97.33	0.002	0.0	0.0	0.0	0.0	0.0	0.0	0.0	0.0
116	105.50	0.002	0.0	0.0	0.0	0.0	0.0	0.0	0.0	0.0
117	102.16	0.002	0.0	0.0	0.0	0.0	0.0	0.0	0.0	0.0
118	162.74	0.001	0.0	0.0	0.0	0.0	0.0	0.0	0.0	0.0
119	348.22	0.000	0.0	0.0	0.0	0.0	0.0	0.0	0.0	0.0
121	116.54	0.002	0.0	0.0	0.0	0.0	0.0	0.0	0.0	0.0
122	39.24	0.009	0.0	0.0	0.0	0.0	0.0	0.0	0.0	0.0
124	116.86	0.002	0.0	0.0	0.0	0.0	0.0	0.0	0.0	0.0
128	503.87	0.000	0.0	0.0	0.0	0.0	0.0	0.0	0.0	0.0
130	230.90	0.001	0.0	0.0	0.0	0.0	0.0	0.0	0.0	0.0
131	1101.72	0.000	0.0	0.0	0.0	0.0	0.0	0.0	0.0	0.0
132	120.35	0.002	0.0	0.0	0.0	0.0	0.0	0.0	0.0	0.0
134	802.12	0.000	0.0	0.0	0.0	0.0	0.0	0.0	0.0	0.0
135	232.63	0.001	0.0	0.0	0.0	0.0	0.0	0.0	0.0	0.0

Table A.15 (continued)

Bus #	**H (s)**	x'_d **(pu)**	x'_q **(pu)**	x_d **(pu)**	x_q **(pu)**	x_l **(pu)**	**S(1.0) (pu)**	**S(1.2) (pu)**	τ'_{d0} **(s)**	τ'_{q0} **(s)**
136	2018.17	0.000	0.0	0.0	0.0	0.0	0.0	0.0	0.0	0.0
137	469.32	0.000	0.0	0.0	0.0	0.0	0.0	0.0	0.0	0.0
139	2210.20	0.000	0.0	0.0	0.0	0.0	0.0	0.0	0.0	0.0
140	899.19	0.000	0.0	0.0	0.0	0.0	0.0	0.0	0.0	0.0
141	1474.22	0.000	0.0	0.0	0.0	0.0	0.0	0.0	0.0	0.0
142	950.80	0.000	0.0	0.0	0.0	0.0	0.0	0.0	0.0	0.0
143	204.30	0.002	0.0	0.0	0.0	0.0	0.0	0.0	0.0	0.0
144	443.22	0.000	0.0	0.0	0.0	0.0	0.0	0.0	0.0	0.0
145	518.08	0.002	0.0	0.0	0.0	0.0	0.0	0.0	0.0	0.0

Table A.16: Exciter data for IEEE 145-bus system

Bus #	K_A	τ_A	τ_C	τ_B	V_{Rmax}	V_{Rmin}
93	185.00	0.020	1.0	1.0	8.89	-2.0
104	253.00	0.015	1.0	1.0	8.86	-7.0
105	54.63	0.468	1.0	1.0	7.38	0.0
106	54.63	0.468	1.0	1.0	7.38	0.0
110	185.00	0.020	1.0	1.0	8.89	-2.0
111	253.00	0.015	1.0	1.0	8.86	-7.0

VITA

Arun Shrestha received his BS in Electrical Engineering from Institute of Engineering, Tribhuvan University, Nepal in 2005 and his MSEE from University of North Carolina at Charlotte in 2009. At present, he is working as an Power Engineer in R&D at Schweitzer Engineering Laboratories Inc. in Charlotte, NC. His research area of interest includes wide-area protection and control, real-time power system modeling and simulation, and power system stability.